

**UNIVERSIDADE FEDERAL DE SÃO CARLOS**  
**CENTRO DE CIÊNCIAS EXATAS E DE TECNOLOGIA**  
**DEPARTAMENTO DE QUÍMICA**  
**PROGRAMA DE PÓS-GRADUAÇÃO EM QUÍMICA**

**“Electrochemistry and STM-assisted Molecular electronics  
study of bimetallic hexaphyrins”**

**Ciro Scheremeta Quintans**

Tese apresentada como parte dos requisitos  
para obtenção do título de DOUTOR EM  
CIÊNCIAS, área de concentração: FÍSICO  
QUÍMICA

**Orientador: Prof. Dr. Ernesto Chaves Pereira**

**\* bolsista FAPESP**

**São Carlos - SP**  
**2019**

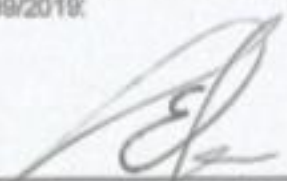


---

Folha de Aprovação

---

Assinaturas dos membros da comissão examinadora que avaliou e aprovou a Defesa de Tese de Doutorado do candidato  
Ciro Scheremeta Quintans, realizada em 23/09/2019:



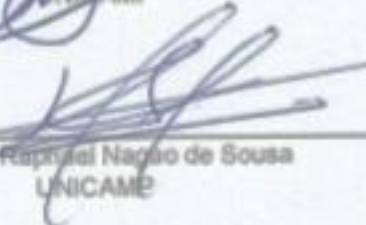
---

Prof. Dr. Ernesto Chaves Pereira de Souza  
UFSCar



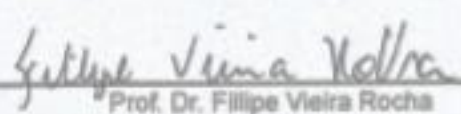
---

Prof. Dr. João Alves Bonacin  
UNICAMP



---

Prof. Dr. Raphael Nogueira de Sousa  
UNICAMP



---

Prof. Dr. Filipe Vieira Rocha  
UFSCar



---

Prof. Dr. Ellen Fabiano Silta  
UFSCar

誰にもさだめは変えられない。  
でも、ただ待つか自ら赴くかは  
決められる。

もののけ姫、宮崎駿

“He was swimming in a sea of other people’s expectations. Men had drowned in seas like that.”

— Robert Jordan

“Sometimes the best way to learn something is by doing it wrong and looking at what you did”

— Neil Gaiman

## **Acknowledgement**

A project made possible by several advisers has its outcome changed depending on each of them. I am thankful not only towards their guidance over the scientific study, and for providing a structure to it, but also to the teachings outside of laboratory. Therefore, I am grateful for the talks in which I was shown that projects never run as smoothly as described on paper while providing support during the toughest times when nothing seemed to work, for showing me that the fun part only starts after bureaucracy is overcome, for reminding me what doing science is all about, and that curiosity should allow us to truly enjoy it. Without any of them, the growth throughout this period would have had different result, and I very much appreciate their collaboration.

Further, I am grateful to my co-workers with whom collaborated during coffee breaks, lunch or over a pint (or two). Often knowledge comes from those who struggled before us.

Lastly, I am grateful to my friends, family and fiancé, whose moral support and encouragement have always helped me move forward during these long years.

This study was financed by the Coordenação de Aperfeiçoamento de Pessoal de Nível Superior - Brasil (CAPES) - Finance Code 001" and by Fundação de Amparo à Pesquisa do Estado de São Paulo (FAPESP) 2016/05363-2

## List of Tables

TABLE 2.1 –MAXIMUM ABSORPTION OF SORET BAND AND Q BAND FOR DISTINCT MESO-TETRAPHENYLPORPHYRIN TETRASULFONATE (TPPS <sub>4</sub> ), AND MESO-TETRAPYRIDYL ETHYLACETATE PORPHYRIN (TPYETACP) IN WATER. (10 <sup>-5</sup> MOL L <sup>-1</sup> ), ADAPTED FROM 108. .....	26
TABLE 4. 1. – WAVELENGTH AND ENERGY ABSORPTION FOR THE ABSORPTION AND EMISSION SPECTRA OF THE HEXAPHYRINS. (VALUES MARKED WITH * WERE REPORTED BUT NOT OBSERVED) .....	52
TABLE 5.1. – HALF WAY POTENTIALS FOR FREE BASE [26] HEXAPHYRIN FOR THIS WORK OVER Pt ELECTRODE AGAINST PSEUDO REFERENCE OF Pt, AND FOR REFERENCE 94, ON GLASSY CARBON AGAINST Fc/Fc <sup>+</sup> .....	65
TABLE 5.2. – HALF WAVE POTENTIAL FOR EACH PROCESS FOR THE MOLECULES OF THIS STUDY.....	77
TABLE 5.3. – DIFFERENCE BETWEEN HALF WAVE POTENTIAL FOR THE GIVEN PROCESSES CHARACTERIZED AS “MACROCYCLE” CENTRED IN FIG. 5.16. E <sub>OX</sub> – HALFWAVE OXIDATION POTENTIAL, E <sub>RED</sub> – HALFWAVE REDUCTION POTENTIAL.....	81
TABLE 5.4. – ELECTROCHEMICAL BAND GAP FOR THE STUDIED MOLECULES .....	82



## LIST OF FIGURES

FIGURE 2.1 – EVOLUTION OF TRANSISTOR DENSITY (LEFT AXIS) AND MINIMUM FEATURE SIZE (RIGHT AXIS) BETWEEN 1970 AND 2011. REPRODUCED FROM .....	4
FIGURE 2.2 – MOLECULAR RECTIFIER SCHEME, WHERE D STANDS FOR THE DONOR ORBITAL AND A THE ACCEPTOR ORBITAL. ....	6
FIGURE 2.3 – NANOPORE JUNCTION SCHEME ADAPTED FROM REFERENCE 35.....	8
FIGURE 2.4 – CROSSWIRE JUNCTION SCHEME ADAPTED FROM REFERENCE 35.....	9
FIGURE 2.5 – HANGING HD DROP JUNCTION JUNCTION SCHEME REPRODUCED FROM REFERNECE 35. ....	9
FIGURE 2.6 – EGAIN APPROACH SCHEME ADAPTED FROM REFERENCE 48.....	10
FIGURE 2.7 – NANOTRANSFER PATTERNING SCHEME ADAPTED FROM REFERENCE 49.....	10
FIGURE 2.8 – NANOPARTICLE BRIDGES SCHEME REPRODUCED FROM REFERENCE 51. ...	11
FIGURE 2.9 – MECHANICALLY CONTROLLED BREAK JUNCTIONS SCHEME ADAPTED FROM REFERENCE 58. ....	12
FIGURE 2.10 – PRINCIPLES OF STM SCHEMATIC. ....	14
FIGURE 2.11 – “SIMULATION OF THE ELONGATION OF A BDT-COATED AU NANOWIRE, LEADING TO THE FORMATION, ELONGATION, AND EVENTUAL RUPTURE OF A Au–BDT–AU JUNCTION.” REPRODUCED FROM REFERENCE .....	15
FIGURE 2.12 – MECHANISM FOR BLINKING METHOD, REPRODUCED FROM REFERENCE 66. ....	16
FIGURE 2.13 – TUNNELLING CURRENT ACCORDINGLY TO SIMMON’S MODEL AT DISTINCT VOLTAGE BIAS.....	20
FIGURE 2.14 – SCHEME FOR COHERENT TUNNELLING, WITHOUT INTERACTING WITH THE MOLECULE, AND FOR INCOHERENT TUNNELLING SUCH AS THE HOPPING TUNNELLING MECHANISM, IN WHICH THE ELECTRON INTERACTS WITH THE MOLECULE.....	22
FIGURE 2.15 – FREE BASE PORPHYRIN REPRESENTATIONS: A) NON-FUNCTIONALIZED (ELUCIDATING ITS INNER HYDROGENS POSITION), B) B-PYRROLIC AND MESO-PYRROLIC FUNCTIONALIZATION AND C) WITH A METAL CENTRE. ....	25
FIGURE 2.16 – FREE BASE PORPHYRIN UV-VIS SPECTRUM AND GOUTERMAN MODEL SCHEME. ....	26
FIGURE 2.17 – REPRESENTATION OF THE MACROCYCLE FOR FREE BASE PORPHYRIN (A), FREE BASE CHLORIN (B), FREE BASE BACTEROCHLORIN (C) AND FREE BASE ISOBACTEROCHLORIN (D).....	28
FIGURE 2.18 – REPRESENTATION OF A FREE BASE CORROLE. ....	28
FIGURE 2.19 – STRUCTURE REPRESENTATION OF THE FREE BASE PHTHALOCYANINE. ....	29
FIGURE 2.20 – REPRESENTATION OF THE OXIDATION STATES OF THE MONO Pd HXP AND HOW ITS STRUCTURE IS AFFECTED. ....	30
FIGURE 2.21 – DUMBBELL AND RECTANGULAR STRUCTURES FOR THE [26] HXP.....	31
FIGURE 4.1 – REACTION SCHEME FOR THE SYNTHESIS OF FREE BASE [26]HXP. ....	37
FIGURE 4.2 - REACTION SCHEME FOR THE SYNTHESIS MONO Pd [28] HEXAPHYRIN, ADAPTED FROM REFERENCE 175.....	38
FIGURE 4.3 - REACTION SCHEME FOR THE SYNTHESIS MONO Pd [26] HEXAPHYRIN, ADAPTED FROM REFERENCE 175.....	39

FIGURE 4.4 - REACTION SCHEME FOR THE SYNTHESIS OF Pd-Pd [26] HEXAPHYRIN, ADAPTED FROM REFERENCE 176.....	39
FIGURE 4.5 - REACTION SCHEME FOR THE SYNTHESIS OF Pd-Ag [26] HEXAPHYRIN.....	40
FIGURE 4.6 - REACTION SCHEME FOR THE SYNTHESIS OF Pd-Cu [26] HEXAPHYRIN.....	41
FIGURE 4.8– <sup>1</sup> H - NMR SPECTRUM OF Pd-Pd [26] HEXAPHYRIN. ....	45
FIGURE 4.10 – <sup>1</sup> H - NMR SPECTRUM OF Pd-Cu [26] HEXAPHYRIN.....	47
FIGURE 4.11 – ABSORPTION (LEFT) AND EMISSION (RIGHT) SPECTRA OF FREE BASE [26] HEXAPHYRIN. $\lambda_{EX} = 560$ NM. ....	49
FIGURE 4.12 – ABSORPTION (LEFT) AND EMISSION (RIGHT) SPECTRA OF MONO Pd [26] HEXAPHYRIN. $\lambda_{EX} = 560$ NM. ....	49
FIGURE 4.13 – ABSORPTION (LEFT) AND EMISSION (RIGHT) SPECTRA OF Pd-Pd [26] HEXAPHYRIN. $\lambda_{EX} = 560$ NM. ....	50
FIGURE 4.14 - ABSORPTION (LEFT) AND EMISSION (RIGHT) SPECTRA OF Pd-Ag [26] HEXAPHYRIN. $\lambda_{EX} = 560$ NM. ....	51
FIGURE 4.15 – ABSORPTION (LEFT) AND EMISSION (RIGHT) SPECTRA OF Pd-Cu [26] HEXAPHYRIN. $\lambda_{EX} = 560$ NM. ....	51
FIGURE 5.1 – CYCLIC VOLTAMMOGRAM OF A METALLATED TETRAPHENYL PORPHYRIN IN DICHLOROMETHANE, ADAPTED FROM REFERENCE 187. ....	56
FIGURE 5.2 – VOLTAMMOGRAM OF THE SYSTEM WITHOUT ANY OF THE MOLECULES FROM THIS STUDY. ELECTROLYTE: 0.10 MOL.L <sup>-1</sup> TBAPF <sub>6</sub> IN DCE. WORK ELECTRODE A PT MICROELECTRODE, REFERENCE AND COUNTER ELECTRODE: PT WIRES. SCANRATE 0.50 V/s. ....	60
FIGURE 5.2 – VOLTAMMOGRAM OF FERROCENE AT 0.100 V/s, OVER A PT MICROELECTRODE. ELECTROLYTE: 0.10 MOL.L <sup>-1</sup> TBAPF <sub>6</sub> IN DCE. REFERENCE AND COUNTER ELECTRODE: PT WIRES. ....	61
FIGURE 5.4 – VOLTAMMOGRAM OF FREE BASE HEXAPHYRIN AT 0.20 V/s AND 0.50 V/s, OVER A PT MICROELECTRODE. ELECTROLYTE: 0.10 MOL.L <sup>-1</sup> TBAPF <sub>6</sub> IN DCE. REFERENCE AND COUNTER ELECTRODE: PT WIRES.....	63
FIGURE 5.5 – VOLTAMMOGRAM OF FREE BASE HEXAPHYRIN WITH ITS PROCESSES TAGGED AT DISTINCT SCAN RATES, OVER A PT MICROELECTRODE. ELECTROLYTE: 0.10 MOL.L <sup>-1</sup> TBAPF <sub>6</sub> IN DICHLOROETHANE. REFERENCE AND COUNTER ELECTRODE: PT WIRES....	64
FIGURE 5.6 – PEAK CURRENT IN FUNCTION OF SQUARE ROOT OF SCAN RATE FOR ALL THE PROCESSES OBSERVED IN THE FREE BASE HEXAPHYRIN TAGGED IN FIG. 5.5.....	65
FIGURE 5.7 – VOLTAMMOGRAM OF MONO Pd HEXAPHYRIN AT 0.20 V/s AND 0.50 V/s, OVER A PT MICROELECTRODE. ELECTROLYTE: 0.10 MOL.L <sup>-1</sup> TBAPF <sub>6</sub> IN DICHLOROETHANE. REFERENCE AND COUNTER ELECTRODE: PT WIRES.....	66
FIGURE 5.8 – VOLTAMMOGRAM OF MONO Pd HEXAPHYRIN WITH ITS PROCESSES TAGGED AT DISTINCT SCAN RATES, OVER A PT MICROELECTRODE. ELECTROLYTE: 0.10 MOL.L <sup>-1</sup> TBAPF <sub>6</sub> IN DICHLOROETHANE. REFERENCE AND COUNTER ELECTRODE: PT WIRES....	67
FIGURE 5.9 – PEAK CURRENT IN FUNCTION OF SQUARE ROOT OF SCAN RATE FOR ALL THE PROCESSES OBSERVED IN THE MONO Pd HEXAPHYRIN TAGGED IN FIG. 5.8.....	68
FIGURE 5.10 – VOLTAMMOGRAM OF Pd-Pd HEXAPHYRIN AT 0.20 V/s AND 0.50 V/s, OVER A PT MICROELECTRODE. ELECTROLYTE: 0.10 MOL.L <sup>-1</sup> TBAPF <sub>6</sub> IN DICHLOROETHANE. REFERENCE AND COUNTER ELECTRODE: PT WIRES.....	69



FIGURE 5.11 – VOLTAMMOGRAM OF Pd-Pd HEXAPHYRIN WITH ITS PROCESSES TAGGED AT DISTINCT SCAN RATES, OVER A Pt MICROELECTRODE. ELECTROLYTE: 0.10 MOL.L-1 TBAPF <sub>6</sub> IN DICHLOROETHANE. REFERENCE AND COUNTER ELECTRODE: Pt WIRES....	70
FIGURE 5.12 – PEAK CURRENT IN FUNCTION OF SQUARE ROOT OF SCANRATE FOR ALL THE PROCESSES OBSERVED IN THE Pd-Pd HEXAPHYRIN TAGGED IN FIG. 5.11.....	70
FIGURE 5.13 – VOLTAMMOGRAM OF Pd-Ag HEXAPHYRIN AT 0.20 V/s AND 0.50 V/s, OVER A Pt MICROELECTRODE. ELECTROLYTE: 0.10 MOL.L-1 TBAPF <sub>6</sub> IN DICHLOROETHANE. REFERENCE AND COUNTER ELECTRODE: Pt WIRES.....	71
FIGURE 5.14 – VOLTAMMOGRAM OF Pd-Ag HEXAPHYRIN WITH ITS PROCESSES TAGGED AT DISTINCT SCAN RATES, OVER A Pt MICROELECTRODE. ELECTROLYTE: 0.1 MOL.L-1 TETRABUTYLAMMONIUM HEXAFLUOROPHOSPHATE IN DICHLOROETHANE. REFERENCE AND COUNTER ELECTRODE: Pt WIRES.....	72
FIGURE 5.15 – PEAK CURRENT IN FUNCTION OF SQUARE ROOT OF SCANRATE FOR ALL THE PROCESSES OBSERVED IN THE Pd-Ag HEXAPHYRIN TAGGED IN FIG. 5.14. ....	73
FIGURE 5.16 – VOLTAMMOGRAM OF Pd-Cu HEXAPHYRIN AT 0.100 V/s AND 0.814 V/s, OVER A Pt MICROELECTRODE. ELECTROLYTE: 0.10 MOL.L-1 TBAPF <sub>6</sub> IN DICHLOROETHANE. REFERENCE AND COUNTER ELECTRODE: Pt WIRES.....	74
FIGURE 5.17 – VOLTAMMOGRAM OF Pd-Cu HEXAPHYRIN WITH ITS PROCESSES TAGGED AT DISTINCT SCAN RATES, OVER A Pt MICROELECTRODE. ELECTROLYTE: 0.10 MOL.L-1 TBAPF <sub>6</sub> IN DICHLOROETHANE. REFERENCE AND COUNTER ELECTRODE: Pt WIRES....	75
FIGURE 5.18 – PEAK CURRENT IN FUNCTION OF SQUARE ROOT OF SCAN RATE FOR ALL THE PROCESSES OBSERVED IN THE Pd-Cu HEXAPHYRIN TAGGED IN FIG. 5.17. ....	76
FIGURE 5.18 – VOLTAMMOGRAM OF STUDIED MOLECULES, OVER A Pt MICROELECTRODE. HIGHLIGHTED PROCESSES ARE SUPPOSED TO BE CENTRED ON THE MACROCYCLE OF THE MATERIAL ELECTROLYTE: 0.10 MOL.L-1 TBAPF <sub>6</sub> IN DICHLOROETHANE. REFERENCE AND COUNTER ELECTRODE: Pt WIRES.....	79
FIGURE 5.19 – SQUARE POTENTIOMETRY FOR SYNTHESIZED MOLECULES, OVER A Pt MICROELECTRODE. ELECTROLYTE: 0.10 MOL.L-1 TBAPF <sub>6</sub> IN DICHLOROETHANE. REFERENCE AND COUNTER ELECTRODE: Pt WIRES.....	80
FIGURE 6.1 – STRUCTURAL PARTS AS CLASSIFIED BY DRAIN <i>ET AL.</i> BASED ON REFERENCE 277. ....	86
FIGURE 6.2 – AXIAL AND ORTHOGONAL COORDINATION BETWEEN GOLD TIPS FOR PORPHYRIN. AND RESULTED CONDUCTANCE HISTOGRAM.....	90
FIGURE 6.3 – REPRESENTATION OF THE CURRENT DECAY ON THE PULLING CYCLE OF TAPPING METHOD (LEFT) AND A 1D CONDUCTANCE HISTOGRAM (RIGHT) CREATED OUT OF CONTACTS FORMED BETWEEN Au STM TIP AND Au MONOCRYSTAL. ....	93
FIGURE 6.4 - REPRESENTATION OF THE CURRENT BLINK (LEFT) AND ITS 2D CONDUCTANCE MAP (RIGHT) CREATED BY THE ACCUMULATION OF BLINKS. THE 2D BLINKING MAPS WERE NORMALIZED VERSUS THE TOTAL AMOUNT OF COUNTS (100 COUNTS REPRESENTING THE MAXIMUM AND 0 REPRESENTING THE MINIMUM) AND A VERTICAL OFFSET TO ZERO CURRENT WAS APPLIED TO THE BASELINE SUCH THAT THE SINGLE-MOLECULE JUNCTION COMPONENT IS DISPLAYED CLEARLY (TUNNELLING BACKGROUND SUBTRACTED). ....	94
FIGURE 6.5 – HISTOGRAMS ACQUIRED THROUGH TAPPING APPROACH FOR FREE BASE HEXAPHYRIN, TCB AS SOLVENT. THE WORKING BIAS VOLTAGE WAS SET ON +10 mV,	

EMPLOYING A TIP ELECTRODE. MEASURED USING 100 nA/V (RIGHT, 36% YIELD) AND 1 nA/V (LEFT, 29% YIELD).....	95
FIGURE 6.6 – HISTOGRAMS ACQUIRED THROUGH TAPPING APPROACH FOR MONO Pd HEXAPHYRIN TCB AS SOLVENT. THE WORKING BIAS VOLTAGE WAS SET ON +10 mV, EMPLOYING A TIP ELECTRODE. MEASURED USING 100 nA/V (RIGHT, 39% YIELD) AND 1 nA/V (LEFT, 32% YIELD).....	96
FIGURE 6.7 – HISTOGRAMS ACQUIRED THROUGH TAPPING APPROACH FOR Pd-Pd HEXAPHYRIN, TCB AS SOLVENT. THE WORKING BIAS VOLTAGE WAS SET ON +10 mV, EMPLOYING A TIP ELECTRODE. MEASURED USING 100 nA/V (RIGHT, 38% YIELD) AND 1 nA/V (LEFT, 41% YIELD).....	96
FIGURE 6.8 – HISTOGRAMS ACQUIRED THROUGH TAPPING APPROACH FOR Pd-Ag HEXAPHYRIN, TCB AS SOLVENT. THE WORKING BIAS VOLTAGE WAS SET ON +10 mV, EMPLOYING A TIP ELECTRODE. MEASURED USING 100 nA/V (RIGHT, 42% YIELD) AND 1 nA/V (LEFT, 32% YIELD).....	97
FIGURE 6.9 – HISTOGRAMS ACQUIRED THROUGH TAPPING APPROACH FOR Pd-Cu HEXAPHYRIN, TCB AS SOLVENT. THE WORKING BIAS VOLTAGE WAS SET ON +10 mV, EMPLOYING A TIP ELECTRODE. MEASURED USING 100 nA/V (RIGHT, 43% YIELD) AND 1 nA/V (LEFT, 34% YIELD).....	97
FIGURE 6.10 – REPRESENTATION SCHEME OF A POSSIBLE INTERACTION BETWEEN 4-MERCAPTOPYRIDINE AND Pd-Ag HXP. THE MESO-PYRROLIC LIGANDS AND HYDROGEN ATOMS HAVE BEEN REMOVED FOR CLARITY.....	98
FIGURE 6.11 – HISTOGRAMS ACQUIRED THROUGH TAPPING ON MPY MODIFIED Au FOR FREE BASE HEXAPHYRIN, TCB AS SOLVENT. THE WORKING BIAS VOLTAGE WAS SET ON +10 mV, EMPLOYING A TIP ELECTRODE. MEASURED USING 100 nA/V (RIGHT, 33% YIELD) AND 1 nA/V (LEFT, 48% YIELD).....	99
FIGURE 6.12 – HISTOGRAMS ACQUIRED THROUGH TAPPING ON MPY MODIFIED Au FOR MONO Pd HEXAPHYRIN, TCB AS SOLVENT. THE WORKING BIAS VOLTAGE WAS SET ON +10 mV, EMPLOYING A TIP ELECTRODE. MEASURED USING 100 nA/V (RIGHT, 38% YIELD) AND 1 nA/V (LEFT, 31% YIELD).....	99
FIGURE 6.13 – HISTOGRAMS ACQUIRED THROUGH TAPPING ON MPY MODIFIED Au FOR Pd-Pd HEXAPHYRIN, TCB AS SOLVENT. THE WORKING BIAS VOLTAGE WAS SET ON +10 mV, EMPLOYING A TIP ELECTRODE. MEASURED USING 100 nA/V (RIGHT, 22% YIELD) AND 1 nA/V (LEFT, 29% YIELD).....	100
FIGURE 6.14 – HISTOGRAMS ACQUIRED THROUGH TAPPING ON MPY MODIFIED Au FOR Pd-Ag HEXAPHYRIN, TCB AS SOLVENT. THE WORKING BIAS VOLTAGE WAS SET ON +10 mV, EMPLOYING A TIP ELECTRODE. MEASURED USING 100 nA/V (RIGHT, 26% YIELD) AND 1 nA/V (LEFT, 27% YIELD).....	100
FIGURE 6.15 – HISTOGRAMS ACQUIRED THROUGH TAPPING ON MPY MODIFIED Au FOR Pd-Cu HEXAPHYRIN, TCB AS SOLVENT. THE WORKING BIAS VOLTAGE WAS SET ON +10 mV, EMPLOYING A TIP ELECTRODE. MEASURED USING 100 nA/V (RIGHT, 21% YIELD) AND 1 nA/V (LEFT, 37% YIELD).....	101
FIGURE 6.16 – 1D HISTOGRAMS ACQUIRED THROUGH BLINKING ON MPY MODIFIED Au FOR Pd-Ag HEXAPHYRIN CONTROL EXPERIMENT WITHOUT MOLECULE, TCB AS SOLVENT.	

THE WORKING BIAS VOLTAGE WAS SET ON +10 mV, EMPLOYING A TIP ELECTRODE. MEASURED USING 100 nA/V AS PRE-AMPLIFIER. ....	102
FIGURE 6.17 – DISTINCT INTERACTIONS POSSIBLE BETWEEN 4-MERCAPTOPYRIDINE AND 4-(THIOMETHYL) PYRIDINE FOR DIPHENYL PORPHYRIN. ....	103
FIGURE 6.18 – HISTOGRAMS ACQUIRED THROUGH BLINKING ON TPY MODIFIED AU FOR THE STUDIED HEXAPHYRINS, TCB AS SOLVENT. THE WORKING BIAS VOLTAGE WAS SET ON +15 mV, EMPLOYING A TIP ELECTRODE. ....	104
FIGURE 6.19 – HISTOGRAMS ACQUIRED THROUGH BLINKING ON 4-(THIOMETHYL) PYRIDINE MODIFIED AU FOR ALL THE MOLECULES SYNTHESIZED AT SETPOINT 0.1 nA OR 1 pA. 1,2,4-TRICHLOROBENZENE AS SOLVENT. THE WORKING BIAS VOLTAGE WAS SET ON +15 mV, EMPLOYING A TIP ELECTRODE. ....	106
FIGURE 6.20 – HISTOGRAMS (LEFT) ACQUIRED THROUGH BLINKING ON TPY MODIFIED AU FOR THE STUDIED HEXAPHYRINS, TCB AS SOLVENT. THE WORKING BIAS VOLTAGE WAS SET ON +15 mV, EMPLOYING A TIP ELECTRODE. THE SETPOINT FOR BLINKS WAS SET AS 1 pA. EXAMPLE OF BLINKS FOR EACH CURRENT SIGNATURE (RIGHT) ON SAME CONDITIONS.....	108
FIGURE 6.21 – 2-DIMENSION BLINKING MAPS WERE BUILT BY THE ACCUMULATION OF HUNDREDS OF BLINKS AT A COMMON TIME X AXIS ORIGIN. ....	109
FIGURE 6.22 – HISTOGRAMS ACQUIRED THROUGH BLINKING ON TPY MODIFIED AU FOR THE STUDIED HEXAPHYRINS, TCB AS SOLVENT. THE WORKING BIAS VOLTAGE WAS SET ON +15 mV, EMPLOYING A TIP ELECTRODE. THE SETPOINT FOR BLINKS WAS SET AS 0.100 nA.....	110



## Resumo

ELECTROCHEMISTRY AND STM-ASSISTED MOLECULAR ELECTRONICS STUDY OF BIMETALLIC HEXAPHYRINS. O transporte eletrônico em porfirinoides está relacionado com diversos bioprocessos na Natureza, da conversão de energia solar em energia química na fotossíntese ao transporte e redução de oxigênio em animais aeróbicos. Devido à essas características, diversas aplicações bioinspiradas utilizam essa classe de materiais, como fotovoltaicos, *water splitting*, catalisadores e terapia fotodinâmica. Para compreender como esses processos ocorrem em porfirinas expandidas, cinco hexafirinas foram sintetizadas em aromaticidade de Hückel, com e sem centros metálicos. Estas moléculas foram caracterizadas por técnicas espectroscópicas, eletroquímicas e por junções moleculares. Os espectros de absorção dessas hexafirinas mostram diversas transições possíveis, nas quais os desdobramento e alargamento das bandas com a adição de centros metálicos estão correlacionados com o a degeneração dos orbitais moleculares da molécula. O *band gap* espectroscópico foi caracterizado através de fluorimetria, elucidando um gap entre 1.12 e 1.20 eV. As medidas eletroquímicas mostram diversos processos quasi-reversíveis. A adição de centros metálicos desloca os potenciais dos processos redox de acordo com a eletronegatividade do metal adicionado. Devido ao grande numero de processos observados, um critério de diagnóstico foi desenvolvido para indicar quais processos ocorrem no centro metálico e quais processos ocorrem no macrociclo do material e seus ligantes. A condutância molecular das hexafirinas foram medidas através de junções moleculares assistidas por um STM, sob substratos de ouro. A funcionalização do ouro se mostrou necessária para observar os processos devido à falta de interações entre as moléculas e os eletrodos metálicos. Diversas “*current signatures*” foram observadas quando o ouro foi modificado com 4-TPy. Isto corresponde a cada possível conformação de junção molecular. Com a adição de centros metálicos, um comportamento similar pode ser observado de acordo com cada metal adicionado, indicando que as propriedades da molécula não influenciam a sua condutância tanto quanto a geometria do fio molecular.

## Abstract

ELECTROCHEMISTRY AND STM-ASSISTED MOLECULAR ELECTRONICS STUDY OF BIMETALLIC HEXAPHYRINS. The electron transport in porphyrinoids are related to several bioprocesses in Nature, from conversion from solar energy to chemical energy in photosynthesis to the transport and reduction of oxygen in aerobic animals. Due to these characteristics, several bioinspired applications have used this class of materials, photovoltaics, water splitting, catalysis and photodynamic therapy. To further understand how this process occurs in expanded porphyrins, 5 hexaphyrins in Hückel aromaticity were synthesized, with and without metal centres. These molecules were characterized by spectroscopy, electrochemistry and through molecular break junctions. The absorption spectrum of hexaphyrins show several possibly transitions, which splits and broadens with the addition of metal centres due to the degeneration of the molecule's orbitals. The spectroscopic band gap was characterized by fluorimetry showing a gap between 1.12 to 1.20 eV for the molecules synthesized. Electrochemistry measurements shows several distinct quasi-reversible redox pairs. The addition of metal centres shifted the processes accordingly to the electronegativity of the metal centres. Due to the severe number of reactions a diagnosis criterium was developed to indicate which peaks corresponds to reactions in the macrocycle or its ligands and which are likely to occur on the metal centres. The molecular conductance of the hexaphyrins were studied with STM assisted break junctions on non-modified and modified gold as electrodes. The gold modification was proved necessary due to the lack of interactions between the molecules and the metal electrodes. Several current signatures were observed on 4-TPy modified gold. This corresponds to all possible molecular junction conformations. Upon the addition of metal centres, a similar trend is observed for each metal, indicating that the molecule properties do not impact as much as the conformation of the molecular wire.

## Contents

1 – Motivation .....	1
2 – Introduction.....	3
2.1 – Molecular Electronics .....	3
2.1.1 – Background .....	3
2.1.2 – Molecular electronics history .....	5
2.1.3 – Techniques.....	7
2.1.4 – STM and its techniques.....	13
2.1.5 – Tunnelling current.....	17
2.1.6 – Electron transport in molecular junctions.....	20
2.2 – Porphyrinoids .....	23
2.2.1 – Porphyrins .....	23
2.2.2 – Other relevant porphyrinoids .....	27
2.2.3 – Expanded porphyrins .....	29
2.2.4 – Hexaphyrins .....	30
3 – Objectives.....	33
4 – Hexaphyrins synthesis and spectroscopic characterization.....	35
4.1 – Synthesis methodology .....	35
4.1.1 – Reactives .....	35
4.1.1 – Free base [26] hexaphyrin synthesis.....	35
4.1.2 – mono Pd – [28]Hexaphyrin synthesis .....	37
4.1.3 – mono Pd – [26] Hexaphyrin synthesis .....	38
4.1.4 – Pd-Pd – [26] Hexaphyrin synthesis .....	39
4.1.5 – Pd-Ag – [26] Hexaphyrin synthesis .....	40
4.1.6 – Pd-Cu – [26] Hexaphyrin synthesis .....	41
4.2 – Nuclear Magnetic Resonance characterization .....	42
4.2.1 – Methods .....	42
4.2.2 – Results .....	42
4.3 – Spectroscopic characterization.....	48
4.3.1 – Methods .....	48
4.3.2 – Results .....	48
5 – Electrochemistry of Hexaphyrins .....	55
5.1 – Introduction – Electrochemistry of porphyrinoids.....	55
5.2 – Methods.....	58

5.2.1 – Reactives .....	58
5.2.2 – Equipment and electrochemical system .....	59
5.3 – Results .....	62
5.3.1 – Voltammograms .....	62
5.3.2 – Comparison between molecules .....	77
5.4 – Partial Conclusion .....	83
6 – Molecular electronic of Hexaphyrins .....	85
6.1 – Introduction– Porphyrinoids in Molecular electronics .....	85
6.2 – Methods.....	90
6.2.1 – Reactives .....	90
6.2.2 – System preparation .....	91
6.2.3 – Electrodes functionalization.....	91
6.2.4 – STM Methods.....	92
6.3 – Results .....	94
6.3.1 – Non modified electrodes.....	94
6.3.2 – 4-mercaptopyridine modified gold .....	98
6.3.3 – 4-(thiomethyl) pyridine modified electrodes.....	103
6.4 – Partial Conclusion .....	111
7 – Conclusion.....	113
8 – References .....	115



## 1 – Motivation

If we look into Nature, we still do not comprehend how the electron flow occurs in complex molecules. This is a whole area that can give further insight to bioprocesses, enzymes activity and to drug behaviour. Having this in mind, porphyrinoids are widely studied not only due to their exceptional properties, such as high visible light absorption, thermal stability and easy to tune properties, but also due to their activities in biological systems, from the conversion of solar energy into chemical energy, in photosynthesis, until the transport and reduction of oxygen in aerobic cells. As a matter of fact, without this class of materials being part of complex proteins, life as we know it would not exist.<sup>1</sup>

Considering this scenario, a class of expanded porphyrinoids, the hexaphyrins, were prepared to be studied. Despite the fact that they were first reported in the 80's, due to its synthesis difficulty, its studies were hindered until the 2000`s when a simpler synthetic pathway was found.<sup>2</sup> Since then, several studies on synthesis show that most transition metals can be chelated in their centre,<sup>3</sup> leading to several electronic and conformational changes. Due to its aromatic properties, it has also been widely used for theoretical simulation, in which molecular dynamics shows that the molecule changes from Hückel to Möbius aromaticity by redox reactions or even by thermal inter-convention.<sup>4-6</sup> However, to date few studies have been carried out on further properties of these materials, such as: coordination chemistry, catalysis, electrochemistry and Molecular Electronics. The latter a new field of study in which main application is the use of molecules as a building block for electronics components.

Therefore, since many complex systems in nature happen through metallated porphyrinoids, we developed 5 expanded porphyrins molecules with and without metal centres for this study, with the common macrocycle of the hexakis(pentafluorophenyl)[26]hexaphyrin. While the desire to understand how the electrons flow this molecule has a bio-inspired argument, the metallic centres added were those that would keep the structure of this molecule completely planar, in Hückel aromaticity.

Some porphyrinoids have been used for molecular electronics research in the past,<sup>7-9</sup> demonstrating its usefulness as a tool to study how coordination chemistry between substrate/tip can be used to tune its conductance. However, this is the first known study on expanded hexaphyrins on this topic.

In this work, we use a series of techniques to try to provide some insight on the fundamental question *“How do electrons move through molecules?”*

Due to the complexity of the work, several issues were faced during its execution. The necessity of a large amount of material influenced the synthetic route chosen for this work, in which the reaction yield and price for synthesizing the hexakis(pentafluorophenyl)[26]hexaphyrin was the leading reason for its use. The inability to functionalize the meso ligands impacted both the electrochemical and molecular electronics study, in which electrodes could not be directly modified with the molecule. Further, the metal centres used were chosen based on the macrocycle planarity and synthesis yield. These were later found to have no application for electrocatalysis and also hindered the molecular electronics study due to the impossibility to coordinate the molecule through its metal centres. Regardless of the issues faced through the project, being responsible both for the synthesis and characterizations of the molecules made it impossible to invest time both to improve its design and the study of electron transport.

## 2 – Introduction

*This chapter provides an overview on the background, the techniques of molecular electronics and on porphyrinoids.*

### 2.1 – Molecular Electronics

#### 2.1.1 – Background

Gordon Moore published an empirical fact between the years of 1959 to 1965: the number of transistors in a single integrated circuit approximately doubled every 18 months maintaining the same price. This was a reflection of the technological advancement and miniaturization of the devices. This exponential increase in transistor density led to the huge technological boom we observed in the last 50 years.<sup>10,11</sup> The observation was later known as Moore's Law and is still in proof in 2019. However, Moore's Law starts to face a deviation with the consecutive delays of the companies to further miniaturize the Si transistors due to the high costs to produce them.

While often the miniaturization of transistors is justified only by the following device miniaturization, an important role that is often overlooked is the so called Dennard's Law.<sup>12</sup> Based on the assumption of maintaining a constant electric field inside the transistor, it was demonstrated that scaling down the device by  $k$  would increase the switching speed by the same factor, reduce the power dissipation by  $k^2$  and improve the power-delay product by  $k^3$ . Therefore, further miniaturization is not only a way to make faster and/or smaller devices, but also a method to improve its energy consumption.

The key component used as reference to track the miniaturization of the technology is the gate length between the "source" and "drain" electrodes in a field-effect transistor (FET). As shown in Fig. 2.1, at Moore's time a single transistor gate had around 10 millimetres and, over the past 50 years, it was reduced to below 100 nm. The current leading technology is by Intel's Coffee Lake (2017-2018), which uses 14 nm FETs. The current approach is facing difficulties that hinder further decreases in transistor sizes, once this is a value extremely close to what is determined as the physical limit, also known as Moore's Limit: 5 nm. Upon further shrinking, the quantum effects of the materials

tend to have a higher influence on the properties of the electronic components, such as current leakage, due to tunnelling.

In summary, we are not only approaching the collapse of Moore’s Law but also its physical limits, and to go beyond implies looking for different approaches. The almost exclusive investment on the Si transistor technology allowed it to persist with no parallel innovation. Hence, a new breakthrough is necessary to further develop this field.

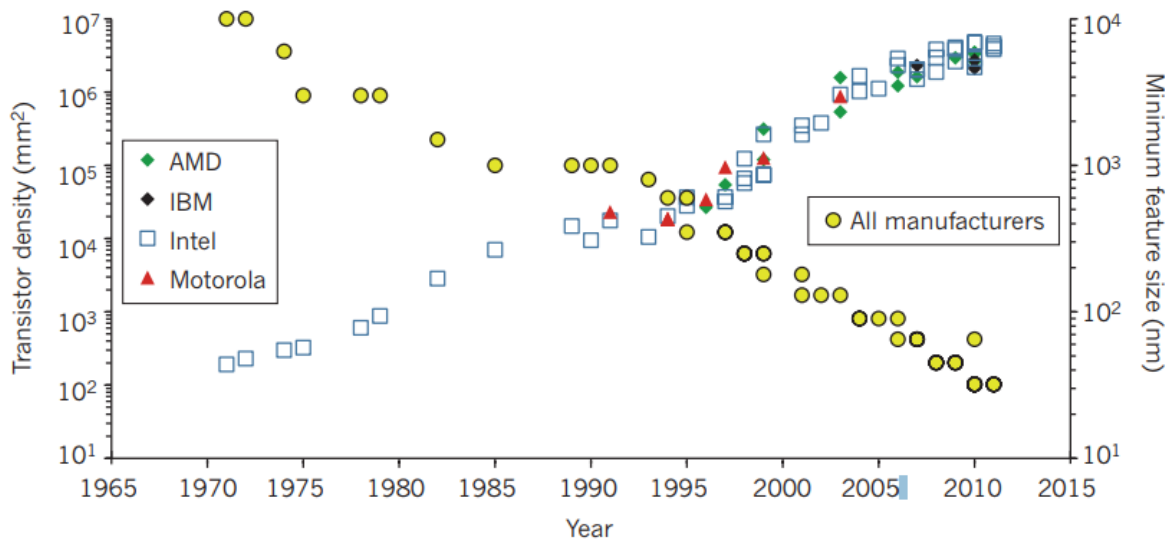


FIGURE 2.1 – Evolution of transistor density (left axis) and minimum feature size (right axis) between 1970 and 2011. Reproduced from 13

In this scenario, there are three possible alternatives to deal with Moore’s Limit:<sup>14-16</sup> “More Moore Approach”, “More than Moore Approach” and “Beyond Moore Approach”.

“More Moore Approach” - consists in keep decreasing the size of electronic transistors while looking for more efficient components and better system architectures as the applications demand, similarly to what has been done up to recent years.

“More than Moore Approach” – Stands for making chips for specific uses instead of just making them smaller and faster, adding new functionalities such as power-management circuits and sensors. In this way, the chips will be

optimized for specific devices. An example of this approach is the cell phone camera, which has photodetectors integrated monolithically to its chip.<sup>17</sup> Interestingly, the first industry road map in which the development plan was on this approach was released in 2018.

“Beyond Moore approach” looks for a way to completely substitute the actual Complementary Metal Oxide Semiconductors (CMOS) for new technologies. There are multiple approaches for beyond Moore as graphene FETs,<sup>18, 19</sup> memristors,<sup>20, 21</sup> the look for new architectures such as neural networks<sup>22</sup> and molecular electronics, topic of this thesis. This approach is the one that would bring forward a “presumptive anomaly”, as stated by Thomas Constant,<sup>23</sup> in which it would be a complete break from any previous technology.

### **2.1.2 – Molecular electronics history**

Nowadays, the idea of molecular electronics can be intuitively understood by blending two main concepts: molecules and electronics. The study of electronics can be described as the study of the behaviour of electron transport in a semiconductor, conductor, vacuum or gas and its application on the design of circuits. By analogy, molecular electronics consist in the study of how the electron current flows through molecules and its possible application as elements to build electronic devices.<sup>24</sup> However, the first grasp on this idea took years to be defined.

Historically, the first proposition that could be related to molecular electronics is that of molecular engineering. In 1956, Arthun von Hippel stated that the development of bottom-up approaches was necessary to further the development of the molecular engineering field, and published a book “Molecular Science and Molecular Engineering” two years later, in 1958. In the same year, the US Air Force in union with the Westinghouse Company organized a conference on “Molecular Electronics”, the first time in record of the use of this term. This conference had the objective to develop the technology in which von Hippel’s ideas were stated. However, the empiric studies of this field were abandoned because they could not follow up with the semiconductor electronics.<sup>25</sup> Molecular electronics stayed dormant for most of the 60’s. In the

late period of this decade, distinct groups started to study the electron transport in molecular monolayer created by Langmuir-Blodgett films.<sup>26</sup> Nevertheless, it was only in 1974 when the iconic paper “Molecular Rectifier”<sup>27</sup> was published by Aviran and Ratner that marks the beginning of modern Molecular Electronics.<sup>28</sup>

In this historical paper, an asymmetric electrical conductivity can occur when electrons tunnel through a single molecule bridging two electronic conductors in a D –  $\sigma$  – A configuration (in which D is an electron donor, A is an electron acceptor, and  $\sigma$  stands for a molecule bridging the gap between them). In analogy to solid state systems, the energy difference between the highest occupied molecular orbital (HOMO) and the lowest occupied molecular orbital (LUMO) can be compared to the “band-gap” in semiconductors, and an electron can be transferred from D to A only if the energy of the Fermi level of the former is higher than that of the bridging molecule’s LUMO, and if the Fermi level of the latter is lower than that of the bridging molecule’s HOMO. This scheme is described in Fig. 2.2.

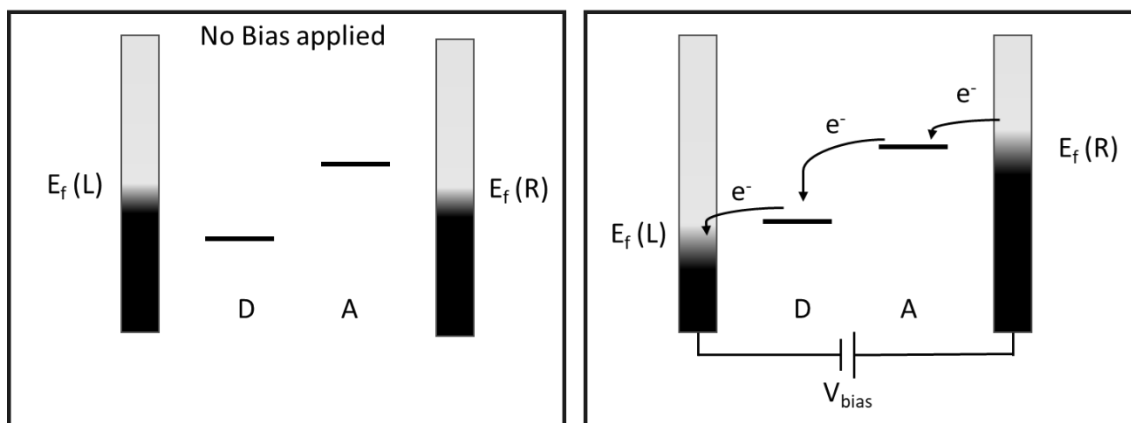


FIGURE 2.2 – Molecular rectifier scheme, where D stands for the donor orbital and A the acceptor orbital.

Despite the challenges of designing a molecule with good rectifying properties, since the molecule has to have high HOMO and low LUMO, without suffering spontaneous reduction,<sup>29</sup> at the time of Aviran’s and Ratner’s proposal it was impossible to fabricate such devices due to the lack of techniques in which molecules could be manipulated. As Ratner described: their proposal was “probably somewhere between science fiction and state-of-the-art”.<sup>30</sup> Therefore, the earlier works on molecular electronics studied an assembly of molecules

instead of monomolecular junctions. Said that, the first work that could be related to molecular electronics predates Aviran and Ratner's work, when Kuhn and Mann reported the conductivity through monolayers of fatty acids with increasing length size, showing the  $\beta$ -decay through the self-assembly layer of fatty acids.<sup>31</sup> However, the approach used was still complicated and difficult to reproduce.

The boom on molecular electronics happened years after the invention of the Scanning Tunnelling Microscope (STM) by Binnig and Rohrer in 1982,<sup>32,33</sup> and by the Atomic Force Microscope (AFM) in 1989, which can be considered the birth event of modern nanoscience and nanotechnology. While some experiments were made in this field, it wasn't until late 90's when Reed et al measured the first reported molecular junction conductivity.<sup>34</sup> While the knowledge of the process was still crawling, the molecular electronics field started to receive massive attention, becoming a research field widely studied.

### **2.1.3 – Techniques**

The main problem that hindered the advance of molecular electronics is how to develop reproductive molecular junctions. Since Aviran's and Ratner's report, multiple approaches have been studied. Generally speaking, the techniques developed are divided in two categories: the molecular array-based devices (MDB), also known as monolayer junction or assembly monojunctions, and single molecule junctions.

#### **2.1.3.1 – Molecular array-based devices**

The MDB approach, historically, predates any concept of molecular electronics. While often ignored, the first report of such method was a measurement capacitance and electronic conductance of fatty acid monolayers created by Langmuir-Blodgett (LB) films in the 30's.<sup>35,36</sup> This approach was more used in the late 60's as the first method for MDB, with the first paper with high reproducibility being published in 1971 on Cd fatty acids salts.<sup>31</sup> Several studies could show how the conductivity would decrease with the molecules length, showing the  $\beta$ -decay of conductivity through alkylic chains. However, this

approach drastically restricts the molecules that could be used since it requires that each termination of the molecule to interact distinctly with the solvent to create a film. Years later with the further development of tools to manipulate molecules, LB films were replaced by self-assembled monolayers (SAM), in which the molecule would have a strong functionalization to bind with the surface of the substrate, as thiols in gold or carboxylates for Pt. The first report of such a case was done by Sagiv,<sup>37</sup> in which he showed that the film preparation method does not induce changes in the conductivity of the monolayer. This kind of method depends on having a functionalization on the molecule that interacts with the substrate, and upon changing this group, it could drastically change the conductivity, depending on the binding groups and the substrate material. Since then, virtually any kind of thin layer technique has been used, from Langmuir-Blodgett to high vacuum electrospray.<sup>38</sup>

The use of advanced techniques contributes to a higher order and lower number of contaminants on the films, such as excess solvent. However, the key point for the study of MDB is to assemble the second electrode on the top of the monolayer to close the electrical circuit, since the metal can easily scrap the monolayer and short-circuit the system. For this reason, several methods have been developed to improve this aspect, such as:

- nanopore junctions:<sup>39,40</sup> a nanopore is created by plasma etching or lithography on an insulating film, such as  $\text{SiO}_2$  or  $\text{Si}_3\text{N}_4$ . This pore will behave as a window between the two sides of the film. A SAM of the molecule of interest will be adsorbed inside the pore and electrical contacts will be made on both sides by sputtering. The resulting assembly is represented in Fig. 2.3.

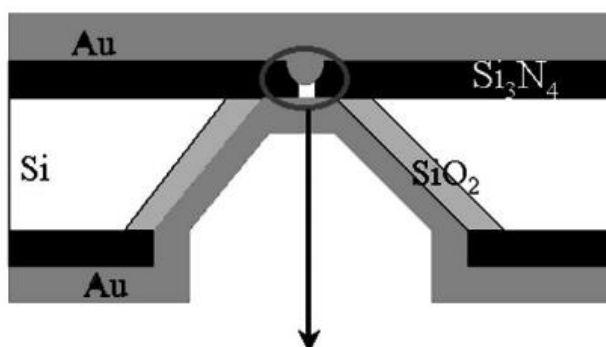


FIGURE 2.3 – Nanopore junction scheme adapted from reference 35.



- cross wire junctions:<sup>41-44</sup> consists in using two long metal wires as electrodes. A SAM is made over one of the wires and the second electrode is soft attached over the SAM in a cross-like geometry, as shown in Fig. 2.4. If the second metal wire is attached perpendicular to a magnetic field, it can be coupled for conductance measurements.

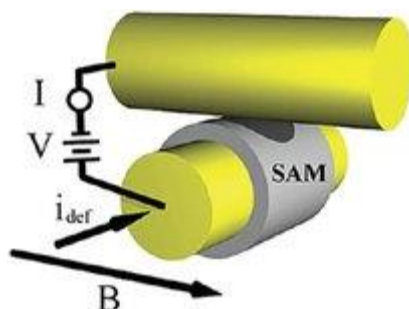


FIGURE 2.4 – Crosswire Junction Scheme adapted from reference 35.

- Hanging Hg drop junction:<sup>45-47</sup> consists in using a Hg drop on a surface of a SAM modified electrode as a second contact. Due to the high mercury surface tension, the odds of shortcircuiting the system decreases. Since the mercury drop is created in the same solution as the SAM was made, usually the measurement has two layers of the molecule. While it is a cheap and practical technique, it has some serious drawbacks related to its toxicity and the fact it easily forms amalgams, short-circuiting the system. Fig. 2.5 shows the scheme of this junction.

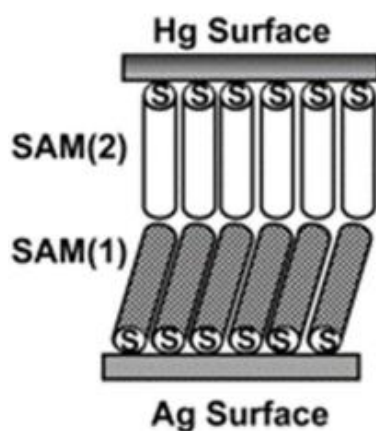


FIGURE 2.5 – Hanging Hd drop junction Junction Scheme reproduced from refernece 35.

- Eutectic gallium-indium (EGaIn):<sup>48</sup> This method was used to overcome the problems of Hg drops approach. In this technique, an EGaIn drop is suspended from a syringe and brought in contact with a bare Ag surface. The syringe is then retracted slowly until the EGaIn forms two conical endings. This ending is then approached to a SAM as the second electrode. This mechanism is described in Fig. 2.6. It is worth noticing that since the EGaIn doesn't form a semi spherical drop, the contact area is drastically reduced when compared to the Hg drop approach.

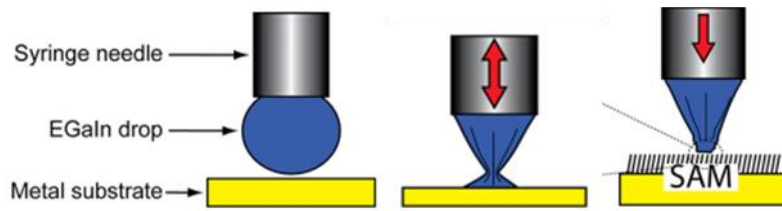


FIGURE 2.6 – EGaIn approach scheme adapted from reference 48.

- Nanotransfer patterning:<sup>49</sup> This method uses an elastomeric stamp, such as polydimethylsiloxane (PDMS), on a Si wafer with features previously defined by lithography. A thin layer of metal is deposited over the stamp which then can be cast over a SAM coated substrate as shown in Figure 2.7. Due to the low interaction between the metal and the stamp, when the stamp is removed the metal layer is transferred in the same pattern as designed.

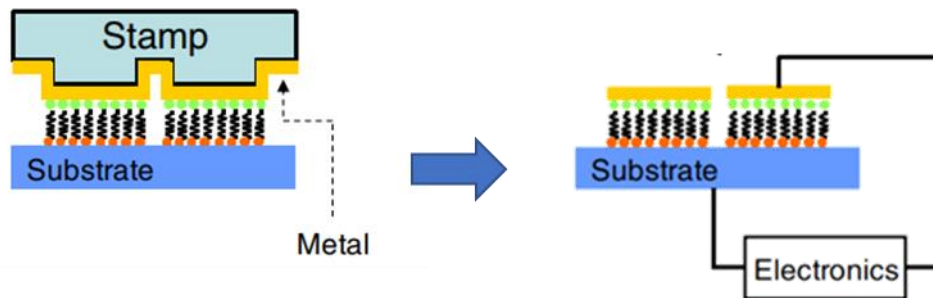


FIGURE 2.7 – Nanotransfer patterning scheme adapted from reference 49.

- Nanoparticle bridges:<sup>50-52</sup> in this approach a nanogap is

created in a wire through ion beam milling. This system is then immersed in a solution containing the molecules to be measured for a period, to allow it to adsorb in its surface. Lastly, gold nanoparticles are trapped in the gap through dielectrophoretic trapping. The final system is shown in Fig. 2.8.

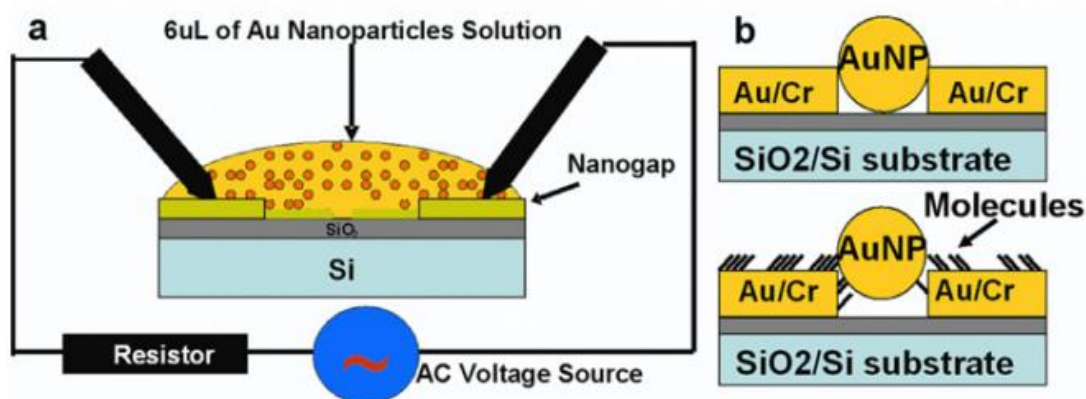


FIGURE 2.8 – nanoparticle bridges scheme reproduced from reference 51.

While there is not an optimal approach for molecular array devices, some of them have advantages over others. Cross wire junctions are extremely easy to be created but also the easiest to cut circuit. Nanotransfer patterning is not a simple technique and has restrictions on the molecules it can be used, but it is a cheap and easy to attach the second metal contact. However, on proper assembled systems there is not a large deviation on the conductance results in the molecules in function of the approach used. Overall, it depends on the expertise of the research group over an optimal study approach.

### 2.1.3.2 – Single molecule devices

Methods for single molecule measurement are not as diversified as those for molecules arrays. This is caused by the difficulty in providing a current signature that identifies as the single measured molecule conductance. The two main methods for this are the mechanically controllable break junctions (MCBJ) and Scanning Tunnelling Microscopy based break junctions (STM-BJ), which will be discussed in the following sub-chapter.

Mechanically controlled break-junctions (MCBJ) <sup>53 - 58</sup> consist in slowly pulling a ductile metal wire until it narrows down and eventually breaks. If the rupture occurs in solution, one or more molecule can spontaneously link between the metal contacts forming a molecular junction. The first reported MCBJ was designed in 1985, in which a Nb-Sn filament fixated on a substrate with epoxy was slowly pulled apart.<sup>56</sup> Nowadays, the technique has further improved and a micro constriction is previously constructed with micro fabrication techniques, such as lithography, increasing the attenuation factor of the break junction, aka the relation between electrode displacement and the bending of the substrate. A higher attenuation factor allows to tune the elongation to a matter of sub-angstrom precision. The general schematic for a MCBJ technique is shown in Fig. 2.9.

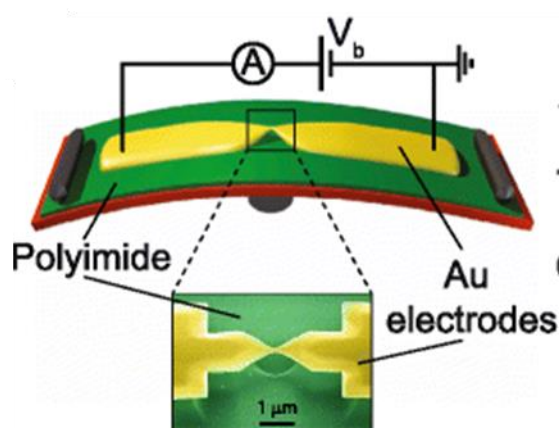


FIGURE 2.9 – Mechanically controlled break junctions scheme adapted from reference 58.

## **2.1.4 – STM and its techniques**

The STM is, usually, an imaging probe-based microscope that consists in the relation between tunnelling current and distance between two electrodes (surface and tip). For proper understanding of the technique, an introduction to the equipment is necessary.

### **2.1.4.1 – The Scanning Tunnelling microscope**

As previously mentioned, the STM was developed by Rohner and Binnig in 1981.<sup>32</sup> This technique allows the imaging of surfaces to atomic level. The instrumentation consists in a sharp conducting tip, a piezodrive, height controller, an isolation system to avoid noise and a computer for interface and scanner control.

The experimental technique, represented in Fig. 2.10, consists in attaching the sharp tip on the piezodrive, which consists in three piezoelectric controllers orthogonal to each other, allowing the control of the tip in x,y,z axis. Applying a voltage to each piezoelectric allows it to expand or contract, moving the tip in the desired direction with sub-angstrom accuracy. Using the height controller and the piezodrive in the z-axis, the tip is approached to the substrate surface up to sub-nanometre distance. Applying a BIAS (V) to the tip allows the wave-function of the tip and substrate to overlap, allowing the passage of a tunnelling current ( $I_t$ ) between tip and substrate. The tunnelling current increases exponentially with the distance and, in case it is measured in function of the x and y axis through the piezodrive control, an image can be created of position in function of height.

The current magnitude and direction that tunnels through this system is dependent of the BIAS applied. Usually the tip of the STM is grounded and the BIAS is applied on the sample. If the BIAS has a positive feedback, the electrons are injected from the tip on the sample. If the BIAS is negative, the opposite will happen and the electrons will tunnel from substrate to the sample. The current in the tip is converted through a current pre amplifier to voltage, allowing the flux of a picoscale currents.

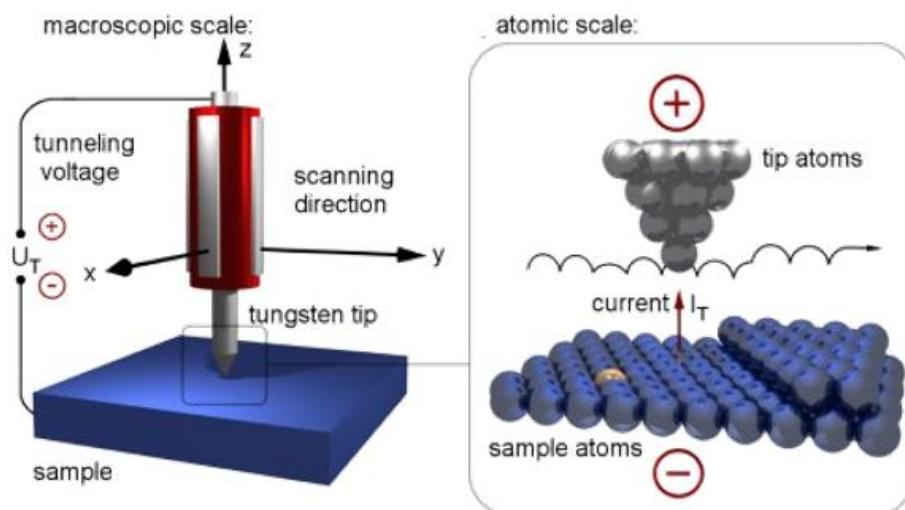


FIGURE 2.10 – Principles of STM schematic. <sup>59</sup>

### 2.1.4.2 – STM-BJ Tapping

The first application of the STM for specific conductance studies was in the 90's conductance through point contact points, <sup>60</sup> showing the conductance quantization of  $2e^2/h$ , where  $e$  is the electron charge and  $h$  is the Planck constant. However, it took several years for the first successful use of the STM on molecular electronics, when Xu and Tao, <sup>61</sup> who designed a tool to create in-situ single-molecule break junctions between the STM tip and the surface electrode.

Upon controlling the distance between them by the piezoelectric transducer (PZE), one can create thousands of in-situ break junctions by quickly approaching and retracting the tip from the surface. This approach will be treated as “*tapping*” for the remaining of this thesis.

Moreover, a secondary technique was developed in which the tip is kept static at fixed distance between both electrodes. When a molecule can spontaneously span the gap between the tip and the surface, a blink of current will be read, characteristic for each molecule. This approach will be treated as blinking<sup>62</sup> for the remaining of this project.

The tapping approach consists in controlling the PZE voltage to drive the tip in and out of contact with the substrate. The mechanism elucidated in Fig. 2.11<sup>63</sup> can be used to describe the regular experiment of tapping, with the

target molecular system either in solution or adsorbed in the electrode substrate. After using the PZE to force the tip into the substrate, crashing it to the substrate and registering a saturation on the read current, it can be pulled from the surface, elongating a metal atomic wire formed between both electrodes. Ideally, there will be a moment in which the atomic wire will be formed by a single atom or quantum point contact, in which the conductance is quantized to  $1 G_0$  (conductance quantum). Upon further pulling, the atomic wire breaks and a molecule might be linked bridging. In this scenario we obtain a single molecule contact and the captured current signal is characteristic for each molecular system. Further pulling of the tip results in the rupture of the system and obtaining the tunnelling current in function of the distance resulting in a current sharp decay.

This mechanism is cyclically repeated several times in order to collect thousands of molecular junctions. While multiple molecules might bridge the rupture gap between the electrodes, upon pulling the tip further from the surface will decrease the number of molecules trapped between electrodes until the moment a single molecule will be in contact. It is important to highlight that ideally the molecules should have strong linkers to promote the interaction with the gold contacts to increase the odds of obtaining a molecular break-junction.

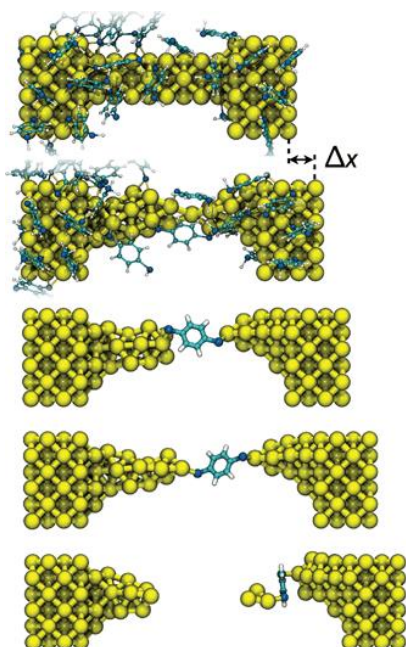


FIGURE 2.11 – “Simulation of the elongation of a BDT-coated Au nanowire, leading to the formation, elongation, and eventual rupture of a Au–BDT–Au junction.” reproduced from reference <sup>64</sup>.



### 2.1.4.3 – STM-BJ Blinking

A year after the appearance of the first STM-BJ studies, Haiss et al proposed an alternative use of the STM for Molecular Electronics study.<sup>65</sup> While using similar set up for the tapping experiments, the molecules would be trapped spontaneously between the electrodes in a motionless mechanism, elucidated in Fig. 2.12<sup>66</sup> The STM tip is set at a constant distance from the substrate and the current is monitored in function of time. In case no molecule bridges the tip – electrode separation, the reading is constant and as function of the tunnelling current through the gap. However, a molecule might be trapped between the electrodes, in which case the circuit is closed and the tunnelling current is redirected through the molecule, yielding a sudden jump in the monitored current which corresponds to the conductance value of the bridged molecule added to the background tunnelling current. As a consequence of these spontaneous contacts, current jumps are observed in the captured current transient, in a telegraphic fashion.

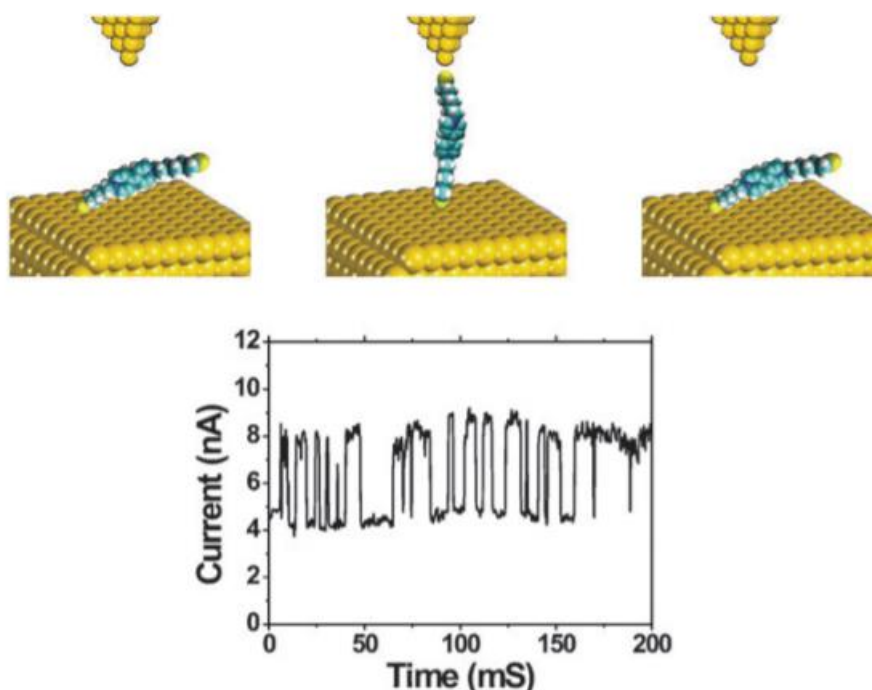


FIGURE 2.12 – Mechanism for blinking method, reproduced from reference 66.

It is important that the distance between electrode and tip in this experiment is compatible with the molecule dimensions. If the distance is too big, a molecule would not be able to bridge the gap. Also, while the lack of strong



linkers to make the gold-molecule interaction will not hinder the blinks to appear, the lifetime of each blink, and its stability, will greatly decrease.

There are several tools that can be applied together with the blinking approach. For example, once the blink happens the tip can be pulled setting a voltage ramp to the PZE, retracting it, while reading the current.<sup>19</sup> We can use it for either proof the presence of the molecular bridge, or to check how the molecule conductivity changes in function of the conformation until the molecular junction is broken. It is also possible to make current- bias voltage curves, checking for possible rectification properties of the studied molecular systems.<sup>67</sup> These tools, while worth mentioning, could not be used in the present work due to the short lifetime of the blinks of the hexaphyrins as discussed in chapter 5.

### 2.1.5 – Tunnelling current

The tunnelling current is a quantum effect where the electron passes through a potential barrier. In the case of the STM, the electrons are injected from the tip to the substrate, or vice-versa, while tunnelling through a non-conductive media: vacuum or a liquid. An extensive discussion of tunnelling current and the resolution of Schrödinger equation can be found elsewhere.<sup>68,69</sup>

The easier approach for tunnelling current through the tip to substrate can be compared to the tunnelling through a rectangular potential barrier, once the distance from the tip to substrate on a nonconductive media has a constant barrier potential with changing distance. The simplified version of the analytical solution can be described as:

$$It = cst * e * V * \exp \left[ \frac{-2\sqrt{2m\Phi}}{\hbar} * d \right] \quad (1)$$

In this equation  $It$  is the tunnelling current,  $cst$  is dependent on the media,  $e$  is the electron charge,  $V$  is the BIAS applied,  $\Phi$  is the work function of the working electrode, as the difference in FERMI energy,  $m$  is the mass of the electron,  $\hbar$  is the Plank constant and  $d$  is the distance. Since most of these values are constant, we can affirm the tunnelling current depends, mostly, on the applied

BIAS, the kind of material and the exponential of the distance between the tip and the substrate. Due to this relation with the distance the tunnelling current changes by one order of magnitude for every 1 angstrom in distance, giving the equipment its high resolution.

Since the 60's simple arguments of molecules as a potential barrier, in which its shape and size would affect conductivity have been made. These predicaments are often related to Simmons's model, which describes the electron transport between metallic electrodes through a tunnelling regiment.<sup>70</sup> This model adopts an approximation in which the electron behaves as a free particle and does not interact with the insulator. The equation that describes the current density is expressed as:

$$J = J_0 \{ \bar{\phi} e^{-A\sqrt{\bar{\phi}}} - (\bar{\phi} + eV) e^{-A\sqrt{\bar{\phi} + eV}} \} \quad (2)$$

Where,

$$J_0 = \frac{e}{2\pi h (\xi \Delta s)^2} \quad (3)$$

$$A = \frac{4\pi \xi \Delta s \sqrt{2m_e}}{h} \quad (4)$$

In which J is the current density, e is the electron charge, h the Plank constant, m is the mass of the electron, V is the BIAS applied,  $\xi$  is a dimensionless correction factor, and  $\bar{\phi}$  is the potential barrier height. Since we are using an approximation in which the potential barrier is rectangular,  $\bar{\phi} = \bar{\phi}_0$ , the height of the potential barrier, and  $\Delta s = s$ , the thickness of the insulating barrier.

As shown in Fig 2.11, these approximations lead us to a model with three regimes depending on the applied BIAS.

- **The Low voltage Range** (Fig. 2.13(a)) – in which the applied voltage is really small and  $eV \sim 0$ . Therefore,  $\bar{\phi}$  can be considered independente of the applied BIAS, the correction factor  $\xi = 1$ , and it yields the following expression:

$$J = J_L V ; J_L = \frac{e^2 \sqrt{2m_e \bar{\phi}}}{4\pi^2 \xi^2 \Delta s} e^{-A\sqrt{\bar{\phi}}} \quad (5)$$

Where  $J_L$  is the current flowing from the left electrode and is a linear function of the applied BIAS.

- **Intermediate Voltage Range (Fig. 2.13(b))** - in which  $eV < \bar{\phi}$ , the  $\bar{\phi}$  is defined as:

$$\bar{\phi} = \frac{\bar{\phi}_1 + \bar{\phi}_2 - eV}{2} \quad (6)$$

Simplifying the expression with the correction factor  $\xi = 1$ , we have:

$$J = J_L (V + \gamma V^3); \gamma = \frac{(Ae)^2}{96\bar{\phi}_0} - \frac{(Ae)^2}{32\bar{\phi}_0^2} \quad (7)$$

In this regime, the current increases in function of the voltage applied.

- **High voltage Range (Fig. 2.13(c))** – if  $eV > \bar{\phi}$ ,  $\bar{\phi}$  is reduced to  $\bar{\phi}_1/2$  and  $\Delta s$  is also reduced. If the applied  $V$  is high enough to make the Fermi energy of the left electrode higher than the right electrode, the tunnelling from the right to the left is not possible since there is no empty states on that electrode to receive electrons. On the opposite direction, since all electrons from the left electrode are on higher energy than the empty states of the right electrode, all electrons can tunnel through it. This is similar to the field emission of electrons in vacuum, in which the work function is necessary to eject it. For this reason,  $J$  can be simplified to :

$$J = \frac{2.2e^3}{8\pi h} \frac{F^2}{\bar{\phi}_1} e^{-\frac{8\pi\sqrt{2m}\bar{\phi}_1^{3/2}}{2.96ehF}} \quad (8)$$

Where  $F$  is the electric field in the insulator,  $F = V/s$ , where  $s$  is the thickness of the insulating field.

According to the equation, this regime currents density increases exponentially with the voltage.

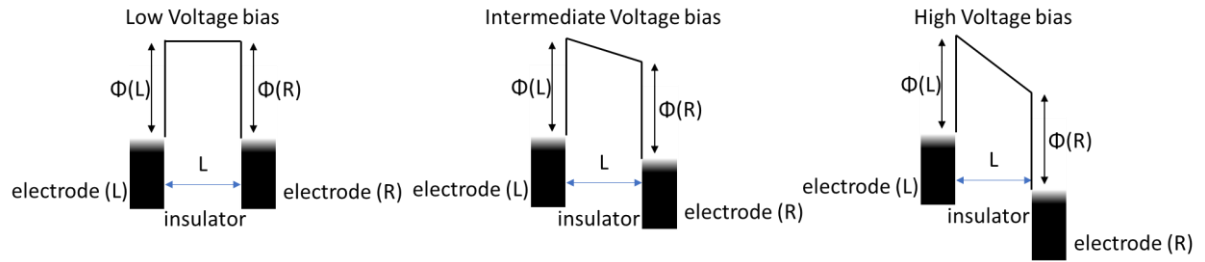


FIGURE 2.13 – tunnelling current accordingly to Simmon's Model at distinct voltage bias.

## 2.1.6 – Electron transport in molecular junctions

Molecular junctions are by definition in atomic scale. Therefore, the transport mechanism phenomenon must be described as a quantum one, and not approached as classical or semi-classical physics. Distinct models have been discussed since the 60's on how the electron can tunnel through atomic systems. Landuaer and Buttkir proposed a system in which the tunnelling could be viewed as a transmission problem<sup>71</sup>. The equation that describes the current for the equations development of Landauer model is described in several references.<sup>72, 73</sup> However, few remarks are important to be done about its resolution.

Due to the Laundauer formalism,<sup>74, 71</sup> the conductance  $G$  is understood as the transmission probability through the junction described as:

$$G = \frac{2e^2}{h} \sum_{n=1}^N T_n \quad (9)$$

The Laundauer expression adds the contribution of each possible conduction channel to the total current. In quantum mechanics viewpoint, this adds each specific current carrying eigenmodes,  $T_n$ , which is each individual transmission to the current. If  $T_1 = 1$ , it means that the specific mode has 1 quantum of conductance. Therefore, the conductance quantum is defined as:

$$G_0 = \frac{2e^2}{h} \sim 77,49 \mu S \quad (10)$$

When we approach a system in which we have two electrodes, the current through it under an electric potential can be described as:

$$I(V) = \frac{2e}{h} \int_{-\infty}^{\infty} dE T(E) [f_L(E) - f_R(E)], \quad (11)$$

This equation is the Landauer formula which correlates current and electron transmission. One of the Landauer formalism achievements is to be able to properly define the conductance quantum. When we have a perfect single channel conductor  $T=1$  between the two electrodes, the finite resistance is the quantum of conductance  $G_0$ , which is also known as Landauer Conductance. This is an important remark because not only the definition of the conductance quantum, but its contrast to the macroscopic definition of ideal conductor (resistance is null), shows that the Landauer approach is able to explain the conductance in nanoscale.

In the case of molecular devices, however, Landauer model is shown too simplistic to consider several further effects, such as: the hybridization of molecular orbital states with the electrodes and the interface dipole moment. Therefore, as Ratner commented, “many slightly flawed theoretical approaches” were done in the beginning of molecular electronics. We still lack complete understanding of these effects, making the modelling of such systems a great challenge.

Nowadays, there are more precise models for transport mechanisms based on Landauer formalism. In this scenario, it is necessary to define coherent and incoherent Tunnelling.

- Coherent tunnelling<sup>75 - 78</sup> - The electron neglects any scattering processes, behaving as a ballistic transport. In this, the molecule is considered a rectangular potential barrier with much higher energy than  $kT$  energy and, due to this, it is independent of the temperature of the system. Direct tunnelling usually occurs in single-molecule conductance measurements when the voltage is much smaller than the potential height. The resolved equation for a coherent tunnelling using Landauer Conductance notation is:

$$G_m = G_0 e^{-\beta l} \quad (12)$$

In which  $G_m$  is the conductance of the molecule,  $G_0$  is the quantum conductance,  $\beta$  is the decay constant in which the conductance exponentially decays with the distance,  $l$ .

- Incoherent tunnelling<sup>72,78</sup> it occurs when scattering effects must be taken in consideration. In this case, the most studied case is the hopping conduction mechanism, represented in Fig. 2.14, in which the electron can be found within the potential barrier well, because the electron transfer does not occur until a favourable situation is achieved, as its molecular conformation. Therefore, hopping mechanisms usually involve thermal motion on the barrier, causing the conductivity to be affected by temperature. It can be understood as the molecules or its environment's necessity to rearrange to allow the electron transfer to occur. The hopping mechanism has its current decaying linearly with the length of the molecule and has an exponential dependence of the temperature:

$$J \sim V e^{-\frac{\phi}{k_b T}} \quad (13)$$

Where  $\phi$  is the activation energy specific for the system,  $k_b$  is the Boltzmann constant and  $T$  is the temperature. The hopping mechanism usually occurs in long molecules with several low energy ( $E$ ) potential barriers ( $N$ ). This concept can allow us to determine a new factor called the transversal tunnelling time ( $\tau$ ).

$$\tau = \frac{N\hbar}{E} \quad (14)$$

The transversal tunnelling time can be defined as the time it takes for the molecule to bridge through the molecule, or in other words, the time it takes "inside the molecular junction". Direct tunnelling mechanisms have lower values than hopping mechanisms, indicating a direct, or faster, passage of the electron through the molecular junction.

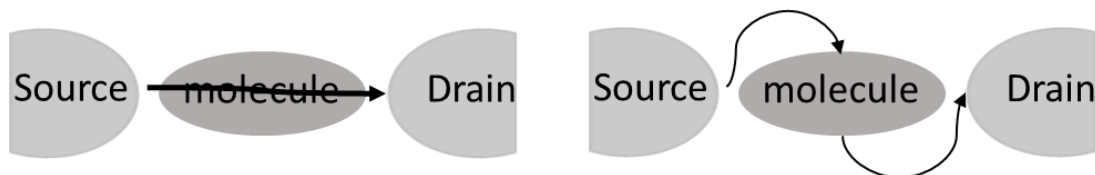


FIGURE 2.14 – Scheme for coherent tunnelling, without interacting with the molecule, and for incoherent tunnelling such as the hopping tunnelling mechanism, in which the electron interacts with the molecule.

While quantum mechanics is the most accurate way to describe the conductance through molecular wires, there are semi classic models which can also describe the electron transfer. In analogy to incoherent tunnelling mechanisms, Marcus<sup>79</sup> describes that, after an initial electron transfer, a relaxation of the system molecule-solvent is necessary prior to a second electronic exchange.<sup>80</sup> While Marcus theory applies to transfer which depend on thermally induced activations, such as vibrational energy, the electron transfer rate can depend on other parameters. On Marcus-Hush theory,<sup>81, 82</sup> it is valid the assumption that the processes are adiabatic, and the activation energy can be provided by a bias or potential applied. A described mathematical solution for such model can be found elsewhere.<sup>83</sup>

## 2.2 – Porphyrinoids

Porphyrinoids consist in a wide class of materials formed by a macrocycle of conjugated pyrroles.<sup>84</sup> Their presence in biological systems allows the existence of aerobic beings in Earth. In plants and bacteria, the green molecules present in chlorophylls are modified porphyrins with a metallic centre of magnesium,<sup>85</sup> which is responsible for the conversion of solar energy in chemical energy in photosynthesis. The oxygen transport in aerobic cells are complex enzymes which active site for oxygen binding are porphyrins with a ferric centre,<sup>86</sup> the haemoglobins. These molecules usually have strong colours and are responsible for vital processes for life and, for this reason, have been named “pigments of life”.<sup>87,88</sup>

### 2.2.1 – Porphyrins

The free base porphyrin, shown in Fig. 2.5(a), is a macrocycle with four pyrroles linked through methine bridges.<sup>89</sup> The porphyrinic macrocycle is highly symmetric with 26  $\pi$  conjugated electrons through the backbone of the molecule, obeying Hückel’s rule for aromaticity. This indicates that the molecule is planar, in the symmetry group  $D_{2h}$ , while in Free base, or  $D_{4h}$ , when metallated. However, many studies indicate that the aromatic pathway in the porphyrins have

only 18  $\pi$  conjugated electrons in the molecule, as in an annulene molecule, which the intern amines groups behaving as inert bridges. <sup>90-92</sup>

There are several ways to tune the properties of porphyrinoids through changes in their structure. These can be divided as core or peripheral.<sup>93</sup> The core functionalization consists in addition of ligands in the positions meso-pyrrolic and  $\beta$ -pyrrolic, Fig. 2.15(b). In this case, the functionalization will directly affect the energy and electronic density of the chromophore and, potentially, introduce distortions in the macrocycle due to steric effects. Therefore, the core functionalization has a direct impact on the optical and electronic properties of the molecule. <sup>94-96</sup> As example, the insertion of highly conjugated ligands tends to red shift the absorption spectra due to the lower electronic density in the macrocycle. <sup>97-99</sup> The insertion of ligands in meso-pyrrolic position also increases the stability of the porphyrins, behaving as a protector to avoid the formation of the meso-hydroxy porphyrins. <sup>100,101</sup> The artificial porphyrins with meso-pyrrolic modifications are historically known as second generation, while those with ligands in position  $\beta$ -pyrrolic are known as the third generation of porphyrins. Due to the higher stability, steric protection and electronic effects, the third generation often presents better catalytic activity properties. <sup>102-104</sup>

The peripheral functionalization consists in a functionalization in the groups meso or  $\beta$ -pyrrolic already in the macrocycle. For this reason, ligands are modified and the changes in the porphyrin ring are negligible, not affecting the optical and electronic properties as the core functionalization. <sup>105</sup> However, there are several properties that are highly impacted by this kind of approach, such as the solubility, potential gradient through the molecule, adsorption through functionalized groups, etc. <sup>106-109</sup> The intern structure of the porphyrin ring has 4 nitrogen atoms that can chelate a metallic ion, as shown in Fig. 2.15(c), with a maximum diameter of 3.7 Å. <sup>110</sup> The optical electronic and catalytic properties are strongly influenced by the presence of a metallic centre.



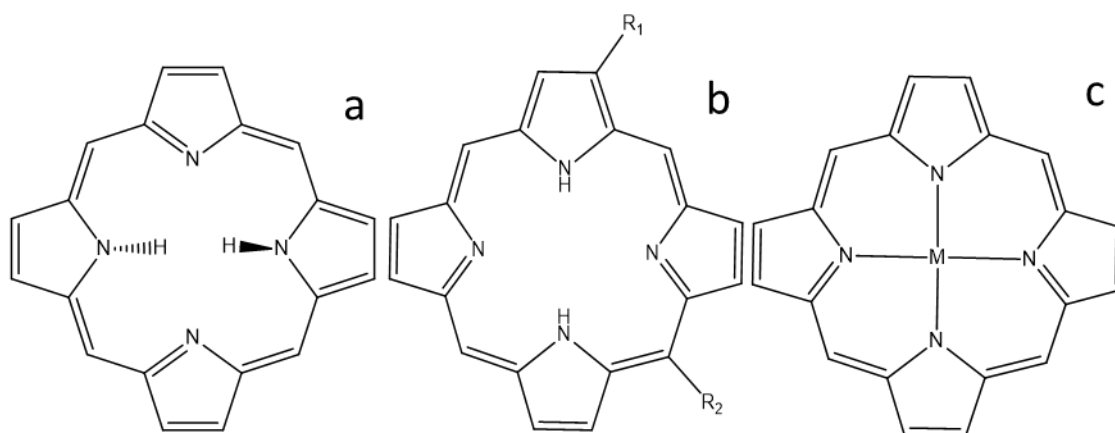


FIGURE 2.15 – Free base porphyrin representations: a) non-functionalized (elucidating its inner Hydrogens position), b)  $\beta$ -pyrrolic and meso-pyrrolic functionalization and c) with a metal centre.

Porphyrin molecules have an intense absorption in the visible spectrum, with molar absorption over  $10^5 \text{ L mol}^{-1} \text{ cm}^{-1}$ . The electronic spectra of porphyrinoids, represented in Fig. 2.16, usually presents a strong absorption between 400 nm and 600 nm, the Soret Band (also known as B band), and a small absorption at higher wavelength, the Q Band. The Soret band is a result from the electronic excitation from the fundamental singlet state to the second excited singlet state,  $S_0$  to  $S_2$ .<sup>107</sup> However, the internal conversion from  $S_2$  to  $S_1$  is a fast process therefore, the only radioactive process observed is from  $S_1$  to  $S_0$ . The Q band is related to the electronic transition between  $S_0$ - $S_1$ . The Q band of the porphyrins is split due to the transition of the fundamental state to two distinct vibrational levels of the excited state. The protons from the pyrrolic nitrogen's break the molecule's symmetry and create two new bands. For these reasons, the Q band is often observed as multiple absorption peaks. Both Soret and Q band are related to electronic transitions from  $\pi$  electrons to  $\pi^*$ .

A more accurate way to explain the metallated porphyrins spectra is through Gouterman four-orbital model,<sup>111</sup> Fig 2.16. While such model is based on the symmetry of the molecule, the symmetry labels become inappropriate for porphyrinoids with lower symmetry, in which case the orbitals are often referred to b1 and b2 (HOMO and HOMO-1) and c1 and c2 (LUMO and LUMO+1). According to this theory, the Soret band corresponds to the electronic transition from an electron from HOMO or HOMO-1 to the second excited orbital, LUMO+1. This usually is the absorption with highest intensity on porphyrins and, often, a

single broad band can be observed in its spectrum. Further absorptions at longer wavelengths correspond to the electronic transition from the HOMO or HOMO -1 to the LUMO. These are denominated Q bands and, while this should lead to two bands in its spectrum, usually several processes are observed due to the degeneration of the vibrational states of the molecule.<sup>112</sup> While all orbitals energies are affected by the presence of a metal centre, the Q band is also heavily influenced by the presence of  $\beta$  or meso-ligands in the pyrroles of the macrocycle, which can lead to different ratios between peaks I to IV.

To elucidate the effect of metal centres on the absorbance spectrum, Table 2.1 shows the absorption value of the Soret band and Q band for porphyrins with distinct chelated metals.<sup>113</sup> For the TPPS<sub>4</sub>, the chelation of Ni does not influence drastically the absorption neither of Soret nor q bands. However, when a Ni is added to the TPyEtAcP, the Soret band suffers a blue shift, towards higher energy, while the Q band has a red shift, to lower energy. This is an example that the chelation of a metal centre is not possible to be directly related to the metal nature, and its effect on the optical and electronic properties depends on all the electronic density and energetic levels of the molecule orbitals.

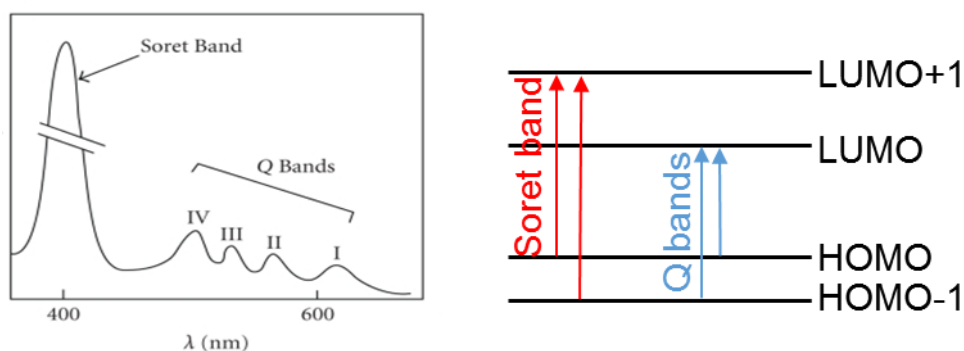


FIGURE 2.16 – free base porphyrin UV-Vis spectrum<sup>114</sup> and Gouterman model scheme.

TABLE 2.1 –MAXIMUM ABSORPTION OF SORET BAND AND Q BAND FOR DISTINCT MESO-TETRAPHENYL PORPHYRIN TETRASULFONATE (TPPS<sub>4</sub>), AND MESO-TETRAPYRIDYL ETHYLACETATE PORPHYRIN (TPYETACP) IN WATER. (10<sup>-5</sup> MOL L<sup>-1</sup>), ADAPTED FROM 113.

Porphyrin	Soret band (nm)	Q Band (nm)

TPPS <sub>4</sub>	413	515 552 579 633
TPPS <sub>4</sub> Ni	413	515 552
TPPS <sub>4</sub> Zn	421	556 595
TPyEtAcP	422	519 557 584 641
TPyEtAcPNi	418	532 562
TPyEtAcPZn	436	563 608

## 2.2.2 – Other relevant porphyrinoids

There are other important families of porphyrinoid, the chlorins, bacterochlorins and isobacterochlorins, which have the same pyrrolic macrocycle as the porphyrin but with distinct saturation. Fig 2.17<sup>115</sup> shows the distinct porphyrinoids in function of the saturation of the macrocycle. These porphyrinoids, however, have Möbius aromaticity and its structure is not planar as the porphyrin. Its properties can be shifted in the same way as regular porphyrins, with metalation and/or addition of ligands in meso or  $\beta$ -pyrrolic position.

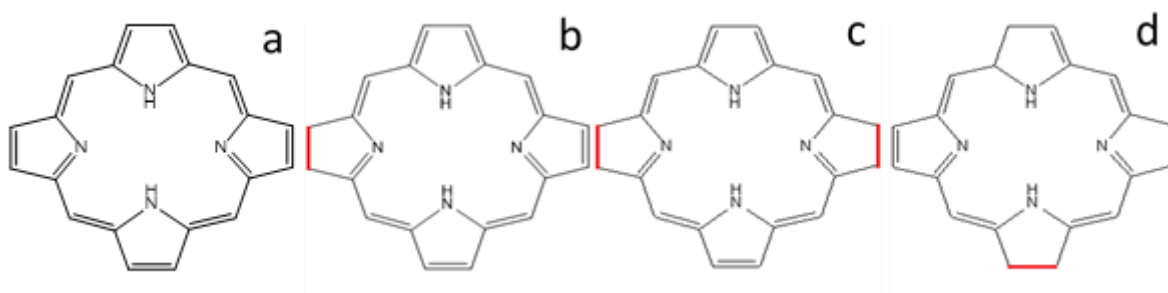


FIGURE 2.17 – Representation of the macrocycle for free base porphyrin (a), free base chlorin (b), free base bacterochlorin (c) and free base isobacterochlorin (d).

There are other porphyrinoids with similar structures to the porphyrin, but with some structural changes. The corroles, in Fig. 2.18 as example, have one of the links between the pyrroles contracted, in which a methinic group is eliminated. In this case several properties are distinct from the porphyrin. While corroles can also coordinate a metal centre, it can only achieve a tridentate chelate, in contrast to the porphyrins that have a tetradentate coordination. Since corroles have a contracted cycle, the space for metallic centres is smaller and, consequentially, its metallic complexes usually have a distortion in its structure.

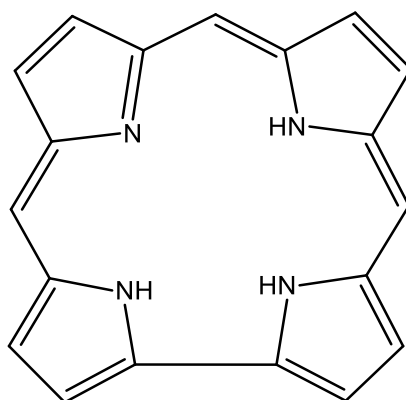


FIGURE 2.18 – Representation of a free base corrole.

A last porphyrinic group important to be mentioned is the phthalocyanines. As shown in Fig. 2.19, the methinics bounds between pyrrolic rings are substituted by amine bounds and  $\beta$ -pyrrolic positions are already functionalized. The phthalocyanines have a higher potential for technological application over porphyrins because those are often more stable chemically, and from a thermal and photochemical perspective. However, its higher stability has the downside of having lower solubility, restricting where it can be used. As other porphyrinoids, further structural changes can deeply affect its properties

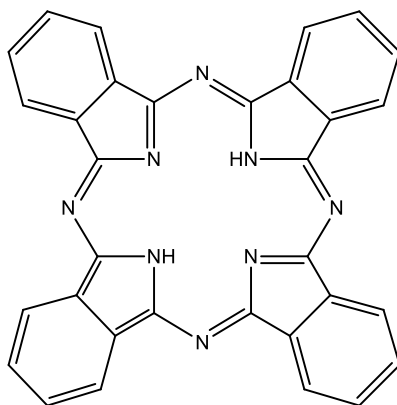


FIGURE 2.19 – Structure representation of the free base phthalocyanine.

Due to the optical, electronic and chemical properties, as well as the many biological functions these materials have in Nature, porphyrinoids have already been widely researched and applied in technological areas, such as: sensors,<sup>116 - 120</sup> catalysts,<sup>121 - 125</sup> photovoltaics,<sup>126 - 129</sup> photodynamic therapy drugs,<sup>130-134</sup> cancer,<sup>135,136</sup> etc. The series of porphyrinoids introduced so far have been widely studied since the 40's and have several reviews.<sup>137-149</sup>

### 2.2.3 – Expanded porphyrins

There is a series of porphyrinoids that is receiving increased attention in recent years: the expanded porphyrins. Sessler defined it as any macrocycle with pyrrole, furan, thiophenes or heterocycles in which the internal macrocycle has at least 17 atoms.<sup>150</sup> However, this definition is too broad and, for this project, the interest will be of those expanded porphyrins that follow Nonn definition: any macrocycle made out of  $n$  pyrrolic rings linked together by methine groups, in which  $n$  is bigger than 4.<sup>151</sup> Through this definition, this group consists of the pentaphyrins, also known as sapphyrins,<sup>152</sup> hexaphyrins, heptaphyrins, octaphyrins, nonaphyrins and homologs with higher number of pyrrolic rings. These molecules have properties analogous to the porphyrins, however, its higher conjugated chain is more flexible. This not only increases its solubility, but also improves its optical properties with a higher molar absorption,<sup>153</sup> photons absorption,<sup>154, 155</sup> and fluorescence on the near-infrared.<sup>156</sup> The expanded macrocycle also has an ordered sequence of amine and imine groups, which allow several electronic states, metallic coordination and hydrogen bond interactions.<sup>157</sup> Distinctly from porphyrins, the conformation of the

expanded porphyrins is not necessarily planar, and is highly dependent of its aromaticity or anti-aromaticity properties. The molecules usually adopt a planar structure when it has a Hückel aromaticity ( $4n+2 \pi$  electrons) or a torsioned structure when in Möbius aromaticity ( $4n \pi$  electrons).<sup>158</sup>

## 2.2.4 – Hexaphyrins

Among the expanded porphyrins of interest, the focus of research often is the hexaphyrin. Its conformation depends of its oxidation state and of its mesopyrrolic ligands.<sup>159</sup> As shown in Fig. 2.20, the hexaphyrin often has two oxidation states which are interconvertible. In case of the mono Pd-Hxp, the reduced state has  $28 \pi$  electrons, in the Nonn nomenclature: the mono Pd [28] Hxp. Its structure is torsioned and has Möbius aromaticity and an intense blue colour. The oxidated state has  $26 \pi$  electrons, the mono Pd[26]Hxp in the Nonn nomenclature, with Hückel aromaticity and an intense violet colour.

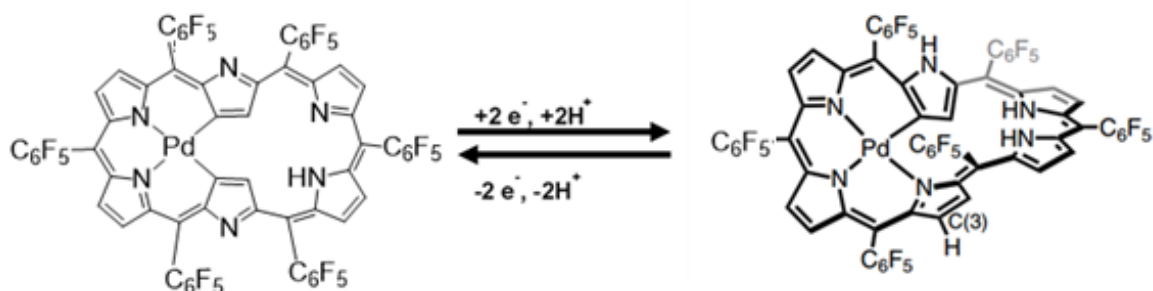


FIGURE 2.20 – Representation of the oxidation states of the mono Pd Hxp and how its structure is affected.

In contrast to porphyrins, the planarity of the [26] Hexaphyrin is highly dependent on its meso-pyrrolic ligands. There are two major structures: rectangular and Dumbbell, also known as Hückel structures and shown in Fig. 21.<sup>160,161</sup> The first has its ligands meso-pyrrolic turned to external side of the macrocycle, adopting a planar structure. The Dumbbell structure, however, has its meso-pyrrolic ligands towards the inner side of the molecule, decreasing its planarity due to the steric interaction. The expanded porphyrins can have its properties changed by core functionalization and/or peripheral one, similar to the

porphyrins. However, due to the impact they can bring to the planarity of the structure, it often has a higher impact on its properties

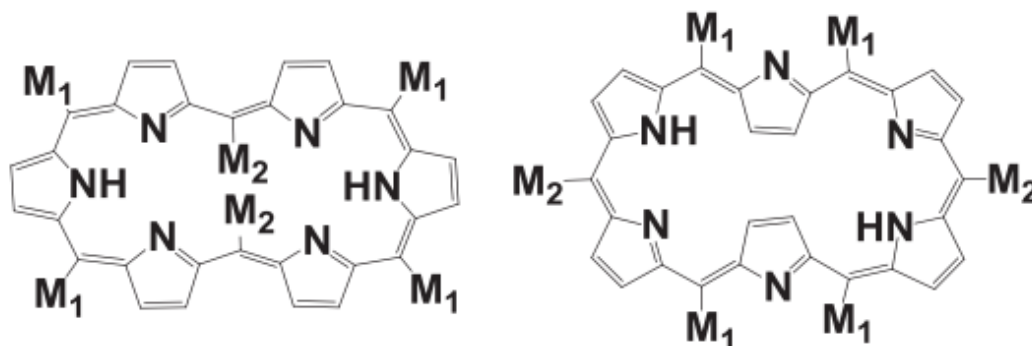


FIGURE 2.21 – Dumbbell and rectangular structures for the [26] Hxp.

To date, most hexaphyrin studies cover its synthesis and the impact of the aromaticity in its optical properties. Distinct materials have been reported with bimetallic centres or heterometallic centres, such as Rh, Cu, Au, Ag, Cu, Zn, Cd, Pd, etc.<sup>162-167</sup> Several synthesis approach have been reported with distinct meso-pyrrolic ligands.<sup>168-170</sup> However, the majority of these studies are done by two groups: Prof. Dr. Sessler, in the United States of America, and Prof. Dr. Osuka, in Japan. Both groups focus mostly on its optical properties<sup>171</sup> and theoretical studies<sup>172-176</sup>, whereas their other characterizations are mostly ignored. For technological applications, these uninvestigated properties are required. To this day, few reports have been done in this sense, such as lanthanide sensors<sup>177</sup> and use of hexaphyrins as photovoltaic dyes, showing an increase in efficiency of 100%.<sup>178</sup>





### **3 – Objectives**

The objective of this thesis is to synthesize distinct bimetallic hexaphyrins, provide some insight on how the metallic centre affects its electron transport properties and try to correlate distinct characterization methods. Originally, such molecules were designed to have thiol terminations, which were not successful. Therefore, we report the synthesis of the achieved molecules and its properties.

The materials were characterized by electrochemistry, spectroscopy and molecular break junction's conductance. The properties of this series of characterizations were cross analysed to see if the information from one can give any insight into the others.



## 4 – Hexaphyrins synthesis and spectroscopic characterization

*The aim of this chapter is to elucidate the synthesis method and the characterization of the materials prepared. Since the thiol modifications couldn't be achieved, this chapter has as objective to describe the synthetic route, reproduced from the literature, and its NMR and spectroscopic characterization as tools to validate the materials obtained.*

### 4.1 – Synthesis methodology

#### 4.1.1 – Reactives

All reactives used in this work were of analytical purity. Pentafluorobenzaldehyde, pyrrol, boron trifluoride ethyl etherate (BF<sub>3</sub>.OT<sub>2</sub>), tris(dibenzylideneacetone)dipalladium(0) (Pd<sub>2</sub>(dba)<sub>3</sub>), tris(4-bomophenyl)aminiumhexafluorantimonate (TBAH), palladium trifluoroacetate (Pd<sub>2</sub>(OCOCF<sub>3</sub>)<sub>2</sub>), copper(I) acetate (Cu(OAc)<sub>2</sub>), silver triflate (AgOTF), and 2,3-dichloro-5,6-dicyano-p-benzoquinone (DDQ) were purchased from Sigma-Aldrich.

With the objective of drying the solvent utilized, all solvents were distilled before used. For the electrochemical measurements, the solvents were distilled and stored in molecular sieve 0.3 nm. Acetonitrile (ACN), methanol(MetOH), dichloromethane (DCM) and dichloroethane (DCE) for high efficiency liquid chromatography (HPLC), were obtained from Merck.

#### 4.1.1 – Free base [26] hexaphyrin synthesis

The synthesis of the hexaphyrins was done as previously reported by Osuka et al<sup>179</sup> and is represented in Fig. 4.1. In a round bottom flask of 100 mL were added: dry DCM (60mL), 1mmol of pyrrol (194 µL, 1mmol), 1 mmol of pentafluorobenzaldehyde (496 µL, 1mmol) and the catalyst BF<sub>3</sub>.OT<sub>2</sub> (100 µL, 0.7 mmol). This system was constantly purged with Ar to create an anaerobic atmosphere. Upon addition of the catalyst, the solution changes from uncoloured to yellow. This system was stirred for a period of 2 hours to allow the formation

of complexes between pyrrols and belzaldeides, which changes the colour from yellow to pink. After the two hours period, the oxidant agent DDQ (2.27g, 10mmol) was added, leading to the synthesis of several different pyrrolic macrocycles.

For the purification of the products, a chromatographic column with common silica was prepared. Due to the high price of this synthesis process, the separation and purification of the sub products, the tetraphenyl porphyrin (TPP) among them, is also desirable. Therefore, the first eluent used is hexane: ethyl acetate, with volume ratio from 9.75 : 0.25 to 9 : 1, with the objective to completely separate the TPP from the other molecules. The TPP fraction was recrystallized in hexane, and was filtered and separated for its use in distinct projects. The fraction with the desired material, Hxp, has a high quantity of expanded porphyrins with 5, 7, 8 and 9 pyrrol groups in its macrocycle, as well as the Hxp in the reduced state, [28]Hxp, which is not of interest of this project but can be oxidized with DDQ and purified as [26]Hxp . Therefore, this second fraction needs a second chromatographic column, with hexane: DCM ratio of 4:2, to purify the material of interest.

The [26] hexaphyrin quantity obtained for each synthesis is around 55 mg (0.038mmol), with a yield as low as 15% for 4 consecutive days on the synthesis process. Due to the high quantity necessary to prepare the metallated molecules, several trials were done to scale up the process. However, despite all efforts, upon increasing the amount of precursor decreases in the reaction yield. Due to the high value for the reactive, it was decided to prepare multiple batches in same condition. For record, upon using this approach the number of chromatographic columns also increases proportionally, otherwise the silica gets easily saturated and cannot be used to purify the products properly.

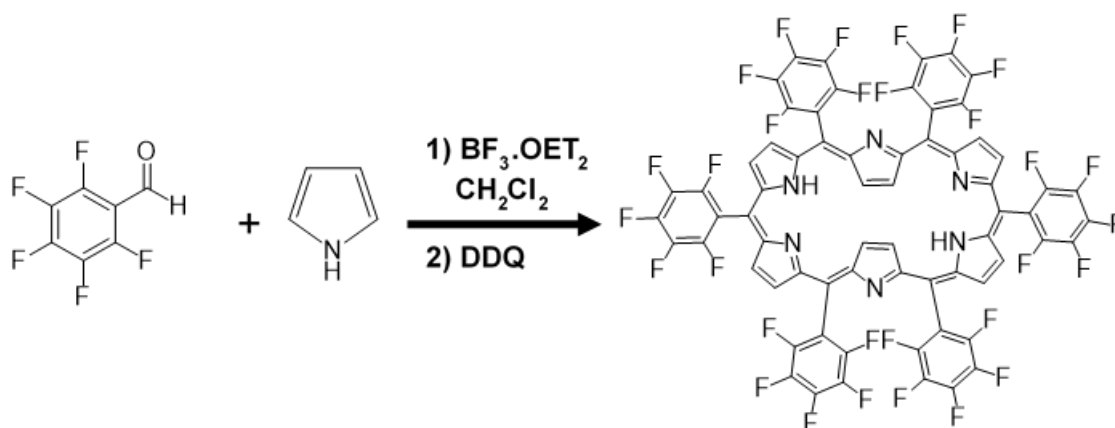


FIGURE 4.1 – Reaction scheme for the synthesis of free base [26]Hxp.

#### 4.1.2 – mono Pd – [28]Hexaphyrin synthesis

The synthesis reaction of the mono Pd- [28]Hxp was previously reported by Osuka et al<sup>180</sup> and its synthesis scheme is represented in Fig. 4.2. In a round bottom flask the following components were added: dry DCM (8.0 mL), MeOH (0.8mL), [26]Hxp (19.7 mg, 0.0135 mmol), NaOAc (10.1 mg, 0.135 mmol) and  $\text{Pd}_2(\text{dba})_3$  (60 mg, 0.675 mmol). The NaOAc is used to deprotonate the [26]Hxp and allow the reaction with the  $\text{Pd}_2(\text{dba})_3$ . The system was stirred for three hours under room temperature.

After the reaction period, the solution was filtered in celite with DCM as eluent, with the objective of complete removal of excess Pd reagent. The DCM solution was then dried under vacuum.

For purification of the product, a single chromatographic column is necessary with silica gel and dichloroethane: n-hexane in ratio 6.4 as eluent. The main product of this reaction is the desired mono Pd- [28]Hxp with an approximate yield of 70% (14.84 mg) per synthesis over 3 days .

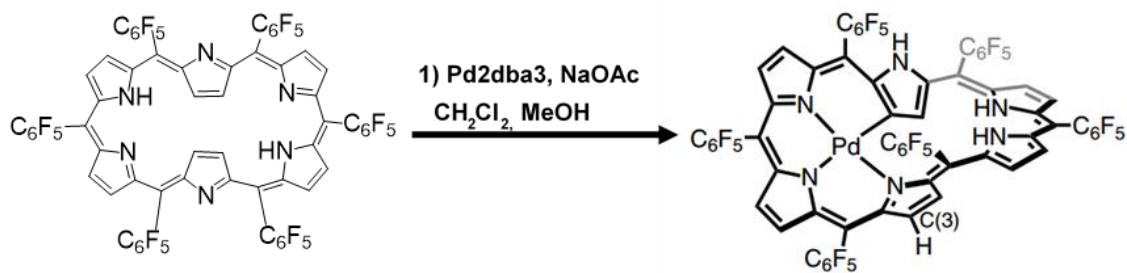


FIGURE 4.2 - Reaction scheme for the synthesis mono Pd [28] hexaphyrin, adapted from reference 180

#### 4.1.3 – mono Pd – [26] Hexaphyrin synthesis

The synthesis of the mono Pd-[26] Hxp was previously reported by Osuka et al <sup>181</sup> and its reaction scheme is represented in Fig. 4.3. In a 100mL round bottom flask the following components were added: ACN (50.0 mL), mono Pd – [28] Hxp (15.7 mg, 0.0101 mmol) and TBAH (179 mg, 0.25 mmol). The reaction was stirred for 30 minutes over an ice bath for temperature control. During the whole reaction time, TLC was used to check on the reaction progress, in which the eluent was a mixture of DCM:hexane at 6:4 volume ratio.

After the reaction period, the solution was washed with Milli-Q, for removal of the excess of TBAH, and the product was extracted with DCM and MeOH. The addition of MeOH is necessary because an emulsion is formed during the extraction. The fraction in DCM, rich in the desired molecule, was dried in anhydrous NaSO<sub>4</sub>, filtered and evaporated.

For the purification of the mono Pd-[26] Hxp a chromatographic column was used with silica gel and a mixture of DCM:hexane of 7:3 in volume as eluent. In this step, the unreacted mono Pd[28] Hxp can be separated from the mono Pd-[26] Hxp and from secondary products from the over oxidation of the molecule.

The average yield of this synthesis is around 80% (13.54 mg) over 1-2 days.

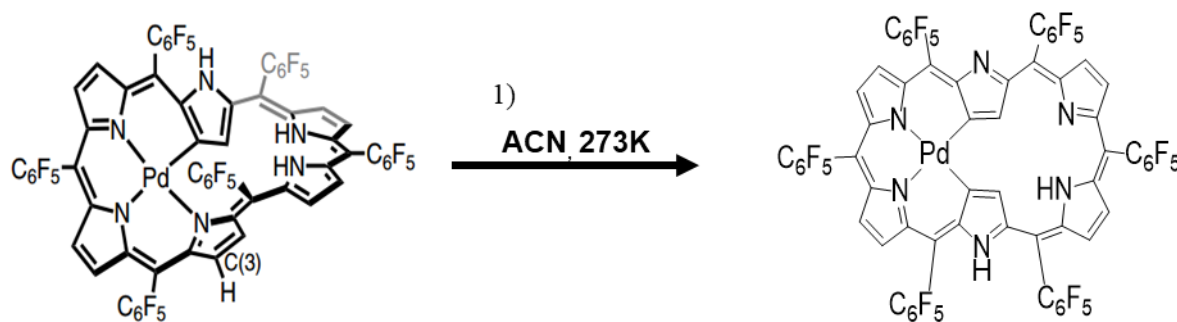


FIGURE 4.3 - Reaction scheme for the synthesis mono Pd [26] hexaphyrin, adapted from reference 180

#### 4.1.4 – Pd-Pd – [26] Hexaphyrin synthesis

Fig. 4.4 shows the reaction scheme for the synthesis of bis Pd Hxp, previously reported by Osuka et al.<sup>181</sup> In a 50 mL round bottom flask the following components were added: dry THF (30 mL), mono Pd [26] Hxp (62.6 mg, 0.040 mmol) and Pd<sub>2</sub>(OCOCF<sub>3</sub>)<sub>2</sub> (16.5 mg, 0.05 mmol). The solution was stirred for 2 hours in an ice bath for temperature control at 0°C while checking the reaction rate with TLC.

After the end of the reaction, the solution was filtered through a celite column to remove the excess of Pd<sub>2</sub>(OCOCF<sub>3</sub>)<sub>2</sub>, while washing with DCM. The solvent was then evaporated under vacuum and a chromatographic column with regular silica was used to purify the Pd-Pd [26] Hxp, using a mixture of DCM : hexane of 6:4.

The average yield of the reaction is 43% (27mg) over 2 consecutive days.



FIGURE 4.4 - Reaction scheme for the synthesis of Pd-Pd [26] hexaphyrin, adapted from reference 176.

### 4.1.5 – Pd-Ag – [26] Hexaphyrin synthesis

The synthesis of the Pd-Ag hexaphyrin was previously reported by Osuka et al<sup>182</sup>, and its reaction scheme is represented in Fig. 4.6. In a round bottom flasks of 100 mL the following components were added: ACN (73.3 mL), mono Pd [26] Hxp (31.3 mg, 20 mmol), AgOTF (51.4 mg, 20mmol) and NaOAc (16.4 mg, 135 mmol). The reaction was stirred for 40 hours while checking the reaction progress with TCL, while using DCM:hexane in 1:1 ratio.

Upon the end of the reaction, the mixture was washed with Milli-Q water and extracted with DCM and MeOH. MeOH was used, as explained in the previous procedures, to decrease the emulsion and allow it to be separated. The aqueous fraction was disposed with the NaOAc and excess of AgOTF. The organic fraction was then dried with NaSO<sub>4</sub> and then evaporated. To separate the reagents from the product a chromatographic column with silica gel was used with a mixture of DCM:hexane at ratio 7:3 as eluent.

This procedure has an average yield of 70% (23.4 mg) over 4 days.

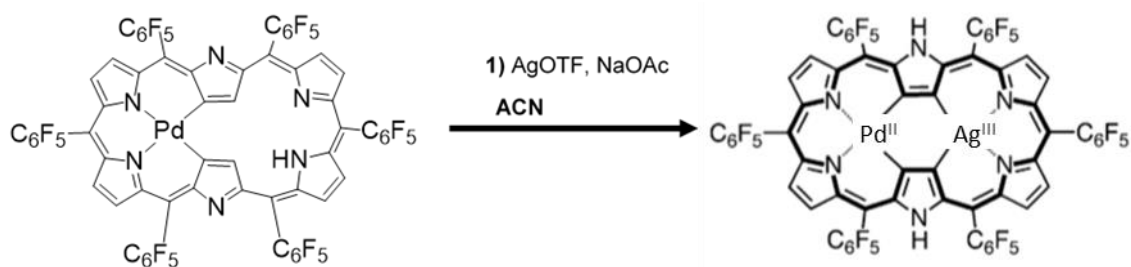


FIGURE 4.5 - Reaction scheme for the synthesis of Pd-Ag [26] hexaphyrin.

It is important to notice that, while this molecule has been previously reported, Ag<sup>III</sup> is not easily achieved and the compounds resulted are usually not stable. Regardless, we trusted the previously reported data and studied its compounds assuming the reports accurate.



#### 4.1.6 – Pd-Cu – [26] Hexaphyrin synthesis

The Pd-Cu [26] Hxp synthesis route was previously reported by Osuka et al<sup>182</sup> and its reaction scheme is shown in Fig. 4.6. In a round bottom flask of 25 mL the following components were added: dry DCM (5.0 mL), MeOH (0.8 mL), mono Pd [26] Hxp (10.1 mg, 0.135 mmol), NaOAc (36.3 mg, 0.02 mmol) and Cu(OAc)<sub>2</sub> (36.3 mg, 0.02 mmol). The MeOH is necessary for the reaction to improve the acetates solubility, which are insoluble in DCM. The NaOAc is used to deprotonate the Hxp macrocycle and allow the electrophilic attack of the Cu(OAc)<sub>2</sub>. The system was stirred for a period of 6 hours while being checked through TLC with a DCM : hexane mixture at 6:4 volume ratio.

After the reaction period, the solution was washed with Milli-Q water and extracted with DCM and a fraction of MeOH. The acetates are insoluble in DCM so can be easily removed in water. The MeOH is necessary, once more, to avoid the emulsion and allow a proper extraction of the system. The organic fraction is then dried with NaSO<sub>4</sub> and the solvent is evaporated.

A chromatographic column with silica gel is used with DCM : hexane in a mixture of 6 : 4 in volume to separate the product from the unreacted mono Pd [26] Hxp and sub products. The average yield of this reaction is 55% (18.0mg), over 2 days process.

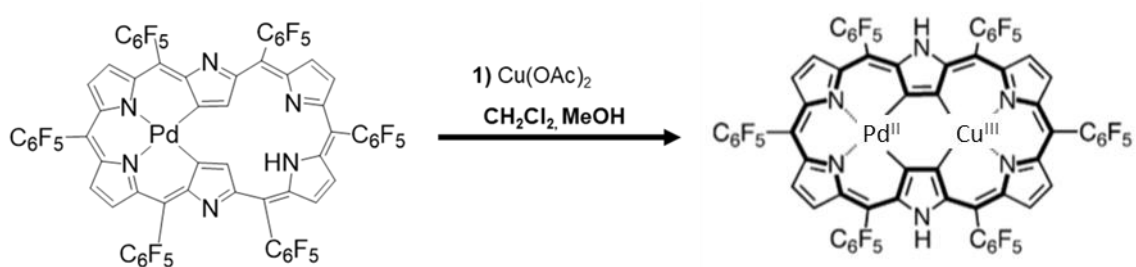


FIGURE 4.6 - Reaction scheme for the synthesis of Pd-Cu [26] hexaphyrin.

As with Ag<sup>III</sup>, Cu<sup>III</sup> compounds are not easily achieved and they are often unstable. These molecules were previously reported and it was studied assuming the reports accurate.

## 4.2 – Nuclear Magnetic Resonance characterization

### 4.2.1 – Methods

The compounds were dried over vacuum for 6 hours before analysis. Deuterated chloroform ( $\text{CDCl}_3$ ) was used to solubilize the prepared molecules over  $^1\text{H}$ -NMR.

The NMR spectrum was measured with the only finality to compare it with reported spectra. Even though a thorough analysis would require also the  $\text{C}^{13}$ -NMR spectrum, the  $^1\text{H}$ -NMR is enough to validate the synthesized material.

### 4.2.2 – Results

#### 4.3.2.1 – Free base [26] hexaphyrin

The NMR was obtained to confirm the synthesis of the material. Fig. 4.7 shows the free base [26] Hxp, with its hydrogens numbered, and its NMR spectrum. The doublet at  $\delta$  -2.43 correspond to the  $\beta$ -pyrrolic protons from the confused pyrroles in the Hxp structure (H1 and H4). The doublets at  $\delta$  9.11 and 9.44 are the remaining pyrrolic hydrogens (H5 to H12). It was expected to observe a singlet at  $\delta$  -1.98, which are the NH hydrogens. However, due to the acidity of these protons and to the deuterated solvent, it is likely that these resonance values are not observed because of its lability with deuterium.<sup>182</sup> Due to the low signal intensity of the Hxp, several others hinder its analysis, such as contaminants and solvents, even though the sample has high purity.

#### 4.3.2.2 – mono Pd-[26] hexaphyrin

The NMR spectrum for the mPd Hxp has not archived. While the molecule was characterized by NMR, in this thesis only its spectroscopic measurements spectroscopic are reported. .

#### 4.3.2.3 – Pd-Pd [26] hexaphyrin

Fig. 4.8 shows the  $^1\text{H-NMR}$  spectrum of the Pd-Pd Hxp. In The singlet at  $\delta$  11.76 correlate to both NH hydrogens on the outside of the macrocycle. The doublets at  $\delta$  9.09,  $\delta$  9.00 and  $\delta$  6.85 are related to the  $\beta$ -pyrrolic hydrogens. Even though we observe a large amount of noise due to the presence of solvents, it is possible to confirm the peaks of the material.<sup>110</sup>

#### 4.3.2.4 – Pd-Ag [26] Hexaphyrin

Fig. 4.9 shows the  $^1\text{H-NMR}$  of the Pd-AgHxp. The singlet at  $\delta$  12.12 correlates to the single NH hydrogen in the molecule. The doublets at  $\delta$  9.62,  $\delta$  9.48,  $\delta$  9.29,  $\delta$  9.27,  $\delta$  9.26 and  $\delta$  9.24, as the multiplet at  $\delta$  9.48, are correlated to all 8  $\beta$ -pyrrolic hydrogens. Therefore, this confirms the molecule we synthesized with that of the literature.

#### 4.3.2.5 – Pd-Cu [26] hexaphyrin

The  $^1\text{H-NMR}$  spectrum of Pd-Cu Hxp is shown in Fig. 4.10 The singlet at  $\delta$  11.15 correlates to the NH hydrogen in the outside of the molecule. The doublets at  $\delta$  9.3 -  $\delta$  8.77 are the signal of the 8  $\beta$ -pyrrolic hydrogens. Even though we have an intense solvent signal, it is possible to confirm the molecule with the spectrum previously reported.



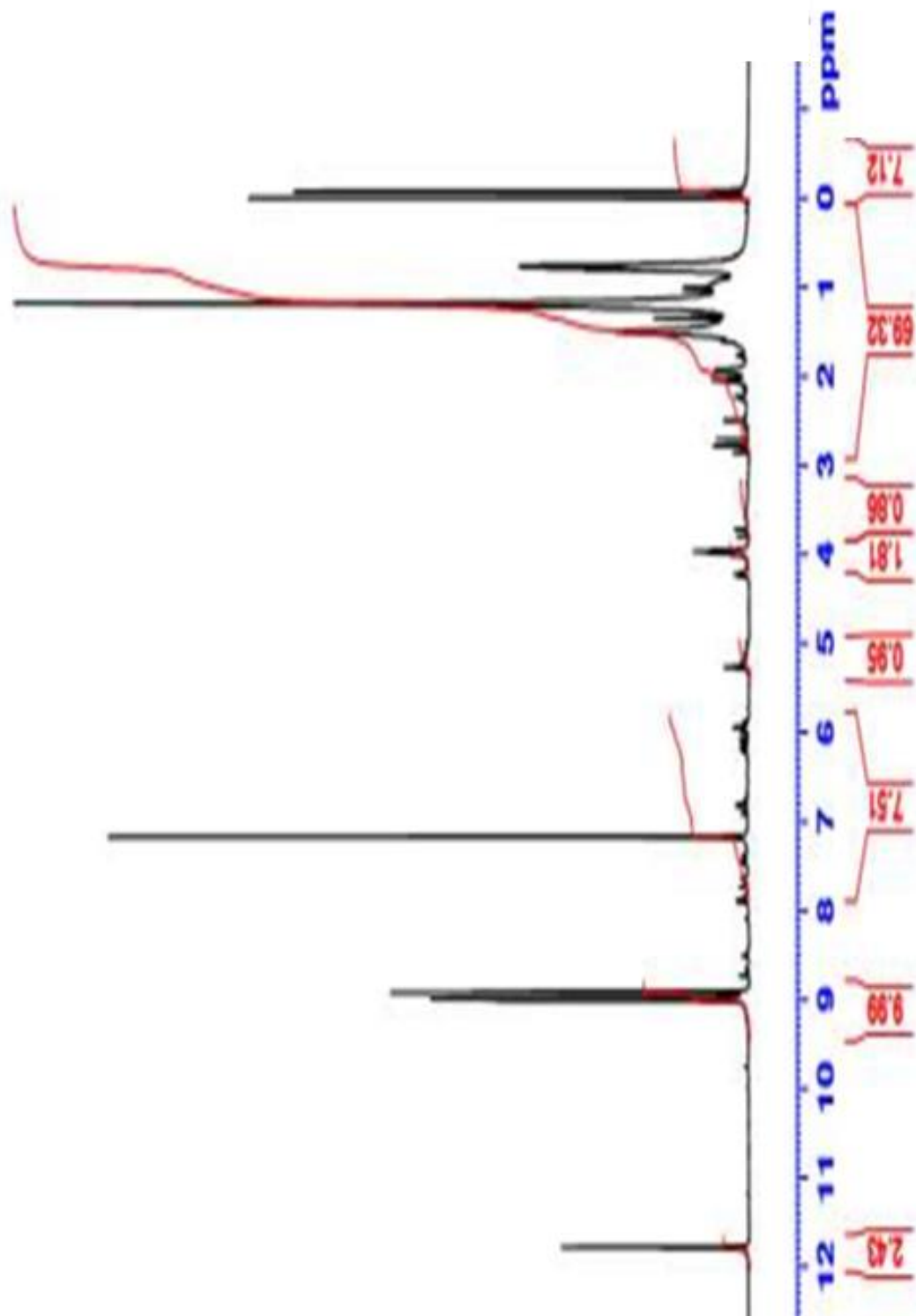


FIGURE 4.8–  $^1\text{H}$  - NMR spectrum of Pd-Pd [26] hexaphyrin.

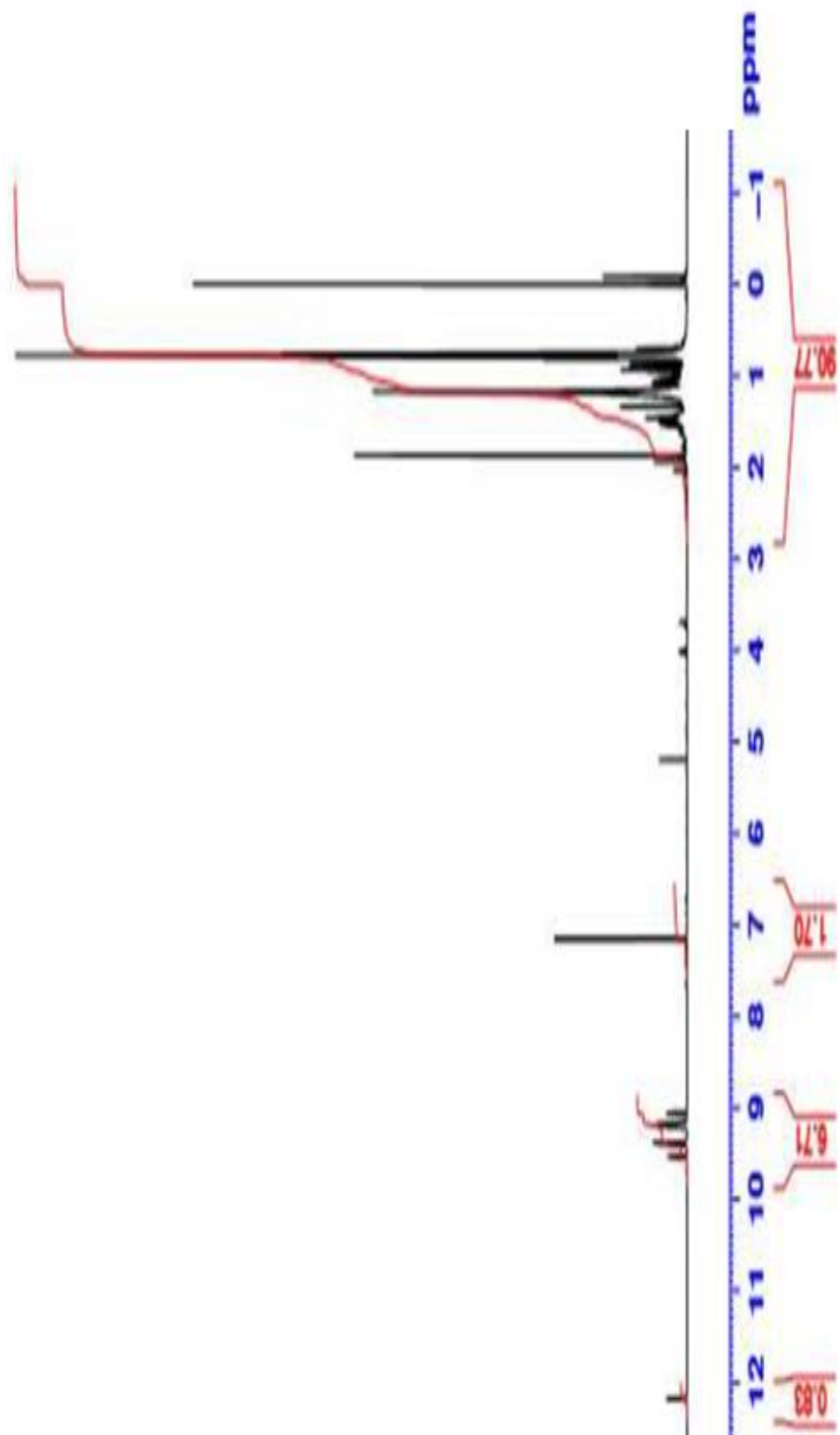


FIGURE 4.9 –  $^1\text{H}$  - NMR spectrum of Pd-Ag [26] hexaphyrin

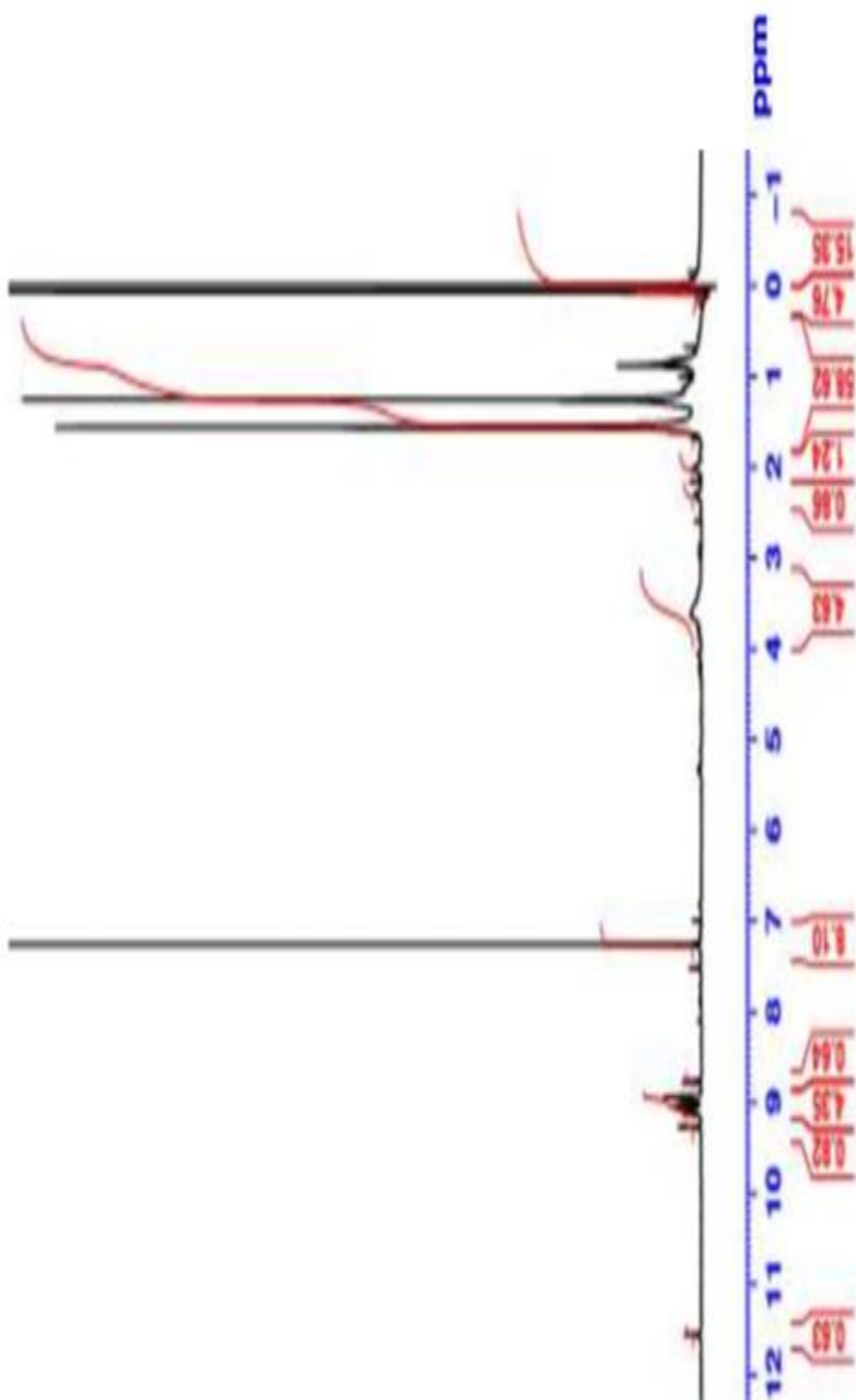


FIGURE 4.10 –  $^1\text{H}$  - NMR spectrum of Pd-Cu [26] hexaphyrin

## 4.3 – Spectroscopic characterization

### 4.3.1 – Methods

The molecules synthesized in 4.1. were characterized by UV-Vis absorption on a Cary 5g UV-Vis-NIR spectrometer and by emission spectroscopy fluorescence (fluorimetry) with an excitation laser of 560 nm. Due to the high specific absorption of these materials, the compounds were diluted to low concentrations in DCM.

As explained in chapter 2.2, spectroscopic methods are usually used to characterize these materials due to the specific optic properties in function of its metal centre and meso or  $\beta$  pyrrolic ligands.

### 4.3.2 – Results

An approach to understand them is to correlate the hexaphyrins properties with those of porphyrins, simpler molecules that have been widely studied. For most porphyrinoids, a four orbital model describes its several distinct electronic transitions, as discussed in Chapter 2.2.1.

The FB [26] Hxp shows a broad Soret band with a peak at 567 nm and Q-bands with absorptions at 711 nm and 767 nm and 1050nm, as shown in Figure 4.11(a). These show a red shift in the absorptions in comparison to the free base porphyrin, which is an expected result due to the longer conjugated macrocycle. There is a shoulder in the Soret absorption at 591 nm that is related to a distinct absorption cross section.<sup>183</sup> Due to the nature of electronic transitions in porphyrinoids, the absorbance spectrum is not a good approach to determine its band gap. For this reason, fluorescence measurements were performed. Fig 4.12.(b) shows the emission spectrum of the FB [26] Hxp, which shows an intense emission at 1056 nm and lower intensity emissions up to 1240 nm. The intensity on 1056 nm corresponds to the transition between states S1 to S0, while the longer wavelengths emission is related to weaker vibronic transitions of the molecule.<sup>184</sup> Therefore, the spectroscopic band gap of the molecule can be determined as 1.174 eV. For the free base hexaphyrin, both the absorption and emission spectra show the HOMO-LUMO transition.



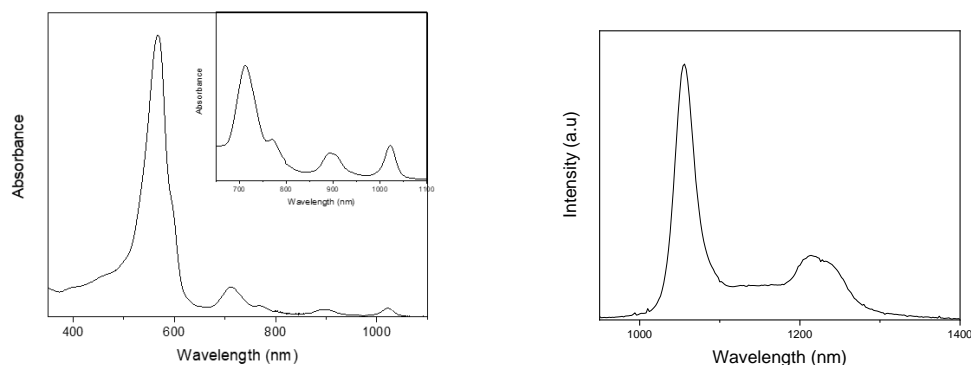


FIGURE 4.11 – Absorption (left) and emission (right) spectra of Free base [26] Hexaphyrin.  $\lambda_{\text{ex}} = 560 \text{ nm}$ .

When a Pd atom is chelated into the macrocycle centre, the mono Pd hexaphyrin on Fig. 4.12, the Soret band absorption is broadened with a peak at 557 nm and a Q band at longer wavelengths, 719 nm and 940 nm. This shows that a single metal centre affects the orbital energies, blue shifting the Soret band while red shifting the Q bands. There are two possibilities for the bands broadening: the stacking of the hexaphyrins through  $\pi$ - $\pi$  interactions or degeneration the orbitals of the macrocycle, broadening the absorption band. The addition of the metallic centre also affects its emission spectra, quenching it to a level that it barely detected in the noise, Fig. 4.12. Upon a smoothing of the plot, it is possible to approximate the maximum emission at 1108 nm, indicating that the band gap of the molecule is around 1.12 eV.

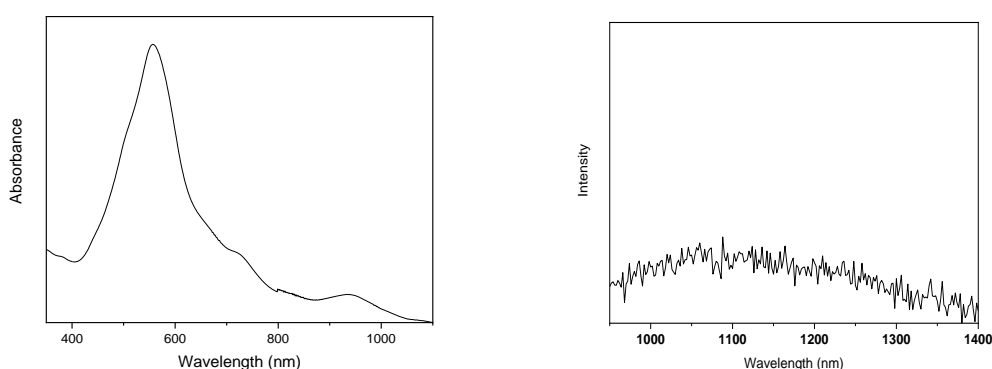


FIGURE 4.12 – Absorption (left) and emission (right) spectra of mono Pd [26] Hexaphyrin.  $\lambda_{\text{ex}} = 560 \text{ nm}$ .

Upon chelation of a second metal atom, distinct behaviours were observed for Cu, Ag and Pd. The Pd-Pd Hxp, Fig. 4.13, has three narrow absorption bands in the Soret region at 493 nm, 579 nm and 629 nm, followed by low intensity processes at Q band region of 889 nm and 1013 nm. In the literature a splitting on the Soret band in several peaks have been previously denominated Soret-like, or B-like, bands. This phenomenon occurs due to the absorption to multiple excited states and/or for distinct absorption values across distinct orthogonal cross sections of the molecule. The emission spectrum of the Pd-Pd Hxp, shown in Fig. 4.13, shows a weak emission with a maximum at 1060 nm, 1.17eV. While the energy is similar to that of the Free Base Hxp, the emission was quenched with the addition of metallic centres.

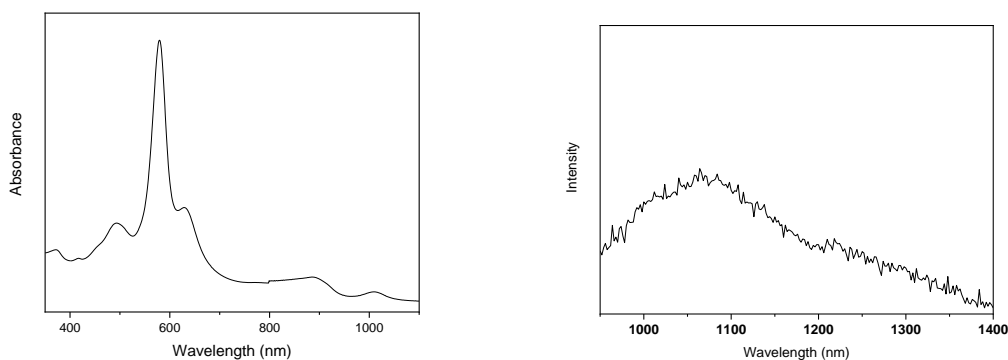


FIGURE 4.13 – Absorption (left) and emission (right) spectra of Pd-Pd [26] Hexaphyrin.  $\lambda_{ex} = 560$  nm.

Similarly, to what happens to the Pd-Pd Hxp, the Pd-Ag Hxp has a Soret-like band with 4 absorption peaks: 525 nm, 583 nm, 698 nm and 751 nm, and Q bands at 867 nm and 1162 nm, as shown in Fig 4.14. The emission spectrum of the molecule is severely quenched in relation to the free base Hxp, but two peaks can be observed at 1035 nm and 1221 nm. It is likely that the first process corresponds to the transition S1 to S0 and the second to vibronic transitions. Therefore, the spectroscopic band gap of the molecule is 1.20 eV.

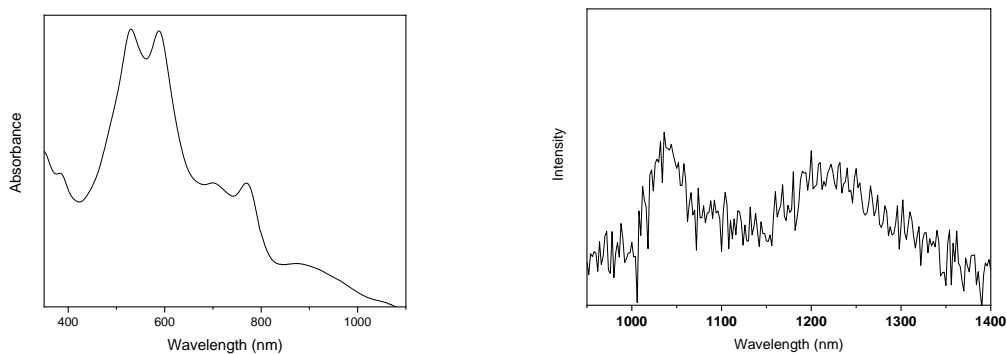


FIGURE 4.14 - Absorption (left) and emission (right) spectra of Pd-Ag [26]  
Hexaphyrin.  $\lambda_{\text{ex}} = 560 \text{ nm}$ .

Lastly, the Pd-Cu Hxp has an absorption spectrum similar to the Pd-Ag hexaphyrin, with a slight shift Soret-like band, with absorptions at 382nm, 530nm and 587 nm, with its Q-like bands at 706 nm, 770 nm and 879 nm, as shown in Fig. 4.15. The emission spectrum of this molecule was recorded but due to the quenching caused by the metal centres it was not possible to separate any possible emission out of the noise of the measurement, as shown in Fig. 4.15.

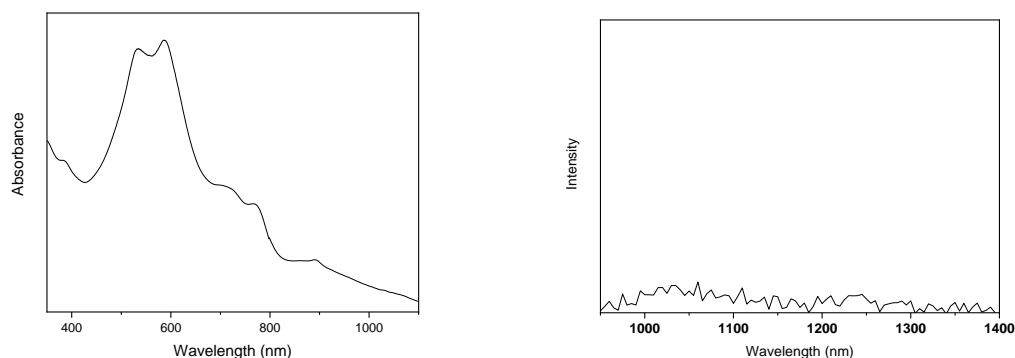


FIGURE 4.15 – Absorption (left) and emission (right) spectra of Pd-Cu [26]  
Hexaphyrin.  $\lambda_{\text{ex}} = 560 \text{ nm}$ .

Table 4.1. summarizes the data of the spectroscopic characterization. The chelating of a metal centre affects the behaviour of the absorption spectra of these molecules, which is due to the shifting and/or creation of new molecular energy levels. Overall, the addition of the metals leads to a blue

shift in the Soret or Soret-like band and a red shift on the Q-band. Additional processes are observed on the molecules Pd-Pd Hxp and Pd-Ag Hxp, which could be due to new energy levels created by the metallic centre and/or distinct absorption values in distinct cross sections. The chelation also affects the emission spectra. The first behaviour that we can observe is the quenching of the emission signal for these molecules, which is similar to other previously reported hexaphyrins.<sup>185</sup> The values of emission for distinct molecules can be related to its band-gap.

TABLE 4. 1. – WAVELENGTH AND ENERGY ABSORPTION FOR THE ABSORPTION AND EMISSION SPECTRA OF THE HEXAPHYRINS. (VALUES MARKED WITH \* WERE REPORTED BUT NOT OBSERVED)

	Soret-like band		Q-like band		Emission	
	(nm)	(eV)	(nm)	(eV)	(nm)	(eV)
Free Base Hxp			711	1.74		
	567	2.19			1056	1.17
			767	1.61		
m-Pd Hxp			1050	1.18		
			719	1.72		
	557	2.26			1108	1.12
Pd-Pd Hxp			940	1.32		
	493	2.51	889	1.39	1060	1.17
	579	2.14	1013*	1.22		
	629	1.97				

Pd-Ag Hxp	525	2.36	867	1.43	1035	1.2
	583	2.13	1152*	1.07		
	698	1.78				
	751	1.65				
Pd-Cu Hxp	382	3.25	879	1.41	-	-
	530	2.34	1157*	1.08		
	587	2.11				
	706	1.76				

#### 4.4. Remarks

While the molecules were successfully synthesized as described by literature and its optical bandgap determined by fluorimetry, the question of the accuracy of its reported metal centres oxidation state was raised. Ideally,  $^{13}\text{C}$  NMR should be done to investigate it.

In the scenario that the reports are not accurate, it is likely that both Cu and Ag are not bound to the carbons of the inner pyrrolic rings, distorting its structure and possibly resulting in a non-planar conformation,



## 5 – Electrochemistry of Hexaphyrins

*Many porphyrins have been applied in electrocatalysis and sensors over the years, inspired for its processes in Nature. Porphyrinoids have unique spectroscopic and electrochemical properties<sup>186</sup> with potential application in wide a range of fields. As previously discussed, their properties can be easily tuned by modifications in its macrocycle. Most porphyrinoids have similar tendencies on its electrochemical reactions based on core or peripheral functionalization. While few studies were conducted on expanded porphyrins, several reviews,<sup>187-193</sup> have been published on the study of other porphyrinoids families. This chapter will consist of a brief discussion in terms of its properties and the effects of the core modifications on the macrocycle of porphyrinoids.*

### 5.1 – Introduction – Electrochemistry of porphyrinoids

Porphyrinoids are electroactive materials with rich electrochemical properties presenting several redox processes, which makes them a constant research topic since the 60's.<sup>194</sup> Up to the 90`s, most of the studies consisted in reporting the effects on its redox properties, based on changes from metallic centre or ligands, and its application as sensors or catalysis. These studies created a library of how core changes affect the molecules electrochemical properties.

The voltammogram of a porphyrin and similar macrocycles usually present at least two pairs of two consecutive redox reactions, as described in Fig. 5.1, forming cations and dications or anions and dianions. For both the free base and metallated porphyrinoids, the oxidations or reductions usually consist on the removal or addition of electrons on the  $\pi$  conjugated macrocycle,<sup>195</sup> which rarer cases in which the metal centre change its oxidation state or its axial ligands.<sup>196</sup>

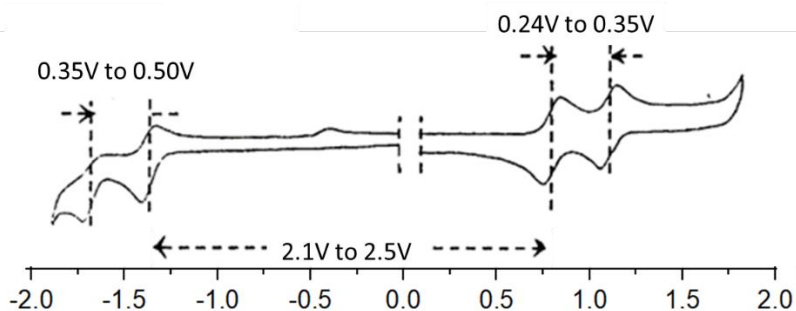


FIGURE 5.1 – Cyclic voltammogram of a metallated tetraphenyl porphyrin in dichloromethane, adapted from reference 192.

Electrochemical techniques can provide information about the orbital energy of a molecule. In a voltammogram, the potential to remove an electron relates to the energy of the HOMO of the molecule, while the potential to inject an electron in it provides the energy associated to its LUMO. The difference in the potential between the first reduction peak, to introduce an electron in the LUMO of the molecule, and the first oxidation peak, where the first electron is removed from the HOMO of the molecule, its electrochemical band gap.<sup>195</sup> Furthermore, the studies from the 60's until the 80's generated an electrochemical criteria that indicates the electron transfer site on the molecule based on its potentials.<sup>197</sup> In porphyrins and tetraphenyl porphyrins the band gap has been extensively studied and often found between 2.1V to 2.5V.<sup>198</sup> The difference in potential between the first and second macrocycle reductions often was between 0.35V and 0.5V and the difference between the two first oxidations between 0.24V and 0.35V.<sup>199-201</sup> These are known as the “diagnosis criteria”, and are often used in these molecules to define if the metal centre is participating or not in the redox properties of the material, where transitions that would occur on ligands or metallic centre would deviate from these mean values.<sup>200</sup> Nevertheless, as the synthesis of porphyrinoids improved and specific functionalization could be achieved it was shown that proper tuning of the molecule properties could be done and reduce its band gap up to 1V.<sup>195</sup> Furthermore, the chelation of transition metals in the 90's indicated that the “diagnosis criteria” lacks proper comprehension for those molecules which metal centre hinders its planarity, such as Fe and Co.<sup>190,203</sup> In these cases, often a two electron transfer was observable at the same potential, which was later characterized as two steps with one electron transfer at similar potential.<sup>204</sup>



Specific studies lead to a vast library of molecules showing trends on how the core modification of these molecules affect its electrochemical properties. As described in Chapter 2.2 of this thesis, several porphyrinoids are distinguished one from another by its macrocycle saturation level in relation to the porphyrin's. For example, we have the phlorines and chloroporphyrin, which conjugation pathway is partially saturated, affecting its planarity and its symmetry group.<sup>205</sup> The same is observable for the comparison between isobacteriochlorin, chlorins and porphyrins, in which the difference in first oxidation potential is up to 0.9V.<sup>206</sup> The modification in planarity of the molecule by its saturation leads to a change in the HOMO and LUMO of the molecule making it easier to oxidize, while having an increase in the absorption wavelength. This trend is observable for all reported porphyrinoid families.<sup>207, 208</sup>

However, one of the most explored tools to tune the electrochemistry of porphyrinoids are the meso and  $\beta$ -ligands to the macrocycle. These can affect its properties, mostly, in two distinct ways. The first is a possible distortion in its macrocycle where several bulky ligands are introduced close to each other. This will correspond to oxidations in lower potentials as the case of saturation of the macrocycle.<sup>209,210</sup> The second, showing a more concise effect, is the electron donation or withdrawal properties of the ligands. The addition of withdrawal groups will lead to a shift of both reduction and oxidation potentials to more positive, while electron donator groups shift it to more negative potentials.  
211-214

Lastly, porphyrinoids are known for chelating with all transition metals,<sup>215,216</sup> including lanthanides and actinides.<sup>217-219</sup> There are several ways in which the nature of the metal will affect the electrochemistry properties of the molecule. First, stable reversible redox pairs, such as  $\text{Fe}^{+2}/\text{Fe}^{+3}$  can lead to an increase of the number of redox reactions in the voltammogram, creating a redox pair specific for the metallic centre.<sup>3,6</sup> However, most metals are not stable in multiple redox states while chelating in the macrocycle, and its effect is mostly by a shift in the oxidation and reduction potentials accordingly to the metal electronegativity.<sup>220</sup>

Porphyrinoids have been used due to their electronic properties in several applications, such as sensors,<sup>221 - 230</sup> electrocatalysts for diverse

reactions,<sup>231-247</sup> photovoltaic dyes,<sup>248-259</sup> etc. It is important to notice that for most applications, not only the properties of the molecule need to be tuned, but also their interaction with an interface and/or target molecule.<sup>260</sup> For this reason the porphyrinoids are often functionalized with terminal thiol or carboxylate groups, and some metals are prioritized for electrocatalysis, such as Fe and Co.

Expanded porphyrinoids have not been as widely studied as porphyrins and phthalocyanines, nevertheless, in the last few years few groups have expanded this area of research, among them, Sessler *et al.* and Osuka *et al.* being the main contributors in this field.

Similar effects to those of the porphyrinoids are observed for hexaphyrins. The addition of electron donating and or withdrawal groups to the  $\beta$ -pyrrolic and meso-pyrrolic positions will affect its redox potentials, shifting it towards more negative or positive potentials, respectively.<sup>261-267</sup> The macrocycle of hexaphyrins also allows multiple conformations by the torsion of its pyrroles, as explained in Section 2.2. of this Thesis. This will affect its aromaticity and, due to the planarity distortion of the molecule, it will also make it easier to oxidize,<sup>268,269</sup> shifting its oxidation potentials to lower potentials. Due to the bigger molecule size in relations to porphyrins, several synthesis procedures lead to the formation of confused macrocycles, which creates a distorted molecule and also affects its redox potentials.<sup>270-272</sup> Several metallic centres have been successfully chelated in hexaphyrins macrocycle. However, the study of its effect on electrochemical properties are still limited, whereas its electrochemical properties are not often reported. Some studies show the same tendency as for remaining porphyrinoids, in which the electronegativity of the metal will affect the redox potentials of the macrocycle and, in some cases, create new redox processes.<sup>273</sup>

This chapter tries to bring further information to this field, studying how distinct metal centres will affect its properties.

## **5.2 – Methods**

### **5.2.1 – Reactives**

Dichloroethane (DCE) HPLC was bought from Sigma and further dried by distilling it and storing in Molecular sieve 0.3 nA, which was acquired

from Sigma-Aldrich. Tetrabutylammonium Hexafluorophosphate (TBAPF<sub>6</sub>) was purchased from Sigma-Aldrich and used as received.

The hexaphyrins were synthesized as described in Chapter 4 of this thesis, with collaboration of Prof. Dr. Kleber T. Oliveira and Dr. Maria C. Donatoni Santos.

Platinum microelectrodes were purchased from “Art Glass Industria e Comercio Ltda ME”.

### **5.2.2 – Equipment and electrochemical system**

The electrochemical experiments were carried out in homemade three-electrode glass cell using an AUTOLAB PGSTAT 302N with SCANGEN250 and FRA32m modules. A homemade Faraday cage was used to decrease the noise on the measurements.

Due to the nature of porphyrinoids, it was not possible to measure it in water. Therefore, an organic system was determined in such a way that a large potential window could be achieved. As shown in Fig. 5.2, a potential window of 3.0 V could be achieved by using DCE as solvent and TBAPF<sub>6</sub> as support electrolyte.

The Pt microelectrode used has a diameter of 50.8 μm. Two Pt wires were used for counter electrode and as a pseudo reference. Lastly, due to the low solution volume used on electrochemical measurements, a gas saturation system was used to previously saturate the Nitrogen through dry dichloroethane before deairing in the cell.

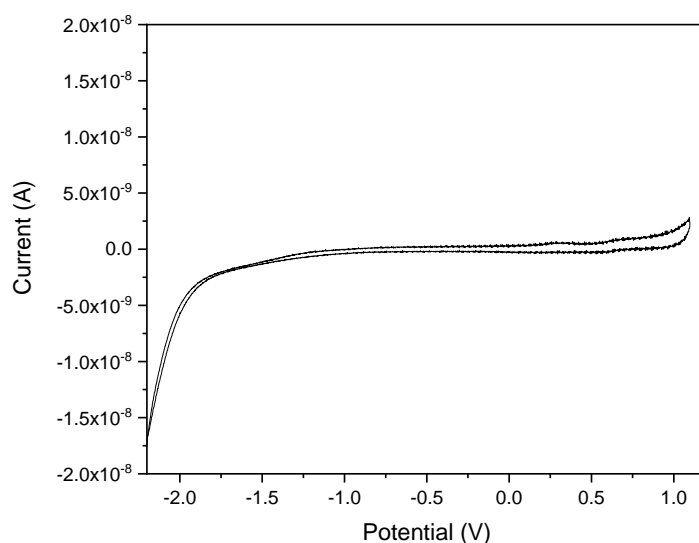


FIGURE 5.2 – Voltammogram of the system without any of the molecules from this study. Electrolyte:  $0.10 \text{ mol.L}^{-1}$  TBAPF<sub>6</sub> in DCE. Work electrode a Pt microelectrode, reference and counter electrode: Pt wires. Scan rate 0.50 V/s.

The molecules were characterized with cyclic voltammetry at room temperature, using a NOVA2.1 routine to scan in distinct scan rates, with anodic sweeps starting on the open potential circuit. The reported voltammograms is the third collected cycle.

Due to the quasireversible or irreversible property of the redox pairs observed, square wave potentiometry measurement was realized with the objective of determining a better approximation of the peak potentials.

All measures were done with a pseudoreference wire of Pt. To avoid degradation and contamination of the hexaphyrins, Ferrocene was measured only in the electrolyte, shown in Fig. 5.3, with a half wave potential of 0.12V. Since there is the possibility of the pseudoreference to slightly shift its potential in the system with the molecules, all the voltammograms presented in this chapter are represented against the pseudoreference value while having in mind the 0.12V shift to ferrocene as reference.

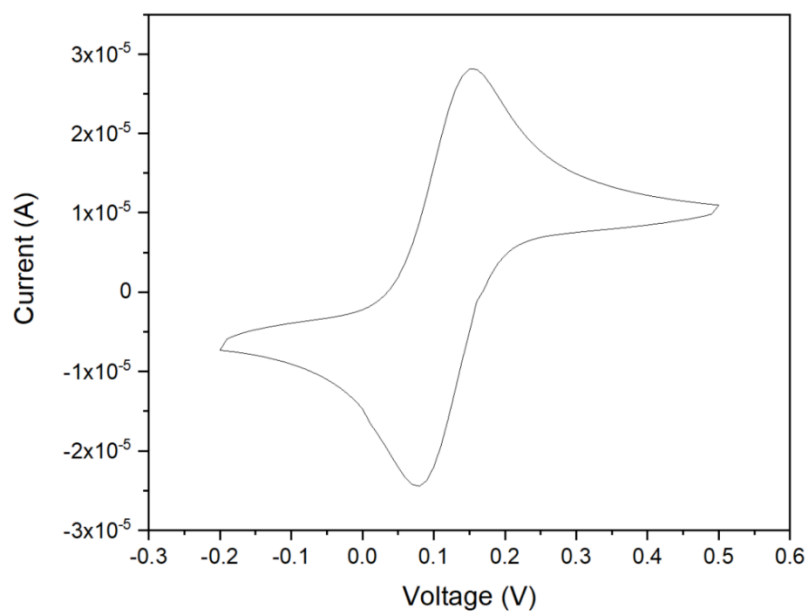


FIGURE 5.2 – Voltammogram of Ferrocene at 0.100 V/s, over a Pt microelectrode. Electrolyte:  $0.10 \text{ mol.L}^{-1}$  TBAPF<sub>6</sub> in DCE. Reference and counter electrode: Pt wires.

## 5.3 – Results

### 5.3.1 – Voltammograms

The cyclic voltammogram for the Free Base Hexaphyrin for the two lowest scan rates, 0.20 V/s and 0.50 V/s, are shown in is shown in Fig. 5.4. The solvent was DCE with 0.10 mol L<sup>-1</sup> TBAPF<sub>6</sub> as supporting electrolyte, the working electrode was a Pt microelectrode, reference and counter electrodes were Pt wires. The redox processes at 0.20 V/s are not as evident as at higher scan rates. One important feature that can be observed between these two voltammograms is the potential shift between the positions of the peaks, indicating that these processes are not reversible, but quasi-reversible. This is also collaborated by the large gap between the current peak for each oxidation and reduction pair, which is often higher than 80 mV. At 0.20 V/s, no oxidation is evident for the molecule, while 4 reductions, can be observed at -0.25V, -0.63V, -0.97V, -1.37V and -1.89V. It is important to notice that there is a trend in which the overall current keeps shifting towards negative upon each new process, indicating that all the previous reactions still occur on the more negative potential. The two first reductions are quasi-reversible in which its reversible oxidation can be observed at -0.19V and -0.59V, while the reductions that occur in more negative potentials seems to be irreversible, which can be caused by the reaction of the molecule with the solvent or due to a change in conformation of the macrocycle, which would affect the reversible step.

At 0.5 V/s, the processes become more evident, but due to the shift of its potential it seems to lose some features. An irreversible oxidation peak can be observed at 0.99V, two quasi-reversible reductions occur at -0.47V and -0.78V, in which its oxidations occur at -0.38V and -0.71V, a third reduction occurs at -1.52V and a last one at -1.89V. The two last reductions follow up with a large current drop in the system, in which could indicate multiple reactions at similar potential or a reaction with multiple electron transfer occurring. From the voltammogram at 0.10 V/s, it is likely that there are two reactions happening at similar potentials and, just like the two more negative reductions in the lower scan rate, irreversible. Supposing that all the electrons added or removed from the molecule are from the conjugated macrocycle, it is expected that the molecule change from [26]hexaphyrin up to [30]hexaphyrin, in which an oxidation towards

[25]hexaphyrin or a further reduction towards [31]hexaphyrin have a chemical process, or a transition of conformation, irreversible.

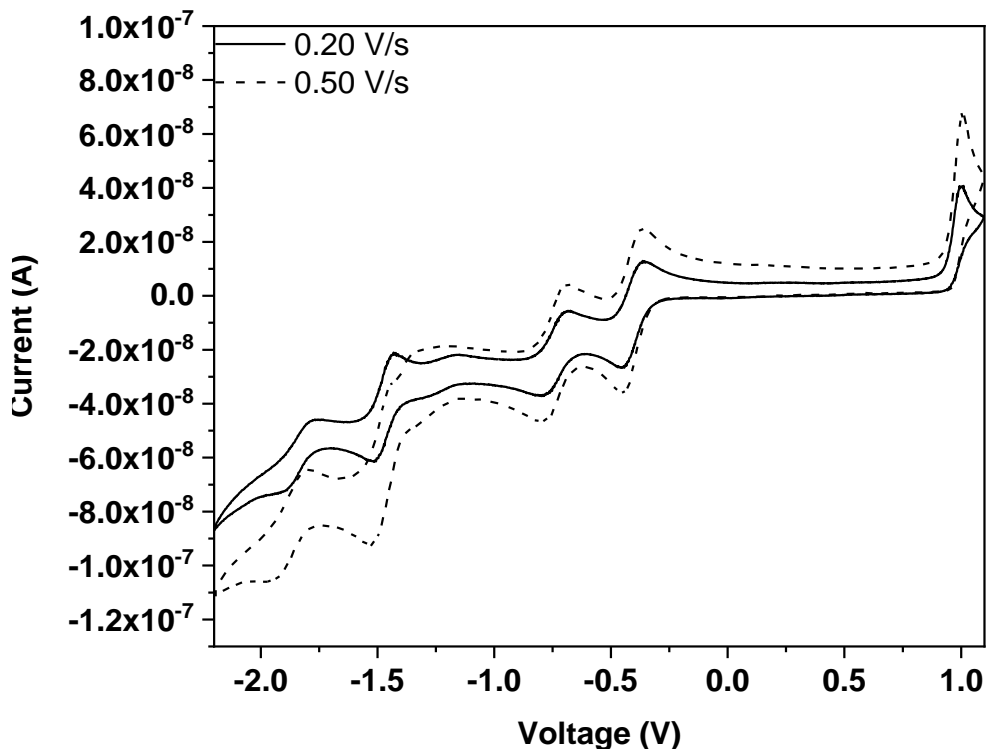


FIGURE 5.4 – Voltammogram of free base hexaphyrin at 0.20 V/s and 0.50 V/s, over a Pt microelectrode. Electrolyte:  $0.10 \text{ mol.L}^{-1}$  TBAPF<sub>6</sub> in DCE. Reference and counter electrode: Pt wires.

Fig. 5.5 shows the scan rate of the Free Base Hxp at distinct scan rates up to  $10.0 \text{ V/s}$ , with each process labelled. The potential of each process changes with increase scan rate due to its quasi-reversible characteristic. More importantly, ultra-fast scan-rates allows the detection of processes that couldn't be observed before. The oxidation at  $1.00 \text{ V}$  (a) that was previously irreversible due to extinction of the molecule possible by a chemical reaction or change in conformation, start to be observable for scan rates higher than  $4.0 \text{ V/s}$  (a'), indicating that at this speed the oxidized molecule can be reduced before the chemical reaction or its conformation is changed. The same occurs with the reduction d', in which the reversible oxidation can be observed at scan rates over  $2.00 \text{ V/s}$ . This indicates the kinetics of the chemical reactions

after the electron transfers, in which at fast scan rates the reverse electron transfer can be observed because it is faster than the chemical change. Lastly, the Half wave potential from the first oxidation process, a, to the first reduction process, b, gives what is determined as the electrical band gap of the material, which is 1.42 V.

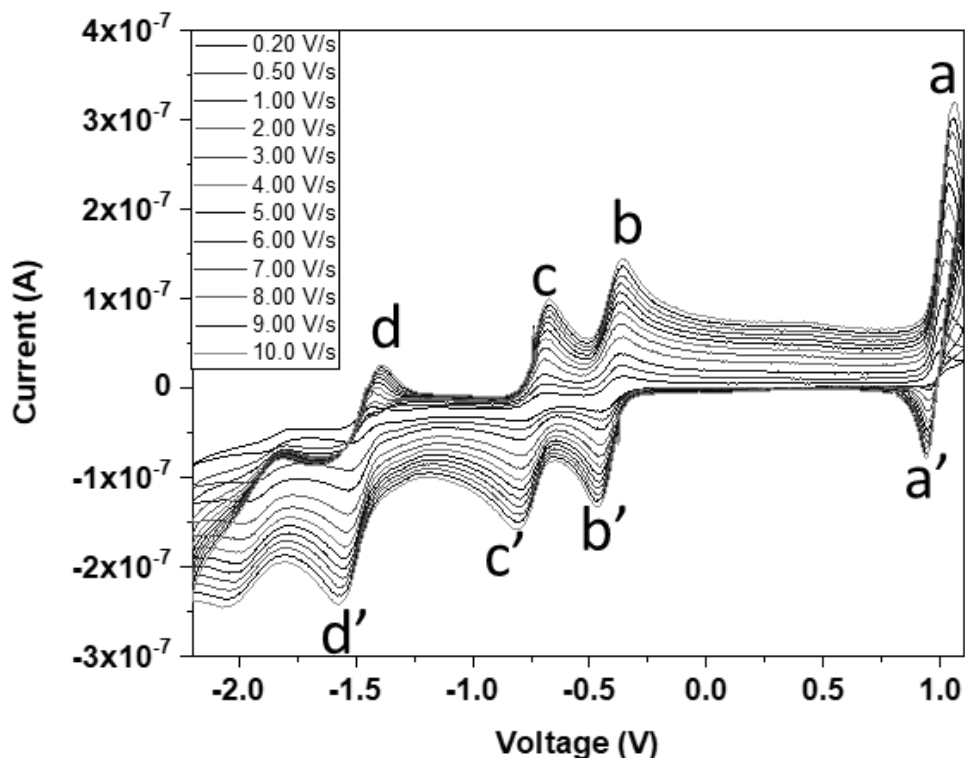


FIGURE 5.5 – Voltammogram of free base hexaphyrin with its processes tagged at distinct scan rates, over a Pt microelectrode. Electrolyte: 0.10 mol.L<sup>-1</sup> TBAPF<sub>6</sub> in dichloroethane. Reference and counter electrode: Pt wires.

Fig. 5.6 shows the peak current for each process tagged in Fig. 5.5 in function of the square root of the scan rate. Due to the linearity between all the processes, it is possible to affirm all of them are predominantly diffusion limited. However, the intersection point of none of the curves crosses the axis Y at 0, indicating that some adsorption occurs at the interface.

Table 5.1. shows the potentials obtained experimentally in comparison to those in the literature.<sup>94</sup> The potentials reported are based on glassy carbon electrode at low scan rate of 0.05 V/s. This will lead to a difference



in the potential observed, but the electrochemical band gap is approximately the same as previously reported.

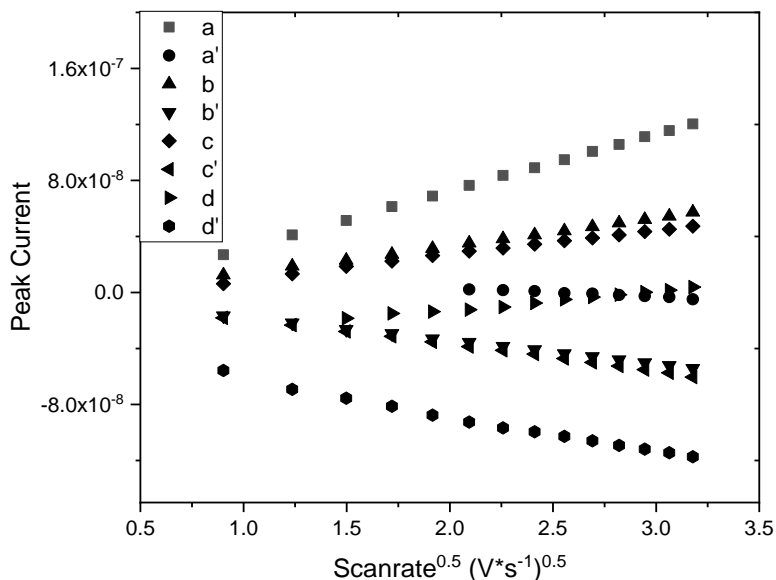


FIGURE 5.6 – Peak current in function of square root of scan rate for all the processes observed in the Free Base Hexaphyrin tagged in Fig. 5.5.

TABLE 5.1. – HALF WAY POTENTIALS FOR FREE BASE [26] HEXAPHYRIN FOR THIS WORK OVER Pt ELECTRODE AGAINST PSEUDO REFERENCE OF Pt, AND FOR REFERENCE 94, ON GLASSY CARBON AGAINST FC/FC<sup>+</sup>.

	E <sup>1/2</sup> ox <sub>1</sub> (V)	E <sup>1/2</sup> red <sub>1</sub> (V)	E <sup>1/2</sup> red <sub>2</sub> (V)	E <sup>1/2</sup> red <sub>3</sub> (V)	BandGap (V)
This work	0.98	-0.43	-0.73	-1.48	1.41
Reference	0.90	-0.57	-0.89	-1.65	1.47

Fig. 5.7 shows the voltammogram of the mono Pd Hxp over Pt microelectrode of Pt at scan rates 0.20 V/s and 0.50 V/s, using 0.10 mol/L TBAPF<sub>6</sub> as electrolyte and Pt both as counter electrode and working electrode. At 0.20 V/s a sigmoidal curve shows two irreversible oxidations, one occurring at

1.01 V, which is a similar potential to the oxidation of the free base hexaphyrin, and a second at 0.17V, which is also irreversible. There are 3 reversible reductions at -0.63V, -1.33 V -1.76V. In comparison to the Free base Hxp, all these reductions occur at potentials more positive than the free base hexaphyrin, indicating that the metal centre affects the HOMO of the molecule by shifting its energy to shallower potentials. Increasing the scan rate to 0.50 V/s the current peaks become more prominent and its  $I_{\text{peak}}$  has its potentials shifted, indicating that these are quasi-reversible processes, an important characteristic upon increasing the scan rate is the separation of some processes. While at 0.20 V/s only 4 reductions could be observed, at higher scan rates 5 processes can be distinguished, which become more visible at even higher scan rates.

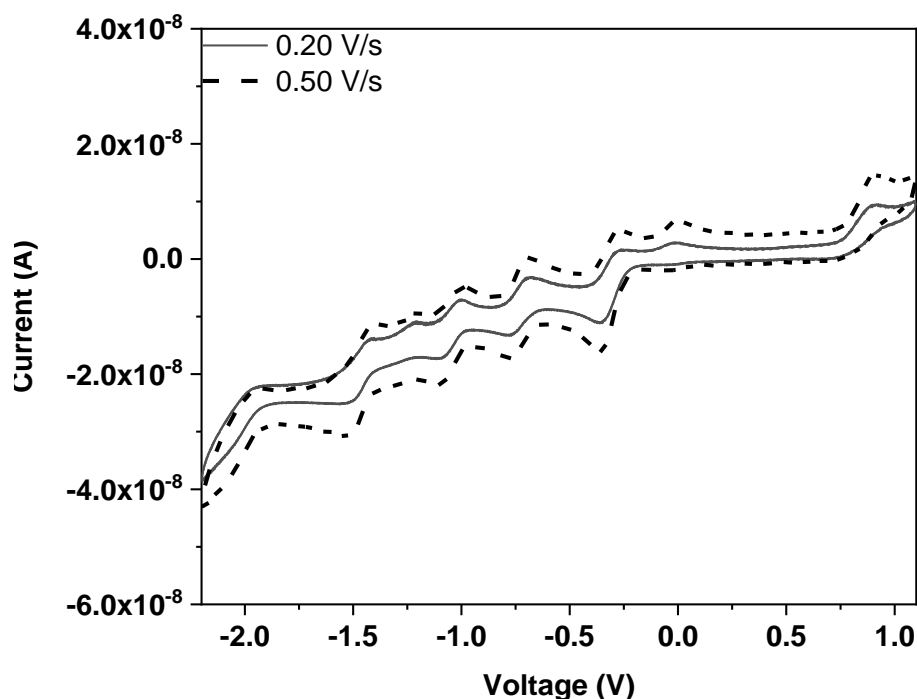


FIGURE 5.7 – Voltammogram of mono Pd hexaphyrin at 0.20 V/s and 0.50 V/s, over a Pt microelectrode. Electrolyte: 0.10 mol.L<sup>-1</sup> TBAPF<sub>6</sub> in dichloroethane.

Reference and counter electrode: Pt wires.

Upon increasing the scan rate, the peaks become more defined and separated, as shown in Fig. 5. 8. With the improved resolution, we can define two oxidation processes, 'a' and 'b'. Process a, at 1.00V, is irreversible even at higher scan-rates, indicating that its coupled chemical reaction or conformation change

to occur extremely fast. Process b, with half wave potential of 0.11V, becomes partially reversible at scan rates faster than 2.00 V/s, indicating a slower chemical step. Processes c to g are quasi-reversible with half wave potentials at -0.24V, -0.64V, -0.96V, -1.13V and -1.36V. Fig. 5.9 shows the current peak for each process in function of the square root of the scan rate, indicating all the processes are predominantly diffusion limited.

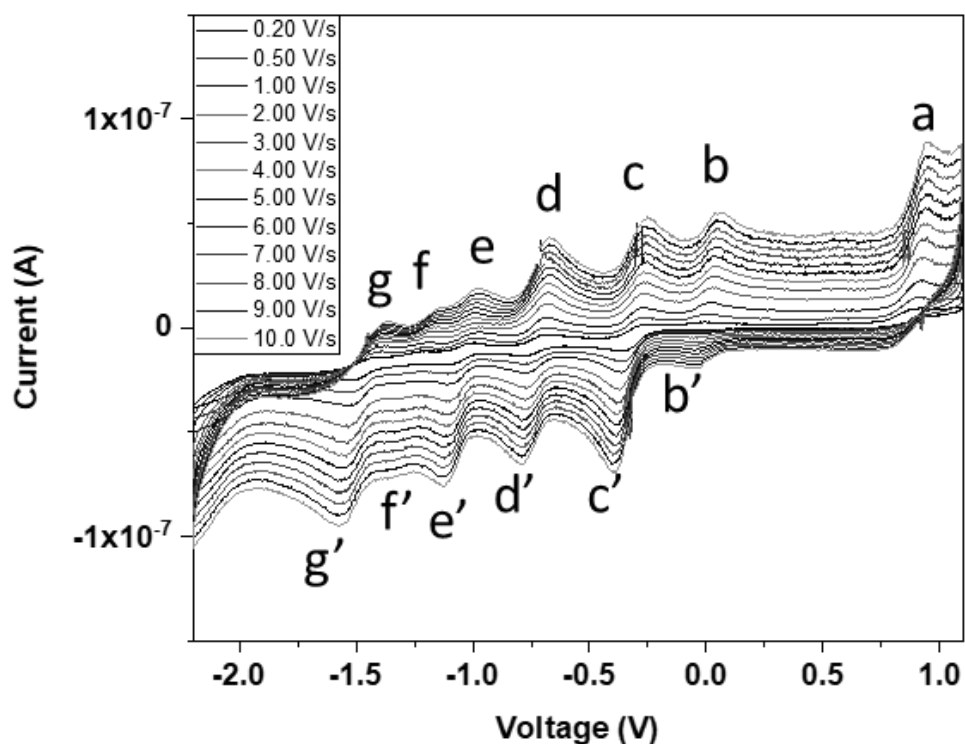


FIGURE 5.8 – Voltammogram of mono Pd hexaphyrin with its processes tagged at distinct scan rates, over a Pt microelectrode. Electrolyte: 0.10 mol.L<sup>-1</sup> TBAPF<sub>6</sub> in dichloroethane. Reference and counter electrode: Pt wires.

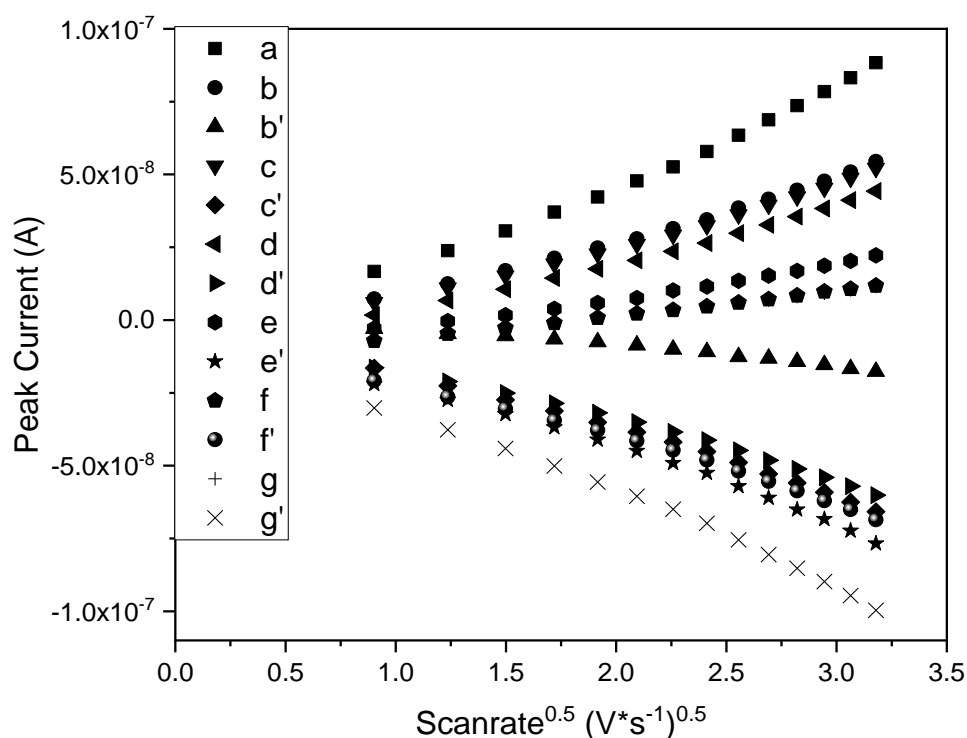


FIGURE 5.9 – Peak current in function of square root of scan rate for all the processes observed in the mono Pd Hexaphyrin tagged in Fig. 5.8.

The voltammograms for the Pd-Pd Hxp at scan rates 0.20 V/s and 0.50V/s are shown in Fig. 5.10. The non-reversible oxidation observed at around 1.00V for Free Base Hxp and Mono Pd Hexaphyrin is present at higher potential: 1.12V. Both capacitance and faradaic currents increase with the scan rate, in which the Faradic processes becoming more prominent at higher scan rates. Four reductions can be observed at -0.26V, -0.68V, -1.38V and -1.87V, with its reversible oxidation at -0.18V, -0.61V, -1.30V and -1.77V.

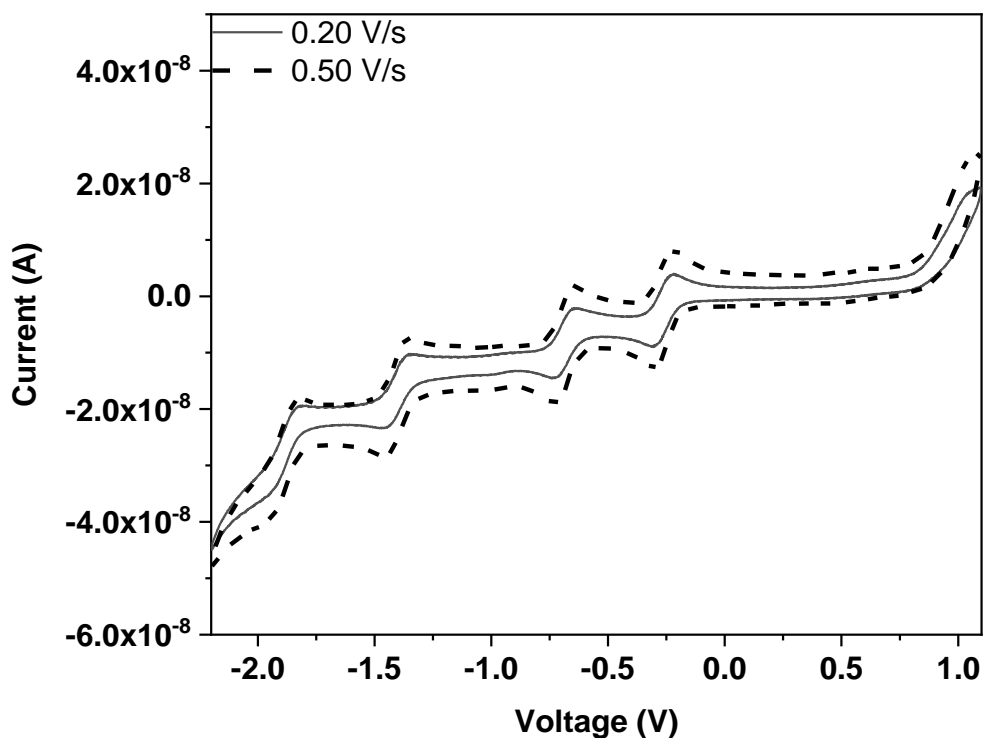


FIGURE 5.10 – Voltammogram of Pd-Pd hexaphyrin at 0.20 V/s and 0.50 V/s, over a Pt microelectrode. Electrolyte: 0.10 mol.L<sup>-1</sup> TBAPF<sub>6</sub> in dichloroethane. Reference and counter electrode: Pt wires.

At higher scan rates the processes become more evident, as shown in Fig. 5.11. Distinct from what happens for the other molecules studied, there is no further separation of the peak potentials with scan-rate for all the voltammograms. This indicates that, with the exception of the oxidation at 1.12V, the processes are reversible for the Pd-Pd hexaphyrin. Even upon fast scan rates no reversibility in the electron transfer could be observed for process 'a', what indicates a fast-chemical step after the electron transfer. Furthermore, the analysis of the current peak in function of the square root of the scan-rate, Fig. 5.12, indicates that all processes are predominantly diffusion limited.

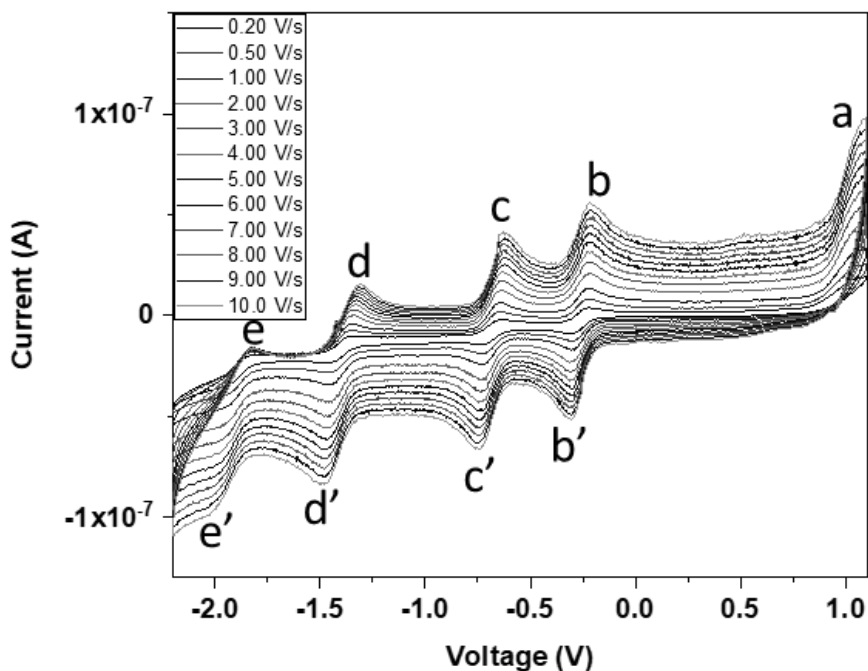


FIGURE 5.11 – Voltammogram of Pd-Pd hexaphyrin with its processes tagged at distinct scan rates, over a Pt microelectrode. Electrolyte: 0.10 mol.L<sup>-1</sup> TBAPF<sub>6</sub> in dichloroethane. Reference and counter electrode: Pt wires.

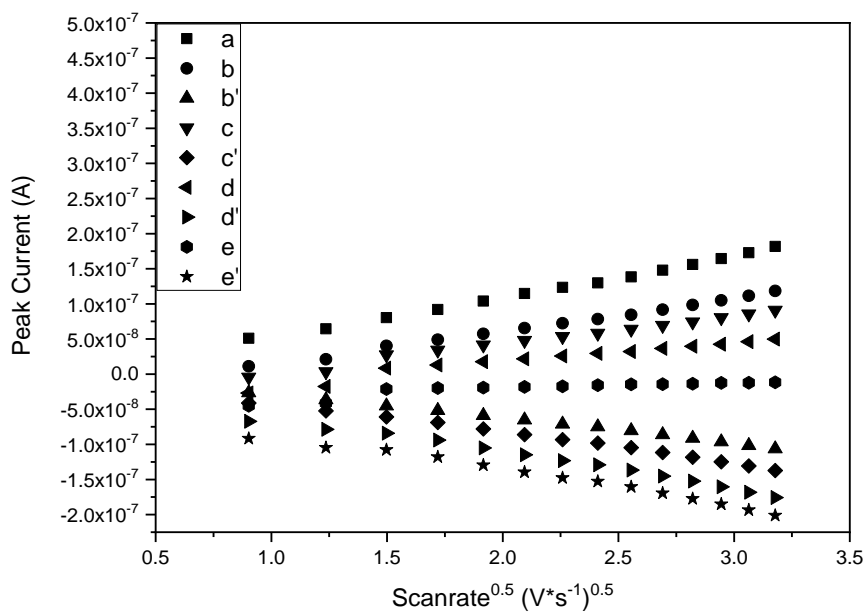


FIGURE 5.12 – Peak current in function of square root of scanrate for all the processes observed in the Pd-Pd Hexaphyrin tagged in Fig. 5.11.

Fig. 5.13 shows the voltammograms for the Pd-Ag Hxp at 0.20 V/s and 0.50 V/s. At low scan-rate the processes are not easily distinguishable due to the low potential difference between them. Upon increasing the scan-rate to 0.50 V/s, the potentials are shifted and the faradaic current increases, making the processes more evident. Three irreversible oxidation peaks can be observed at 0.10V, 0.60V and at 0.97V. While the first two process are not observable for the free base Hxp, the last oxidation potential is similar to the one presented in the other molecules. Six distinct reduction potentials can be observed, in which some are quasi-reversible and others are irreversible.

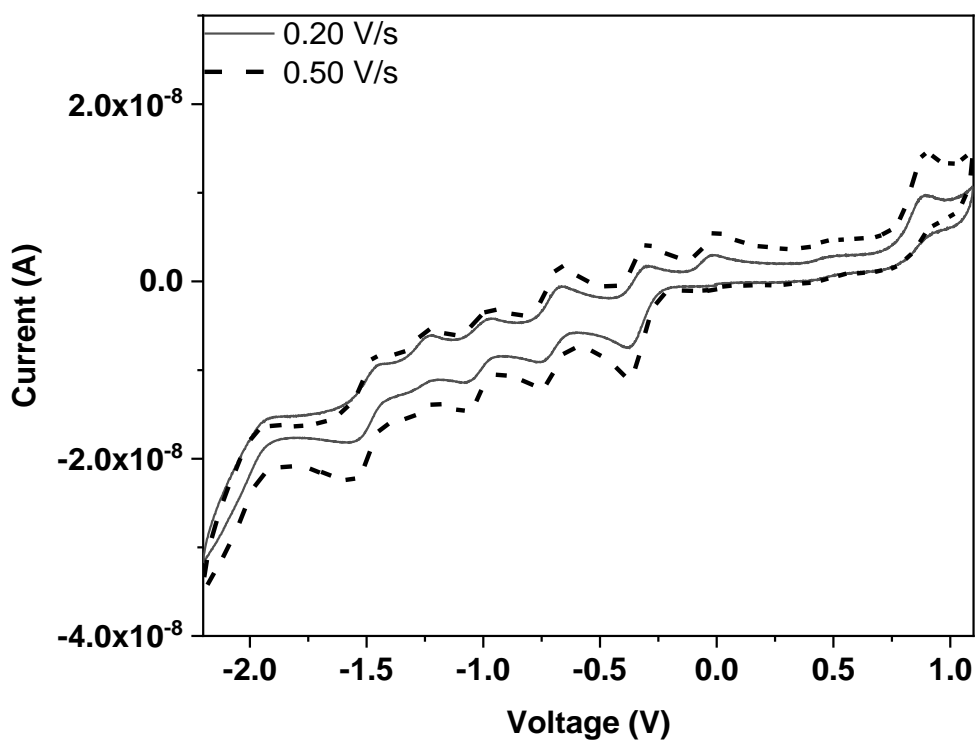


FIGURE 5.13 – Voltammogram of Pd-Ag hexaphyrin at 0.20 V/s and 0.50 V/s, over a Pt microelectrode. Electrolyte: 0.10 mol.L<sup>-1</sup> TBAPF<sub>6</sub> in dichloroethane. Reference and counter electrode: Pt wires.

To better understand this system, faster scan-rates are necessary, as shown in Fig. 5.14. At a faster scan-rate the first oxidation peak is shifted towards a higher potential while being covered by the capacitive current, becoming less noticeable. Both processes 'a' and 'b' are irreversible at low scan-

rates, but its reverse electron transfer can be observable at higher scan-rates, with a half wave potential at 0.58 and 0.90V. Processes 'c' to 'h' have narrow potential gaps and are not reversible, with half wave potentials at -0.27V, -0.62V, -0.93V, -1.18V, -1.44V and -1.82V. Process 'f' and 'h' have a sharp decrease in the current. This can be caused by a two-electron reaction or by multiple reactions at similar potentials, similar to what is observed on the Free Base Hexaphyrin.

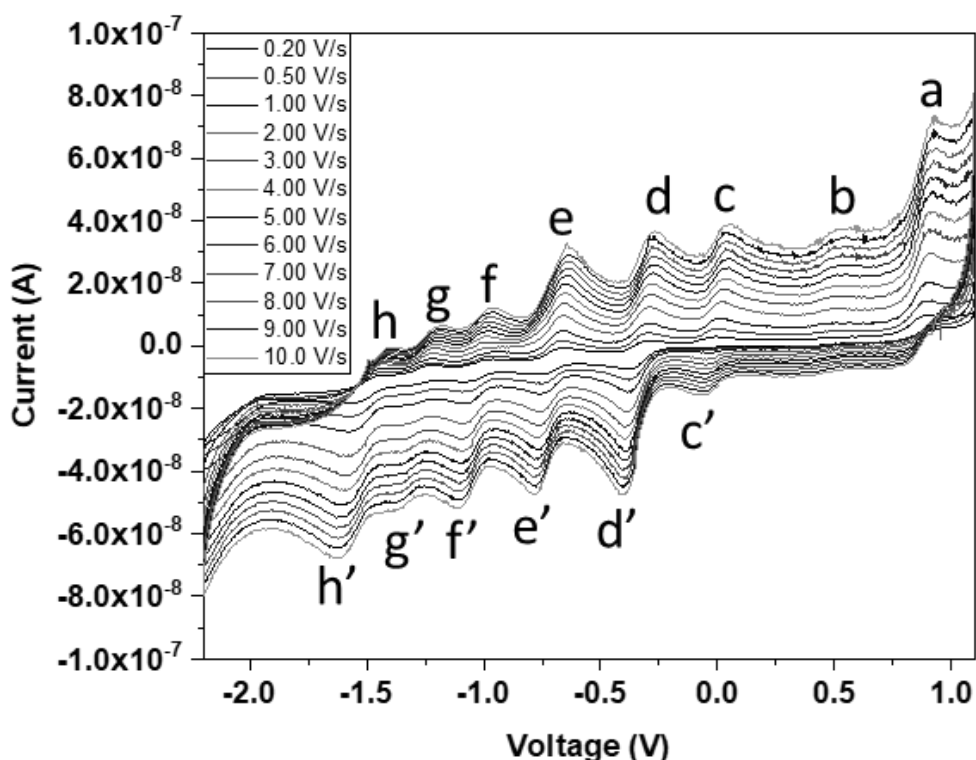


FIGURE 5.14 – Voltammogram of Pd-Ag hexaphyrin with its processes tagged at distinct scan rates, over a Pt microelectrode. Electrolyte: 0.1 mol.L<sup>-1</sup> tetrabutylammonium hexafluorophosphate in dichloroethane. Reference and counter electrode: Pt wires.

Fig. 5.15 shows the peak current for each process labelled in Fig. 5.14 in function of the square root of the scan-rate. The processes are predominantly diffusion limited, due to the linearity of its function.



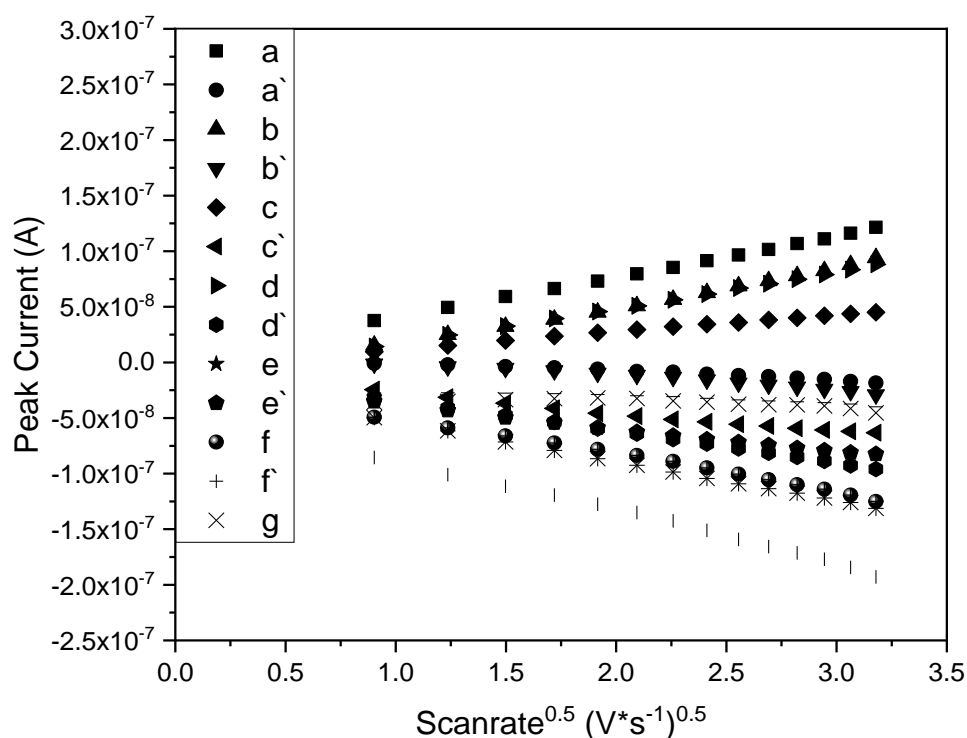


FIGURE 5.15 – Peak current in function of square root of scanrate for all the processes observed in the Pd-Ag Hexaphyrin tagged in Fig. 5.14.

Lastly, Fig. 5.16. shows the voltammogram of the Pd-Cu Hxp over a Pt microelectrode in DCE with TBAPF<sub>6</sub> as support electrolyte. Several distinct processes can be observed, but at lower scan rates, some of them are not easy to point out due to the small potential gap between them. Two non-reversible oxidation processes are observable at 0.10 V and at 0.99 V. There is a total of five reduction processes occurring with short potential gap between them, which becomes more featured at higher scan rates.

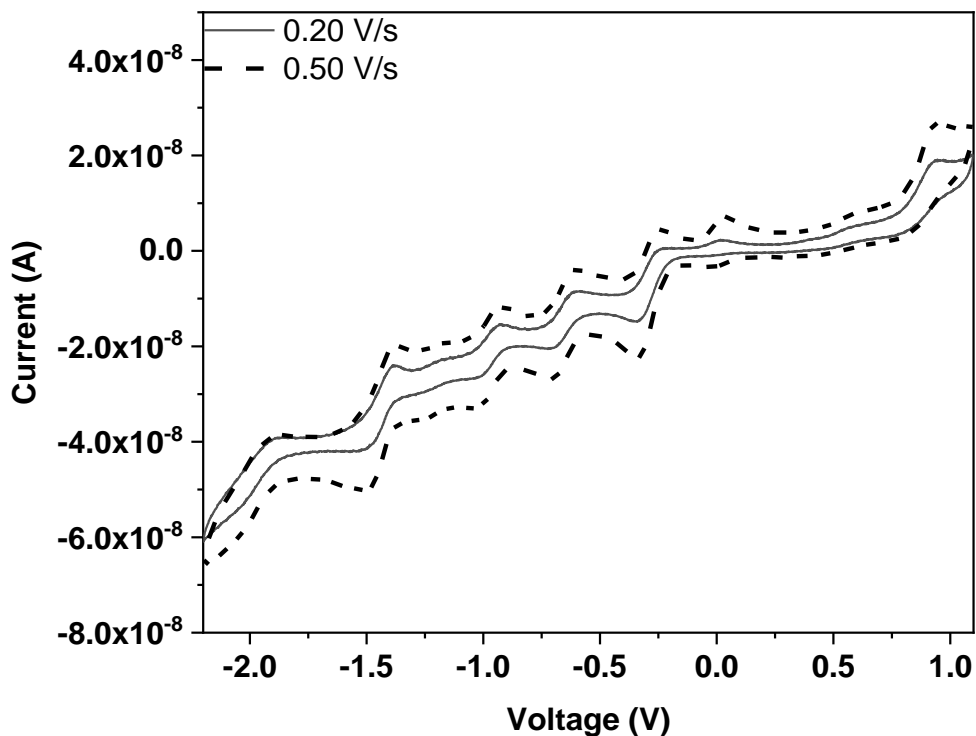


FIGURE 5.16 – Voltammogram of Pd-Cu hexaphyrin at 0.100 V/s and 0.814 V/s, over a Pt microelectrode. Electrolyte: 0.10 mol.L<sup>-1</sup> TBAPF<sub>6</sub> in dichloroethane. Reference and counter electrode: Pt wires.

Fig. 5.17 shows the voltammograms of the Pd-Cu at scan-rates up to 10 V/s. With increasing scan-rates, a third non reversible process is observed, 'b', at 0.67V, and the reverse electron transfer of the first oxidation process, 'c', can be observed. Processes 'd' through 'h' are quasi-reversible with half wave potentials of -0.24V, -0.60V, -0.92V, -1.16V and -1.38V. The process 'h' is followed by a sharp decrease in current similar to that observed for the Free Base Hxp, which may indicate a two-electron transfer or two processes at similar potential. Fig. 5.18 shows the peak current for each process in Fig. 5.17 in function of the square root of scan rate. Due to the linearity of each function, it is supposed that most of these processes are controlled predominantly by diffusion.

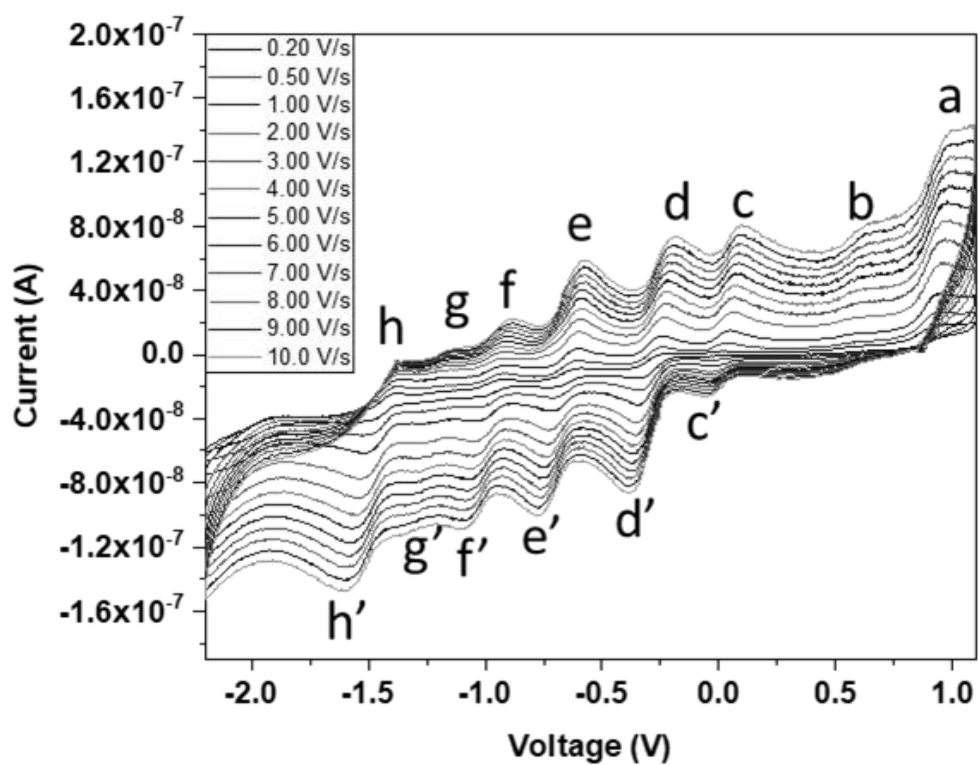


FIGURE 5.17 – Voltammogram of Pd-Cu hexaphyrin with its processes tagged at distinct scan rates, over a Pt microelectrode. Electrolyte: 0.10 mol.L<sup>-1</sup> TBAPF<sub>6</sub> in dichloroethane. Reference and counter electrode: Pt wires.

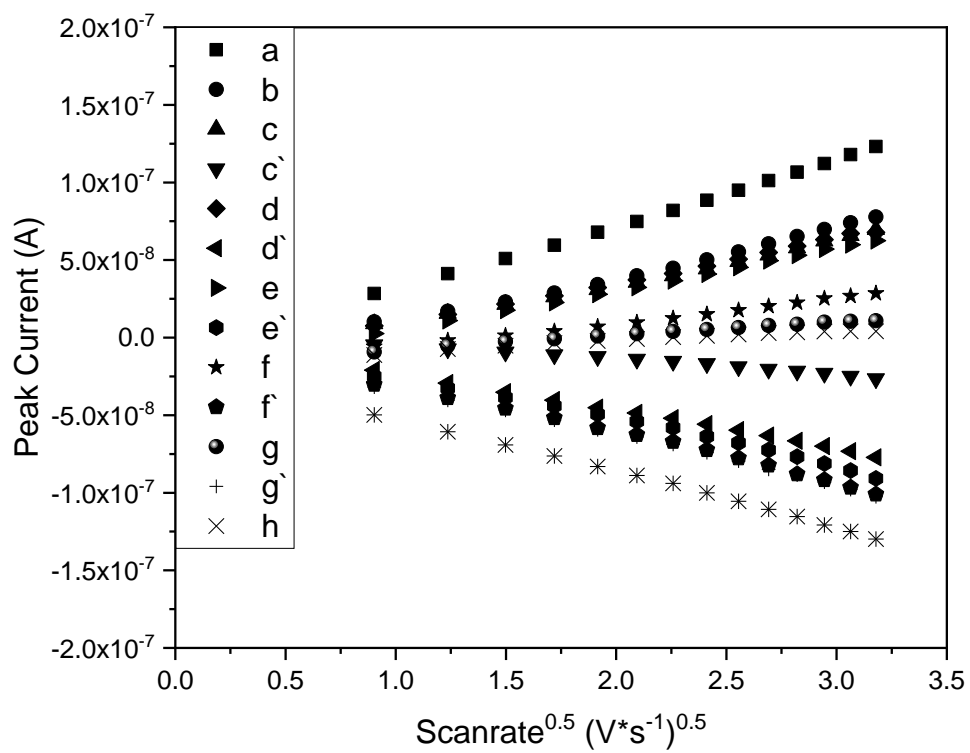


FIGURE 5.18 – Peak current in function of square root of scan rate for all the processes observed in the Pd-Cu Hexaphyrin tagged in Fig. 5.17.

### 5.3.2 – Comparison between molecules

Fig. 5.19 shows the voltammograms at 1.00 V/s for all molecules of this study and Fig. 5.20 shows the square wave potentiometry. Table 5.2. shows the half wave potential for each process, aligned to corresponding processes in the other molecules. Several processes in all molecules can be related to similar potentials. The free base hexaphyrin has a single oxidation occurring at 1.00V and four reductions on its macrocycle, presumed consecutive, at -0.43V, -0.73V, -1.49V and -1.93V. As shown in Fig. 5.17, the non-reversible reductions at -1.49V and -1.93V follows up with a larger decrease in the current, indicating multiple processes at similar potential or two electron transfers reductions.

TABLE 5.2. – HALF WAVE POTENTIAL FOR EACH PROCESS FOR THE MOLECULES OF THIS STUDY.

	<i>Half wave potential (V)</i>								
<i>FB Hxp</i>	1.00			-0.43	-0.73			-1.49	-1.89
<i>mPd Hxp</i>	1.08	0.12		-0.24	-0.63	-0.96	-1.14	-1.38	
<i>PdPd Hxp</i>	1.13			-0.22	-0.64			-1.34	-1.82
<i>PdAg Hxp</i>	0.91	0.58		-0.27	-0.62	-0.95	-1.19	-1.46	-1.87
<i>PdCu Hxp</i>	1.05	0.69	0.08	-0.23	-0.60	-0.92	-1.15	-1.37	-1.86

As observed for other porphyrinoids, the addition of a metal centre will shift potentials of the macrocycle accordingly to the electronegativity of the metal. The addition of a Pd shifts all molecule potentials to more positive, as shown in Table 5.2. The non-reversible oxidation at higher potentials at 1.08V has a faster coupled chemical reaction, and its reverse electron transfer cannot be observed even at higher scanrates. The two first reductions shift from -0.43V and -0.73V to -0.24V and -0.63V, respectively. The multiple processes, or multiple electron transfer process, observed at -1.49V can be observed at -1.38V. These processes are assumed to be electron transfers on the macrocycle of the molecule, in which consecutive electrons are added or removed from its conjugated backbone. However, this molecule presents three other processes that are not observable in the free base Hxp. An oxidation at 0.12V and two reductions at -0.96V and -1.14V. This could occur for two specific reasons: the

first is the change in the redox state of the Pd, in which case the macrocycle doesn't participate in the electron transfer, and the second is the change in orbital energies of the molecule due to the presence of the Pd and, because of this, multiple orbitals at narrower energies can participate on electron transfers, allowing it to donate/withdraw multiple electrons on the backbone of the molecule. The presence of similar behaviour for oxidation and reduction reactions to the free base Hxp could indicate that these redox reactions are centred at the metal instead of the backbone of the molecule. However, without specific tools to measure the intermediate nature for each reaction, it is difficult to affirm the mechanism of these processes.

Upon the addition of a second metal centre, distinct behaviours are observed accordingly to its nature. The Pd-Pd Hxp voltammogram can be compared to the one of the free base Hxp, with a shift in its potential to more positive. A single oxidation process is observable at 1.13V, non-reversible. Four distinct reductions can be observed: at -0.22V, -0.64V, -1.34V and -1.82V. The correlation with the Free base Hxp indicates that all these processes are related to the conjugated  $\pi$  backbone of the macrocycle.

The Ag on the PdAg Hxp influences its electrochemical properties in two distinct ways. Firstly, the oxidation potential common to all the molecules at around 1 V has its potential shifted towards more negative values: to 0.91V. A second oxidation potential, not observable for previous molecules, is observable at 0.58V. Due to the lack of this process on the free base Hxp and monoPd Hxp, it is likely that this represents a process centred on the Ag centre. Several reduction processes can be observed at -0.27V, -0.62V, -0.95V, -1.19V, -1.46V and -1.87V. The two first and two last can be comparable to those of the free base hexaphyrin, whereas the firsts are shifted to higher potential and the lasts to lower potential. The processes at -0.95V and -1.19V are not related to any that happens on the free base molecule, and might happen on a metal centre.

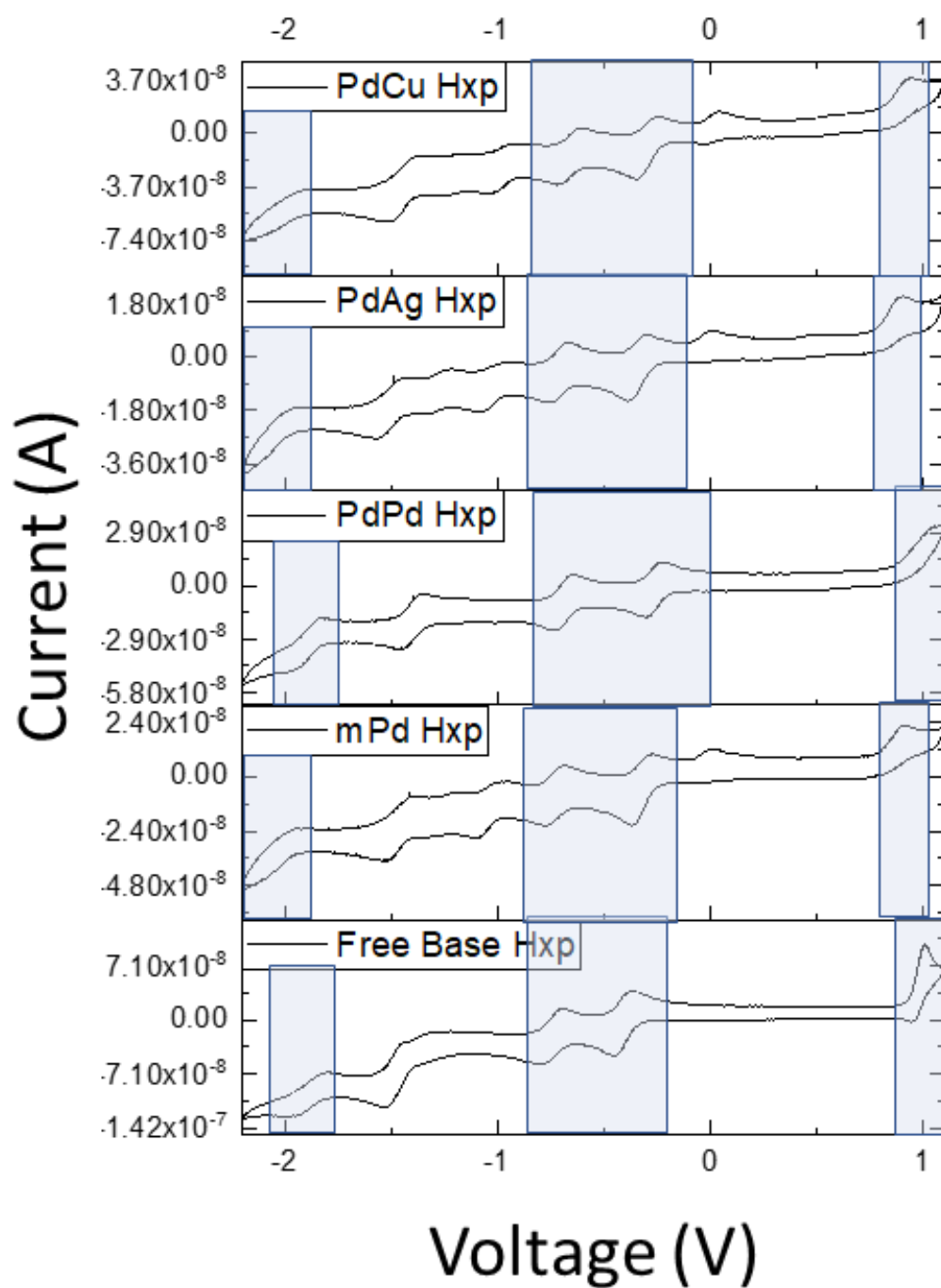


FIGURE 5.18 – Voltammogram of studied molecules, over a Pt microelectrode. Highlighted processes are supposed to be centred on the macrocycle of the material Electrolyte: 0.10 mol.L<sup>-1</sup> TBAPF<sub>6</sub> in dichloroethane. Reference and counter electrode: Pt wires.

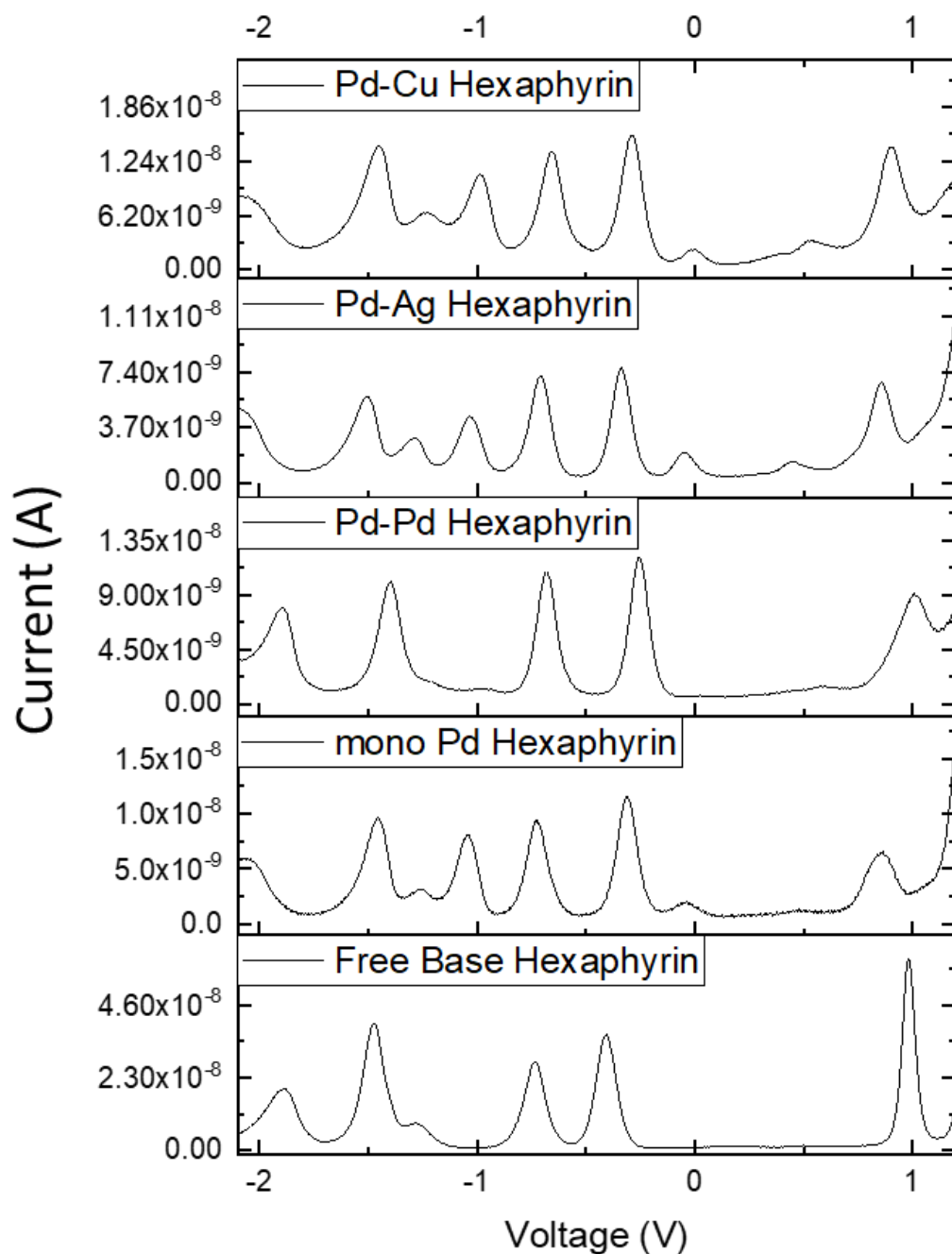


FIGURE 5.19 – Square potentiometry for synthesized molecules, over a Pt microelectrode. Electrolyte: 0.10 mol.L<sup>-1</sup> TBAPF<sub>6</sub> in dichloroethane. Reference and counter electrode: Pt wires.

Lastly, the Pd-Cu Hxp is the molecule with highest number of processes among the studied ones. The non-reversible oxidation at around 1.0V



is shifted towards more positive potentials, at 1.05V. Two other oxidation processes are observable, one comparable to the mono Pd and one to the Pd Ag, at 0.08V and 0.69V, respectively. It is possible that these processes occur on the metal centre of the molecule. Six distinct reductions can be observed for this molecule. The two shallower and two more negative processes, at -0.23V, -0.60V, -1.37V and -1.86V can be related to those reductions on the macrocycle observed to all other molecules. Two other reductions can be observed at -0.92V and -1.15V, which are in the same range as the reductions of the mono Pd Hxp and the Pd-Ag Hxp. These reductions occur, possibly, on the metal centre of the molecule. Due to the similarity to the other molecules, possibly it is caused by the Pd centre, while having its potential shifted by the second metal.

Based on the hypothesis of the flagged processes are either centred on its metal or its macrocycle, checking the potential gap between each process half wave potential can give some insight as a characteristic criterion for the hexakis(pentafluorophenyl) [26] hexaphyrin electrochemistry. Table 5.3 presents the gap between the half wave potentials previously shown in Figure 5.16 as macrocycle centred. The difference of the first oxidation half wave to the first reduction is present around 1.18V to 1.43V. The Pd-Ag Hxp shows an unusually low oxidation potential which shifts the tendency of the material to present a process at around 1.30V. The difference of energy between the first and second reduction half wave process is between 0.30V and 0.42V, between the second and third is between 0.70V and 0.84V and lastly the difference between the two last processes is from 0.41 to 0.49V. Within a margin of error, these potential differences can be considered within the same range. The remaining processes are most likely metal centred, in which no specific trend can be observed since it is highly dependent on the nature of the metal.

TABLE 5.3. – DIFFERENCE BETWEEN HALF WAVE POTENTIAL FOR THE GIVEN PROCESSES CHARACTERIZED AS “MACROCYCLE” CENTRED IN FIG. 5.16.  $E_{ox}$  – HALFWAVE OXIDATION POTENTIAL,  $E_{red}$  – HALFWAVE REDUCTION POTENTIAL

	$E^1_{ox} - E^1_{red}$	$E^1_{red} - E^2_{red}$	$E^2_{red} - E^3_{red}$	$E^3_{red} - E^4_{red}$
<i>FB Hxp</i>	1.43	0.3	0.76	0.44
<i>mPd Hxp</i>	1.32	0.39	0.75	0.49

<i>PdPd Hxp</i>	1.35	0.42	0.7	0.48
<i>PdAg Hxp</i>	1.18	0.35	0.84	0.41
<i>PdCu Hxp</i>	1.28	0.37	0.77	0.49

The electrochemical band gap can be defined as the potential difference between the first oxidation half wave potential and the first reduction half wave potential. Table 5.4. shows the electrical band gap for the molecules of this study. Due to the oxidation centred on the metal for some of these hexaphyrins, some band gaps are unusually narrow, as for the *PdCu Hxp* and *mPd Hxp*. As described in the introduction of this chapter, the electrochemical band gap can provide the energy level of the HOMO and LUMO of the molecule. The determination of this value was important to try to correlate the electrochemical and spectroscopic data. However, while the spectroscopic data has several forbidden transitions, the electrochemical processes are limited by the energy to add or remove an electron. Therefore, the values of the electrochemical band gap are too narrow for this comparison.

TABLE 5.4. – ELECTROCHEMICAL BAND GAP FOR THE STUDIED MOLECULES

Band-Gap (V)	
<i>FB Hxp</i>	1.43
<i>mPd Hxp</i>	0.36
<i>PdPd Hxp</i>	1.35
<i>PdAg Hxp</i>	0.85
<i>PdCu Hxp</i>	0.31

## 5.4 – Partial Conclusion

The electrochemical characterization of the hexaphyrins were successfully performed. Several processes could be detected depending on the metal centres in the molecule. Several peaks could have a source in common for its oxidation and/or reduction: the macrocycle of the molecule. Several electrons could be donated to the  $\pi$ -conjugated backbone, at similar potentials and potential gaps in between each process, creating a criterion for its selection. Due to the lack of further characterizations of metallated [26] hexaphyrins in Hückel aromaticity in the literature, this criterion could not be expanded to check its validity. This is with acceptance with the literature of hexaphyrins since it has multiple conjugated backbones reported, from 26 electrons to 32 electrons. The remaining processes observed are characteristic for each metal.

Further information could be achieved with the use of coupled electrochemical techniques, such as electron paramagnetic resonance or UV-Vis. These techniques could provide details on the redox mechanism of the molecule and guarantee that the assumptions of each process occurring in the conjugated macrocycle on the metal centre are correct. While EPR analysis could not be achieved due to the high concentration needed for the electrochemical characterization, in-situ spectroscopy has not been investigated.

While it was desired these molecules would have activity towards electrocatalysis for reactions of interest, the metal centres added were chosen based on the aromaticity of the macrocycle, whereas their coordination geometry, at that moment was ignored.  $\text{Pd}^{+2}$ ,  $\text{Cu}^{+3}$  and  $\text{Ag}^{+3}$  have square planar geometry which are not expected to be able to coordinate molecules of interest. Further, the interaction between molecule and electrodes are weak and it could only be characterized in high concentrations solutions. Trials to support it on an electrode yielded no result. The use of specific ligands on meso-pyrrolic positions could improve this, as explained in the introduction of this chapter. Therefore, any electrocatalysis for this molecule would compete with the activity over the bare

electrode. In this scenario, oxygen reduction reaction has been tested to show a decrease in efficiency with the molecule in solution.

## 6 – Molecular electronic of Hexaphyrins

*As previously introduced, many bioprocesses occur through porphyrinoids, from catalysis, oxygen transport, electron transport and energy harvesting and conversion. Therefore, the importance of the study and comprehension of their electronic properties and functions is evident. Due to the ease with which the porphyrinoids properties are changed by structural modifications on its macrocycle, it is also a potential class of molecules to be the building blocks for the next generation of electronic devices based on molecules. However, despite of years of research the charge separation and electron transfer are not easily predicted from its structural properties.<sup>274,275</sup>*

### 6.1 – Introduction– Porphyrinoids in Molecular electronics

Porphyrin have been previously used in molecular electronics both in molecular array-based devices and as single molecule junctions.<sup>276</sup> In Molecular array-based studies the development of a mono-layer is necessary, where a common method is to use self-assembled monolayers.<sup>277</sup> Supramolecular chemistry plays a role in developing better systems to improve the assembly strategies and the way to package molecules in layers. The self-assembly of porphyrinoids has been a topic of wide variety of studies due to its proved relation to the application in electrocatalysis, photoelectric dyes, and sensors.<sup>278-281</sup>

Earlier porphyrinoid studies can be briefly explained by Drain *et al.* classification of its structure. It is divided in four parts that directly affects the molecular electronics properties: the surface-reactive functional group, the tether, the linker (exemplified in Fig. 6.1) and the electronically active part.<sup>282</sup>

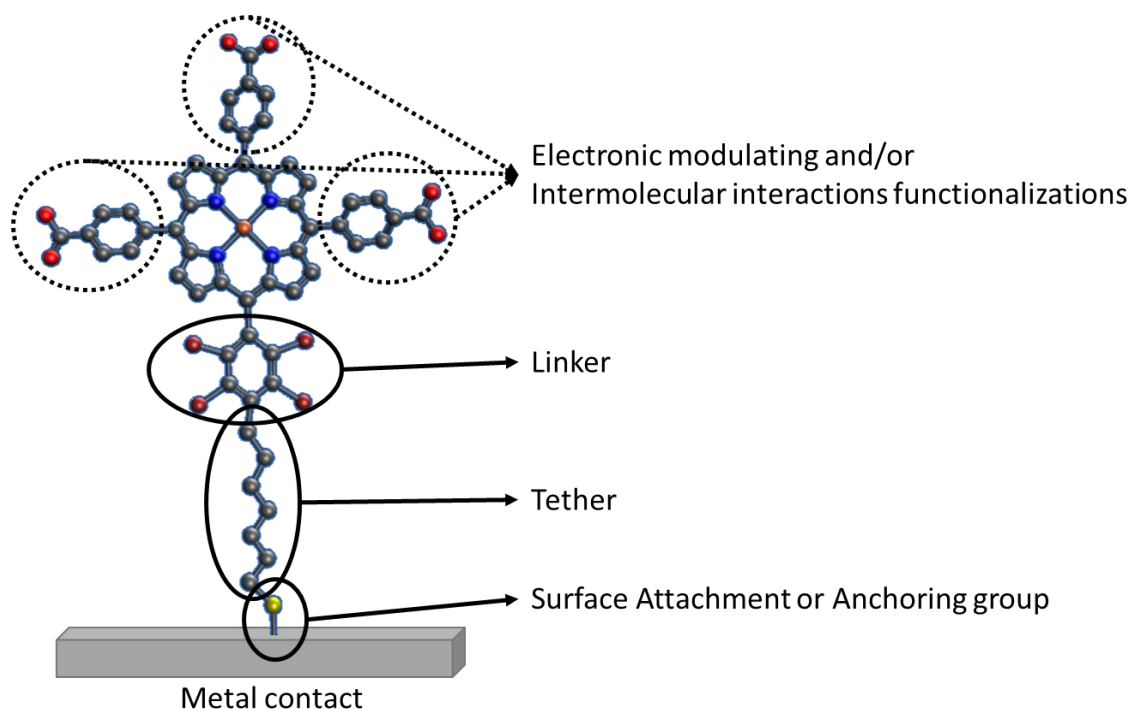


FIGURE 6.1 – Structural parts as classified by Drain *et al.* Based on reference 282.

The surface attachment, also defined as anchoring group, is a molecule terminal group with a high affinity for the electrode. It is responsible for the interaction between the molecule and the surface, which plays an important role in electron-transport properties.<sup>283</sup> The atomic configuration on the surface of a monocrystal can lead to distinct conductance as shown for thiols over gold,<sup>284</sup> where a coordination by a single bound or a symmetric multiple coordinated site over a monocrystal can lead to a variation on the conductance by a factor of 1.5. Further, the coupling of the orbitals between the substrate and the molecule, which relates to its adsorption strength, will also affect the electron transport properties,<sup>285</sup> whereas strong interactions are preferable due to a lower energy barrier for the electron to tunnel through.<sup>286,287</sup> For this reason, specific groups are often used in function of the employed metal substrates. On gold surfaces, thiol and disulfate groups are often used to link the molecules,<sup>288,289</sup> but several other groups have been successfully used as pyridines,<sup>290</sup> amines<sup>291</sup>, cyanines,<sup>292</sup> carboxylates,<sup>293</sup> etc. If the working metal is distinct, several other groups can be used such as carboxylates for Pt, diphosphines for Pd<sup>294</sup> and phosphonates for oxides.<sup>295,296</sup> Even though not ideal for molecular electronics,

porphyrinoids can be attached to the surface through weaker interactions. This scenario is not ideal due to the higher tunnelling barrier created by the lack of coupling between molecule and electrodes orbitals. However, interactions such as  $\pi$ - $\pi$  stackings or through an indirect anchoring group that can chelate with a metal centre can be achieved. The latest can also be used as a tool to guarantee that the orientation of the porphyrin will be parallel to the surface.

The tether allows the distance between the electroactive part and the surface to be changed, increasing or decreasing it. The nature of the tether will also influence the conductance, where a high conjugated one will have a lower  $\beta$ -decay than an alkylic chain, for example.<sup>297</sup> While a long tether hinders the electron tunnelling since it behaves as an extra potential barrier,<sup>298</sup> it is also used as a spacer between the electronically active part and the surface. While it is not desired for molecular electronics application, this spacing allows the correlation between the electronic transport properties and possible applications. A larger spacing allows bigger molecules to interact with the porphyrinoid and lead to improvements on its use for sensor and catalysis.<sup>299</sup>

The linker is the porphyrin macrocycle modification in which the tether and the surface attachment will be added. The linker has a strong influence as a core modification, and the electronic properties of the molecule will be affected by its electron donating or withdrawal properties.

Lastly, the electronically active part consists on the macrocycle with its functionalization. The conductance properties are strongly dependent on the energy levels of the molecule and its core functionalization, in which the metal centre or the  $\beta$  or meso ligands will influence the final properties. However, on molecular array devices the interactions between molecules play an important role. Therefore, the ligands used in the molecule can guarantee a low electronic intermolecular interaction, in which the properties of the molecule will have its properties evaluated, or groups in which the intermolecular interaction will be maximized can be used. In this case, it is expected a higher density of molecules and a distinct property due to the coupling of nearby molecules orbitals.<sup>300</sup> Further, porphyrinoids have two main orientations on the surface: parallel to the substrate, which shall be referred as orthogonal, or perpendicular to it, which will

be referred as axial. Changes in the electronically active part of the molecule will favour one orientation over the other.<sup>301-303</sup> While it is easier to functionalize the macrocycle for its study in axial conformation, in biosystems the porphyrin ring is perpendicular to the main pathway of the electron flow, in an orthogonal conformation linked through chemical ligands.<sup>304,305</sup>

The definition of Drain is consistent to the “first generation” of molecular arrays with porphyrins, whereas recent studies have moved towards more complex systems including linked molecules and controlled multi-layer of porphyrinoids. Through these approaches, several studies have been conducted showing a strong potential for its application in information storage,<sup>306-310</sup> and others such as current routers,<sup>311-314</sup> organic FETs,<sup>315</sup> spintronic devices<sup>316</sup> and, through the understanding of the electron transfer, on photovoltaic dyes.<sup>317</sup>

The molecule design for porphyrinoids study on mono molecular junctions can be done in analogy with the previous explained definition by Drain. However, there are several difficulties on the single molecule junction formation, and further details should be considered. A structural requirement is that the molecule has to connect simultaneously with two electrodes.<sup>318</sup> The probability for the break-junction to happen and its stability depends on how this interaction occurs.<sup>319</sup> As previously described, the conductance through a molecular<sup>320</sup> wire is highly influenced by the coupling of the orbitals between the molecule and electrodes,<sup>321</sup> and in this scenario a good molecule design should have anchoring groups adequate to the metal electrodes.

On STM-BJ experimental conditions, higher vibrational and rotational energy of molecules, variable distance of tip-substrate and the molecule environment can lead to the observation of multiple current signatures. In a simple molecule as an oligoene, for example, the electrical contact can happen by a terminal thiol group or through the conjugated  $\pi$ -system.<sup>318,322</sup> For more complexes molecules, it can be observed several current signatures, where they may have similar conductance, resulting in a broad distribution of signals in the same range, or conductance distinct by several order of magnitudes. In this scenario multiple approaches have been used to restrict the number of signals observed to those of interest, as the use of bulky or longer anchoring groups to



favour specific anchoring configurations,<sup>323, 324</sup> the addition of insulating orthogonal groups,<sup>325,326</sup> and even wrapping the desired molecule in larger macromolecules.<sup>327</sup>

Lastly, due to the lack of neighbouring molecules, the environment can directly affect its conductance. The STM-BJ of 1,4-benzenediamine (BDA) on gold changes up to 50% depending on the solvent used for the measurement, once the solvent molecules can bind to uncoordinated Au sites around the break-junction, changing the work function of the metal.<sup>324</sup> Furthermore, the solvent can lead to different solvation and distinct conformations, which might be favoured on the electrodes.<sup>324</sup>

On the case of porphyrinoids, several distinct molecules have been studied by molecular junctions.<sup>328-336</sup> While a proper use of anchoring groups can lead to higher junction stability,<sup>337</sup> a secondary influence of the anchoring group is the variety of molecular geometries that the molecule can acquire, each with different conductance values.<sup>338</sup> It is important to notice that the anchoring group position can also hinder the formation of a molecular junction in case it has any kind of steric hindrance.<sup>339</sup>

Often a metal centre is present and anchoring groups can be used to chelate on it, such as pyridines. As previously explained, two distinct conformations are possible: an axial and an orthogonal one, as described in Figure 6.2.<sup>340</sup> On the case of the diphenyl-porphyrin(DPP) and the Co-diphenil-porphyrin (Co-DPP), the conductance through the macrocycle doesn't suffer strong influence from the metal centre, showing two current signatures around  $3 \times 10^{-3}$  Go and  $8 \times 10^{-3}$  Go. The addition of the metal centre allows a new conformation with a higher current signature specific for the metal, at  $3 \times 10^{-2}$  Go. This same behaviour is also observed with other metal centres such as Zn, Ni and Cu.<sup>341</sup>

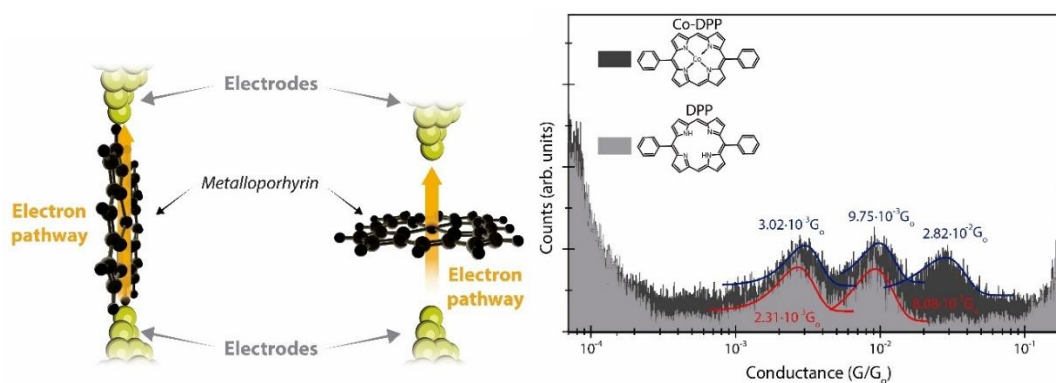


FIGURE 6.2 – Axial and orthogonal coordination between gold tips for porphyrin. And resulted conductance histogram.

A second stage on the porphyrinoids studies are from its derivatives. Molecular break junction can give insights in how porphyrin stackings work as antenna effect, and for this reason often linked porphyrins are studied.<sup>342</sup> Linked porphyrins have shown low to ultra-low attenuation factor,<sup>343-346</sup> and it is often in function of the coupling of its orbitals.<sup>347</sup> Fused porphyrin rings, however, have shown a negative  $\beta$ -decay, indicating an increase of conductivity with length.<sup>348</sup>

To date the only report in which hexaphyrins have been used for molecular electronic is a theoretical study on the conductance switching on free base hexaphyrins due to the aromaticity change from Hückel to Mobius.<sup>349</sup> Hence, this work tries to provide further information on this class of molecules.

## 6.2 – Methods

### 6.2.1 – Reactives

All reactive used in this work were of analytical purity. Hydrogen peroxide, sulfuric acid, 4-mercaptopyridine (MPy) and ethanol were purchased from Sigma-Aldrich and used as received. 1,2,4-trichlorobenze (TCB) were purchased from Merck and used as received. 4-(thiomethyl) pyridine (TPy) was received from Dr. Arantzazu Gonzalez Campo from Materials Science Institute of Barcelona.

The hexaphyrins were synthesized with collaboration of Prof. Dr. Kleber T. Oliveira and Dr. Maria C. Donatoni Santos as explained in Chapter 4 of this thesis.

Gold (111) monocrystals (10 mm x 1 mm) of 99.9999% purity and orientation accuracy <0.1 degrees were acquired from MaTeck.

### **6.2.2 – System preparation**

All glassware, PTFE tweezers and the homemade STM PTFE cell were cleaned with freshly prepared piranha solution, made with 3:1 volume ratio of sulfuric acid to hydrogen peroxide, for a period of 20 minutes. All items were rinsed with Milli-Q water (Millipore) in abundance.

The gold monocrystals used as substrates electrodes were annealed in hydrogen flame for a period of 6 minutes, followed by a brand surface electropolishing process. The oxidation was done in 0.1 mol.L<sup>-1</sup> sulfuric acid during 3 minutes to eliminate possible residual contamination in the surface of the electrode followed by a strapping of the Au oxide layers on the surface by immersing the monocrystal in a 1 mol.L<sup>-1</sup> hydrochloric acid solution. The gold was then re-annealed in hydrogen flame for 6 minutes and cooled down in Ar atmosphere to avoid molecules adsorption on the surface, such as oxygen.

The STM tips were mechanically cut, briefly annealed and then installed in the STM and immersed in the sample solution.

A solution of each analyte was prepared in sub  $\mu$ molar concentration and added to the cell after its assembly.

### **6.2.3 – Electrodes functionalization**

Au tips and substrates were functionalized after annealing. The gold was immersed in 1 mM Ar-purged ethanol solution of 4-mercaptopyridine or 1mM 4-(thiomethyl) pyridine for a period of 24h under an Ar inert atmosphere.

The gold was then rinsed with EtOH and Milli-Q water and dried with Ar before being assembled in the STM.

## 6.2.4 – STM Methods

STM – BJ techniques were discussed in session 1.1. and its relevant papers are referred properly. All experiments were carried out using a homemade Teflon STM cell on a magnetic plate. The experiments were carried out on a PicoSPM II Microscope head controlled using Picoscan 2500 electronics, all from Agilent (USA). The system was completely isolated mechanically and electronically to avoid noise. The data was acquired through a NI-DAQmx/BNC-2110 National Instruments (LabVIEW data acquisition System), with data collection and analysis with LabVIEW code designed by Diez-Perez Group at King's College London.

The equipment has a current pre-amplification system that can be manually swapped in between experiments. LabVIEW interface reads the data in the converted voltage from the tunnelling current detected. So, the reading could be converted to conductivity by the formula:

$$I_t = V * P; \quad G = \frac{I_t}{U_{applied}} * \frac{1}{G_0}$$

Where  $I_t$  is the tunnelling current in Ampere,  $V$  is the current output captured as voltage (in volts),  $P$  is the pre amplification used in A/V,  $G$  is the molecule conductance and the  $U_{applied}$  is the bias applied between the grounded tip and the substrate.  $G_0$  is the quantum conductance:  $7.7480 * 10^{-5}$  S.

### 6.2.4.1 – Tapping (Iz)

After the system assembly, the STM tip is brought to tunnelling regime over the surface electrode area. The STM feedback is then turned off and the piezo control over the tip electrode is done through the LabView tool. The STM tip is brought in and out of contact with the substrate at a constant speed, in V/s, from 0.5 to 2 V/s, controlling the approach and retraction from the surface through the current tunnelling through the tip. This creates a two-point feedback used to collect thousands of current decays during the tip retracting cycle, 350 as

exemplified in Fig. 6.3. The saturation level at the beginning of the curve (a) corresponds to the maximum current reading of the equipment, where the tip is touching the surface of the monocrystal. When the tip is withdrawn from the surface in tunnelling regime, an exponential current decay can be observed. If a molecule junction is formed, there will be steps or *plateaus* in the tunnelling decay (b), where the conductance of the molecule can be determined. Lastly, upon separation between tip and substrate the current reading will decay until an open circuit current will be read (c), without any current flow.

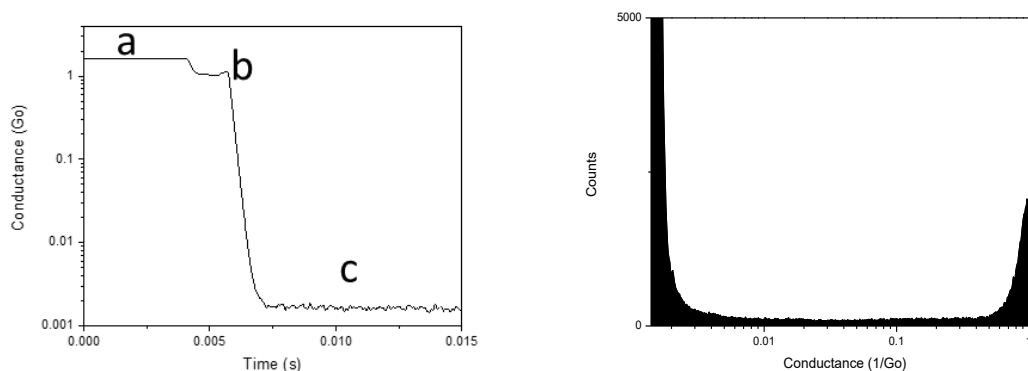


FIGURE 6.3 – Representation of the current decay on the pulling cycle of tapping method (left) and a 1D conductance histogram (right) created out of contacts formed between Au STM tip and Au monocrystal.

The decays containing current signatures were selected using selection criteria. Curves that are too noisy or decays were no plateau could be observed have been rejected sure to the lack of molecular junctions. The selected current decays with the observed plateaus were accumulated in semi-log conductance histograms, where the observed plateaus provide an average single molecule conductance value.

#### 6.2.4.2 – Blinking (It)

After the system assembly, the STM tip is brought to an initial set-point tunnelling current. The STM feedback is then turned off and the tunnelling current is monitored for the formation of molecular bridges. The spontaneous

molecular events, coined as “blinks”, appear due to the spontaneous formation of molecular bridges as explained in section 2.1.2. The blinking data is plotted either as a 1D conductance histogram or as a 2D conductance, shown in Fig. 6.4., using a LabVIEW tool/code.

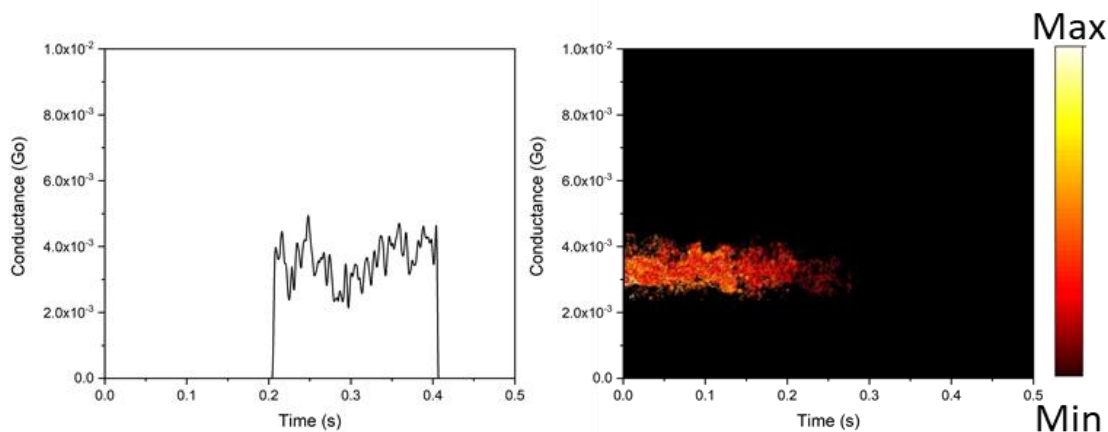


FIGURE 6.4 - Representation of the current blink (left) and its 2d conductance map (right) created by the accumulation of blinks. The 2D blinking maps were normalized versus the total amount of counts (100 counts representing the maximum and 0 representing the minimum) and a vertical offset to zero current was applied to the baseline such that the single-molecule junction component is displayed clearly (tunnelling background subtracted).

## 6.3 – Results

### 6.3.1 – Non modified electrodes

The first approach to the study of the molecules was through tapping method employing non-modified gold electrodes. Due to the limitation on the current detection range, two pre-amplifications were used: 100 nA/V and 1 nA/V, so conductance in the range from 1 Go to 10<sup>-6</sup> Go could be obtained under the applied bias voltages. After setting the experiment, over five thousand break junctions were collected with the objective of obtaining a histogram of possible current signatures.

From Fig. 6.5 to Fig. 6.9, the 1D conductance histogram for each molecule in each pre-amplification range is shown. All the molecules have a peak at 1 Go, corresponding to the gold quantum contact point ( $2e^2/h = 77.45 \text{ } \square\text{S}$ ). The non-modified surface did not show any current signature of the molecule possibly because of the weak interaction with gold. This could be caused by the lack of chemical affinity between the gold and the molecule meso-ligands. An alternative explanation regarding the lack of current signatures is the possibility of the molecule having a high resistance, in which case the current signature could be below the equipment detection limit. This high resistance is not expected on highly conjugated molecules, so it is unlikely to be the case. Some of the histograms for the pre-amplifier at 1nA/ show a sharp increase in counts around  $4 \cdot 10^{-5}$  Go while others show a broad increase. Both signals correspond to the baseline current, and the profile is because of the use of distinct pre-amplifiers of the same range and their inherent current detection limits.

The blinking approach was used for these molecules, but no signal was observed.

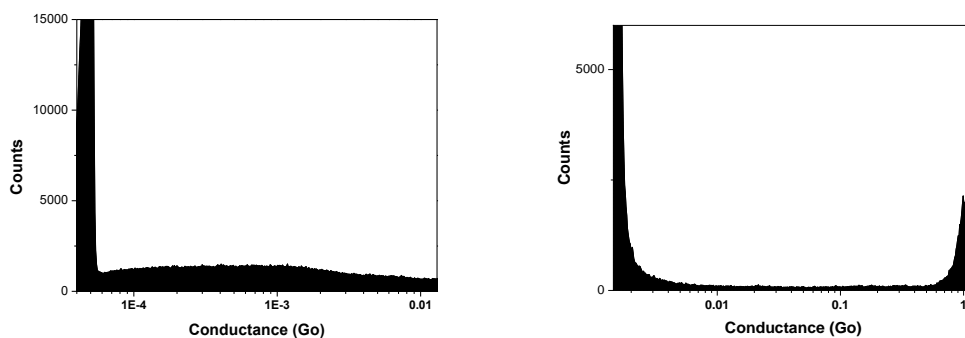


FIGURE 6.5 – Histograms acquired through tapping approach for Free base Hexaphyrin, TCB as solvent. The working bias voltage was set on +10 mV, employing a tip electrode. Measured using 100 nA/V (right, 36% yield) and 1 nA/V (left, 29% yield).

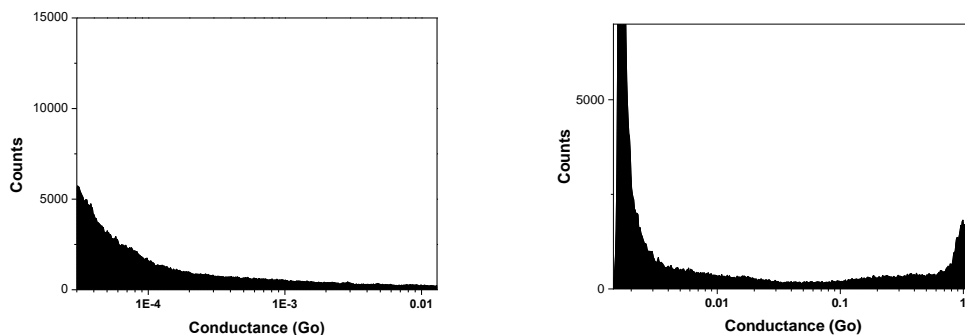


FIGURE 6.6 – Histograms acquired through tapping approach for mono Pd Hexaphyrin TCB as solvent. The working bias voltage was set on +10 mV, employing a tip electrode. Measured using 100 nA/V (right, 39% yield) and 1 nA/V (left, 32% yield).

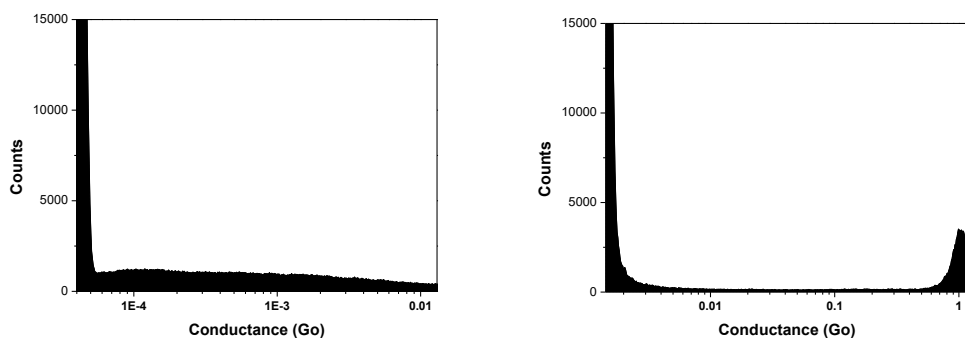


FIGURE 6.7 – Histograms acquired through tapping approach for Pd-Pd Hexaphyrin, TCB as solvent. The working bias voltage was set on +10 mV, employing a tip electrode. Measured using 100 nA/V (right, 38% yield) and 1 nA/V (left, 41% yield).



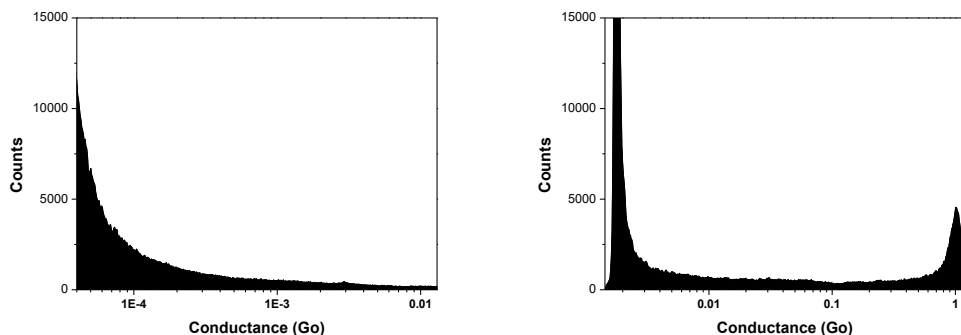


FIGURE 6.8 – Histograms acquired through tapping approach for Pd-Ag Hexaphyrin, TCB as solvent. The working bias voltage was set on +10 mV, employing a tip electrode. Measured using 100 nA/V (right, 42% yield) and 1 nA/V (left, 32% yield).

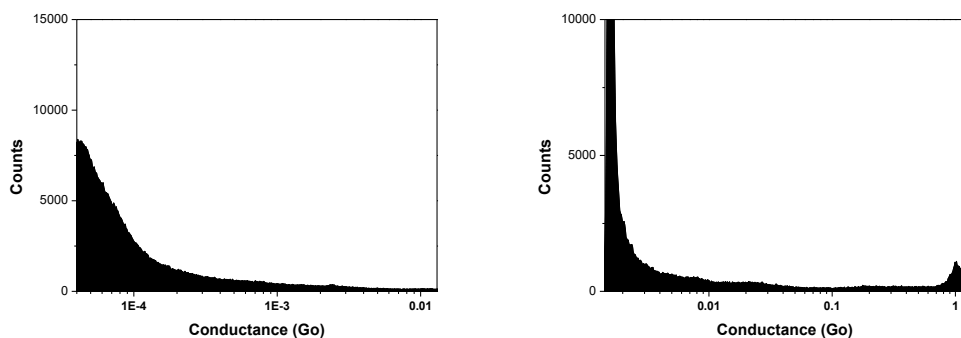


FIGURE 6.9 – Histograms acquired through tapping approach for Pd-Cu Hexaphyrin, TCB as solvent. The working bias voltage was set on +10 mV, employing a tip electrode. Measured using 100 nA/V (right, 43% yield) and 1 nA/V (left, 34% yield).

### 6.3.2 – 4-mercaptopyridine modified gold

The following step was to measure the molecule with a gold modified tip and substrate electrodes. At this moment, the used molecule to anchor the target molecule was 4-mercaptopyridine. While the molecules synthesized do not seem to have a direct interaction with the gold, the metal centres could be used to anchor the molecules perpendicularly to the surface through the linker as described in Fig. 6.10.

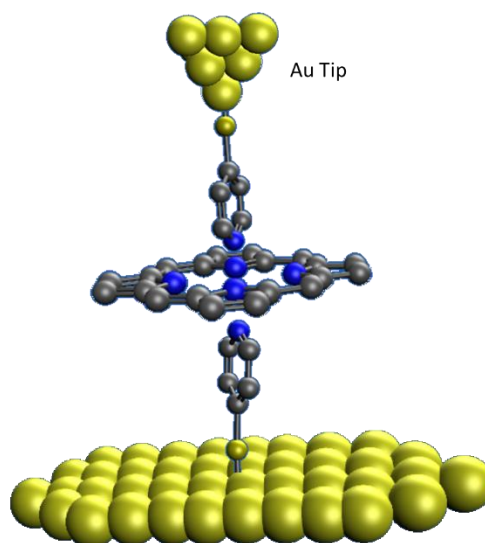


FIGURE 6.10 – Representation scheme of a possible interaction between 4-mercaptopyridine and Pd-Ag Hxp. The meso-pyrrolic ligands and hydrogen atoms have been removed for clarity.

The 1d conductance histograms for the molecules of this study are represented from Fig. 6.11. to Fig. 6.15. Similarly, to what was observed for the non-modified gold, on low pre-amplification,  $100\text{nAV}^{-1}$ , the peak corresponding to 1 Go is observed. However, no other current signature band can be observed in either pre amplification.

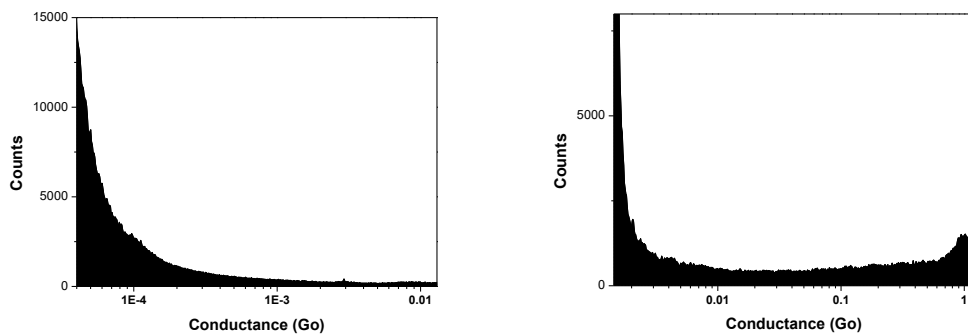


FIGURE 6.11 – Histograms acquired through tapping on MPy modified Au for Free base Hexaphyrin, TCB as solvent. The working bias voltage was set on +10 mV, employing a tip electrode. Measured using 100 nA/V (right, 33% yield) and 1 nA/V (left, 48% yield).

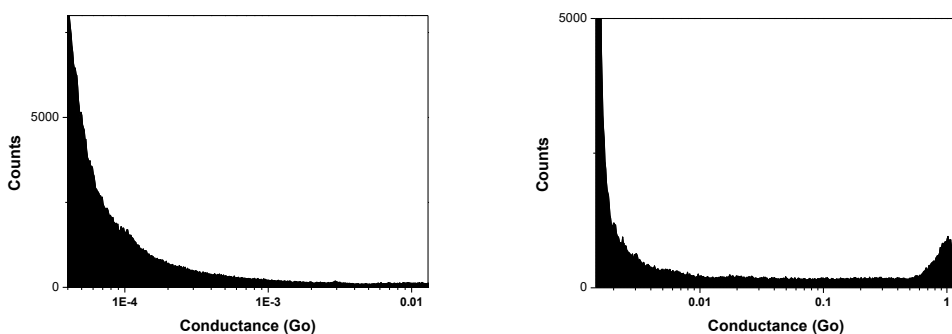


FIGURE 6.12 – Histograms acquired through tapping on MPy modified Au for mono Pd Hexaphyrin, TCB as solvent. The working bias voltage was set on +10 mV, employing a tip electrode. Measured using 100 nA/V (right, 38% yield) and 1 nA/V (left, 31% yield).

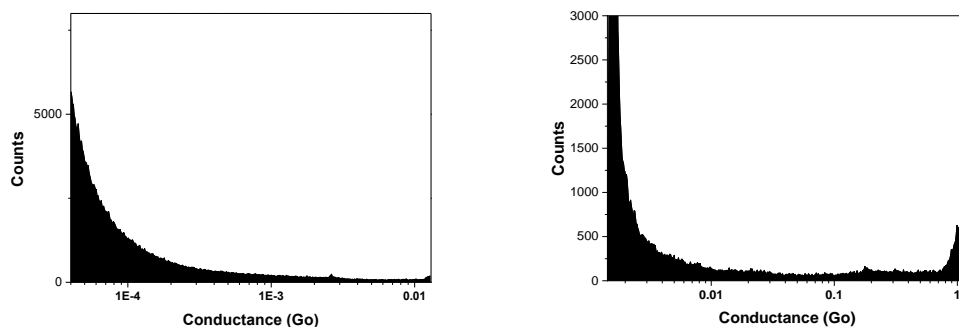


FIGURE 6.13 – Histograms acquired through tapping on MPy modified Au for Pd-Pd Hexaphyrin, TCB as solvent. The working bias voltage was set on +10 mV, employing a tip electrode. Measured using 100 nA/V (right, 22% yield) and 1 nA/V (left, 29% yield).

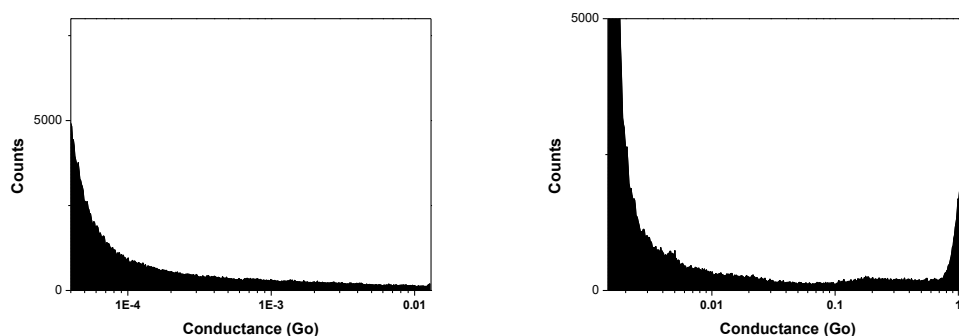


FIGURE 6.14 – Histograms acquired through tapping on MPy modified Au for Pd-Ag Hexaphyrin, TCB as solvent. The working bias voltage was set on +10 mV, employing a tip electrode. Measured using 100 nA/V (right, 26% yield) and 1 nA/V (left, 27% yield).

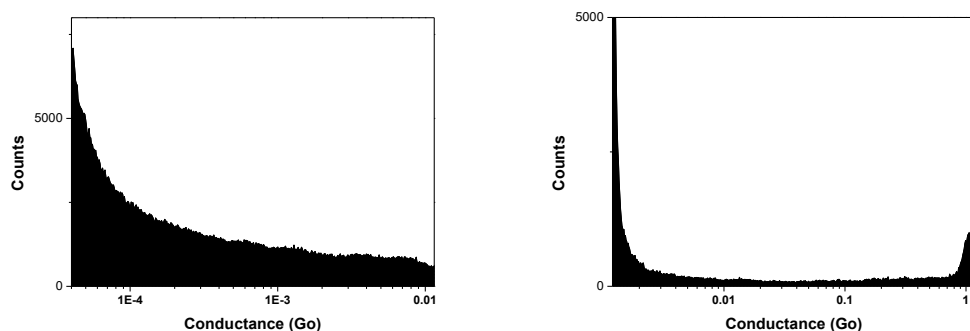


FIGURE 6.15 – Histograms acquired through tapping on MPy modified Au for Pd-Cu Hexaphyrin, TCB as solvent. The working bias voltage was set on +10 mV, employing a tip electrode. Measured using 100 nA/V (right, 21% yield) and 1 nA/V (left, 37% yield).

While it is likely no signal could be observed due to the lack of interaction between molecule and modified electrodes, a second reason that could lead to the lack of signals is the fact the tapping approach is not the optimal technique to use on modified electrodes. The constant crashing between gold surface and the tip may lead to a defunctionalisation by coverage of the tip and/or migration of the 4-mercaptopyridine. Furthermore, the interactions between the anchor with the metal centres are expected to be weak due to the preferable d4 geometry of the metal centres, in which case the molecular junctions would have a lifetime too short to be capturable with the amplifier resolution. For this reason, the blinking technique was also used to characterize these molecules. A single signal was observed for these molecules as shown in Fig. 6.16, however, this signal corresponds to the molecular junction of the 4-mercaptopyridine itself, showing that the tentative to coordinate the molecule was not succeeded, in which there is a higher affinity between the linker molecules than the linker-macrocycle.

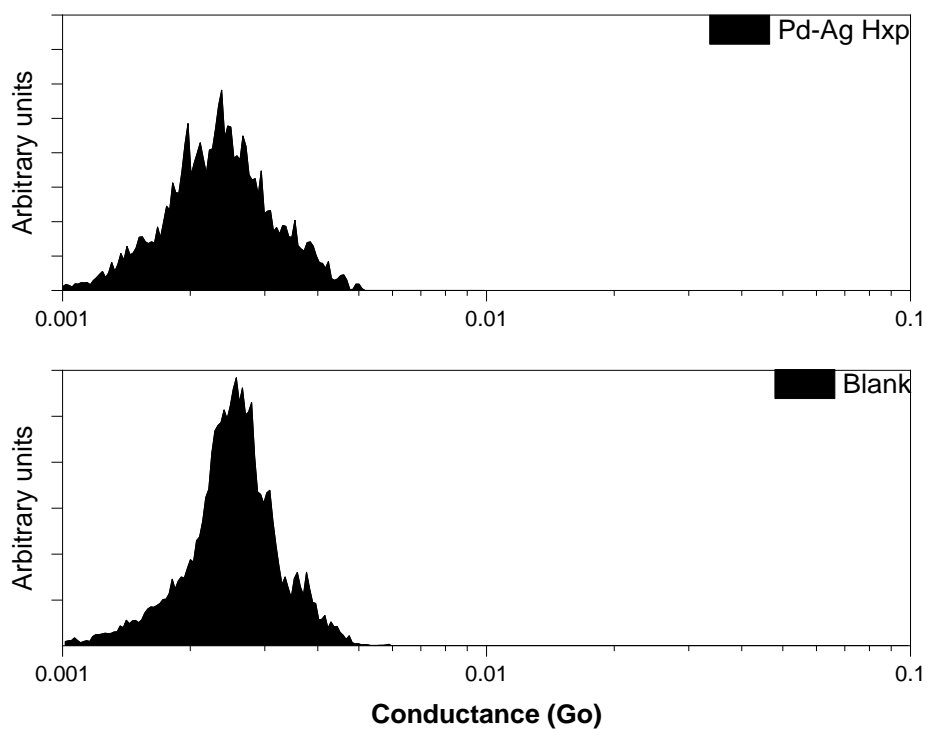


FIGURE 6.16 – 1d Histograms acquired through blinking on MPy modified Au for Pd-Ag Hexaphyrin control experiment without molecule, TCB as solvent. The working bias voltage was set on +10 mV, employing a tip electrode. Measured using 100 nA/V as pre-amplifier.

### 6.3.3 – 4-(thiomethyl) pyridine modified electrodes

Previous results in porphyrins showed a better response on 4-(thiomethyl) pyridine modified gold over 4-mercaptopyridine due to the possibility of  $\pi$ - $\pi$  stacking in addition to the complexing over the metal centre,<sup>351352</sup> as schematized for diphenylporphyrin in Fig. 6.17. Analogously, there is the possibility of the interaction between the TPy and the conjugated  $\pi$  macrocycle of the hexaphyrins. Due to the gold functionalization, tapping was not used as an approach at this stage.

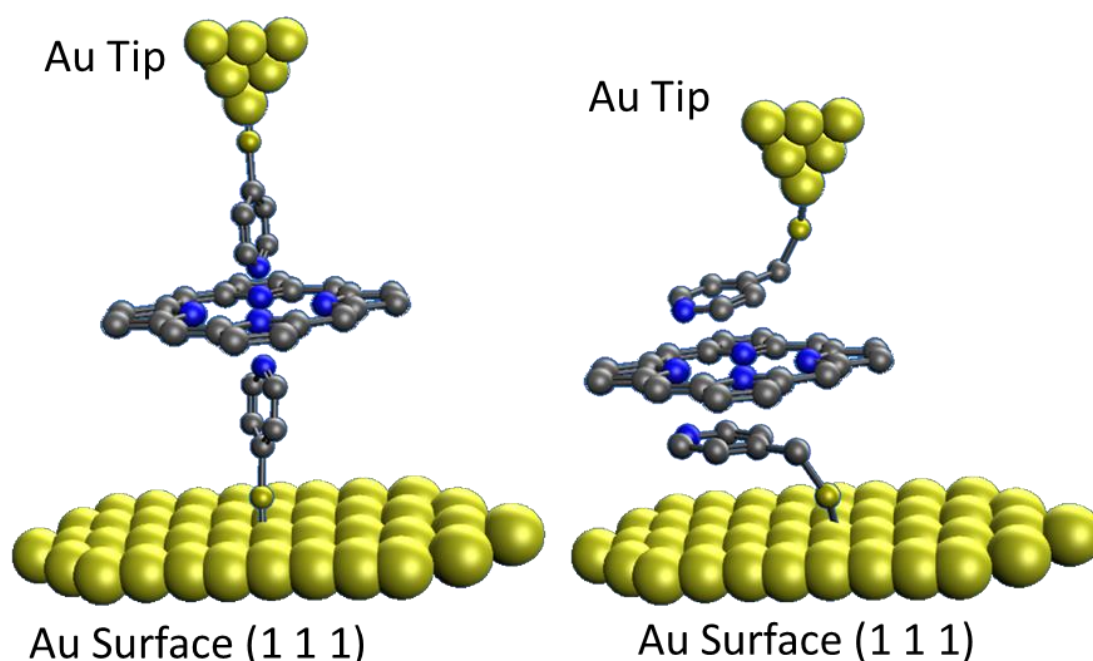


FIGURE 6.17 – Distinct interactions possible between 4-mercaptopyridine and 4-(thiomethyl) pyridine for diphenyl porphyrin.

The 1d histograms acquired through blinking for all the molecules are represented Fig. 6.18. All histograms show broad bands over 4 orders of magnitude, from  $10^{-6}$  Go to  $10^{-2}$  Go. This happens due to the molecule's design, as there are many possible interaction points between the modified gold and the molecule. Distinct interaction corresponds to distinct current signatures.<sup>353</sup>

The Free base hexaphyrin, Fig. 6.18, shows all the current signatures through the macrocycle. When compared to the molecules with metal centres, a noticeable change in the profile of the conductance bands is noted,

even though, all the processes still occur in the same range as the macrocycle current signatures.

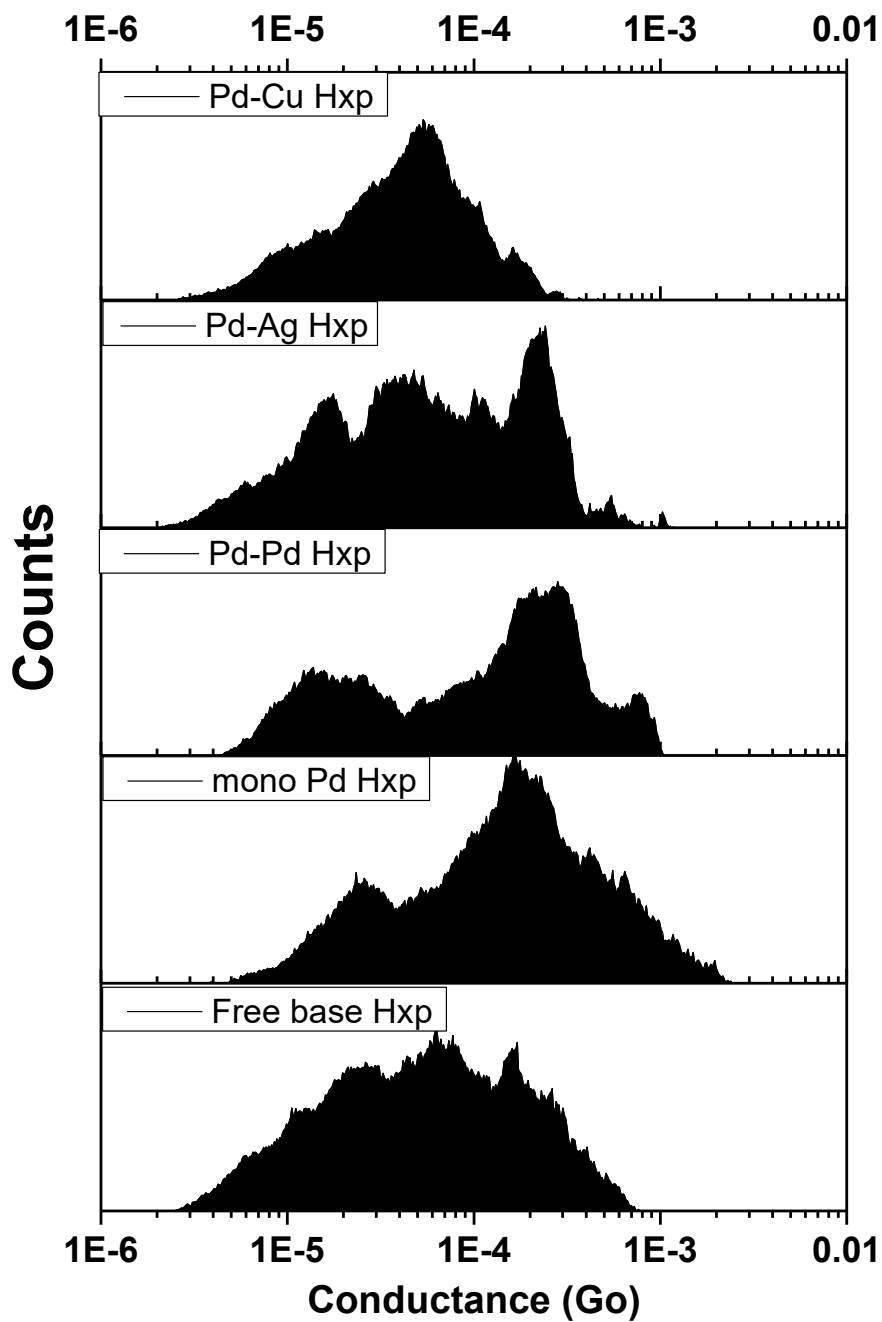


FIGURE 6.18 – Histograms acquired through blinking on TPy modified Au for the studied hexaphyrins, TCB as solvent. The working bias voltage was set on +15 mV, employing a tip electrode.



A tool to decrease or restrict the number of signals is necessary to understand what is happening. As previously discussed, the distance between tip and surface can restrict the possible conformations the molecular bridge can assume. Therefore, two distinct tunnelling currents setpoints were used as parameters to collect blinks: 1 pA and 0.100 nA. Considering a coherent electron tunnelling as described in section 2.1, the  $\beta$ -decay of the measured systems could be estimated as approximately  $8.2 \text{ nm}^{-1}$ . Therefore, a difference of 0.6 nm can be expected between the setpoints, where the setpoint 1pA should be at 1.7nm from the surface and the setpoint 0.1 nA should be at 1.1 nm from the surface. The axial coordination between Au-TPy-CoDPP-TPy-Au was shown by DFT calculations to require around  $1.8\text{nm}^{340}$  and, from this estimative, it is expected that the 1pA setpoint to be able to coordinate through the metal centre while at closer tip-surface distance other interactions between TPy and molecule to occur.

Fig. 6.19 shows the 1d conductance histogram for each molecule at the new pre-set parameters. Upon approaching the tip setpoint from 1 pA to 0.1 nA, a similar behaviour occurred to all molecules. The current signatures at the range of  $10^{-5} \text{ Go}$  do not show up, which is caused by the hinder of some conformations by the hexaphyrin with the proximity with electrode, whereas in further tip-substrate distance a molecular junction through the axial conformation is more likely.<sup>340</sup>

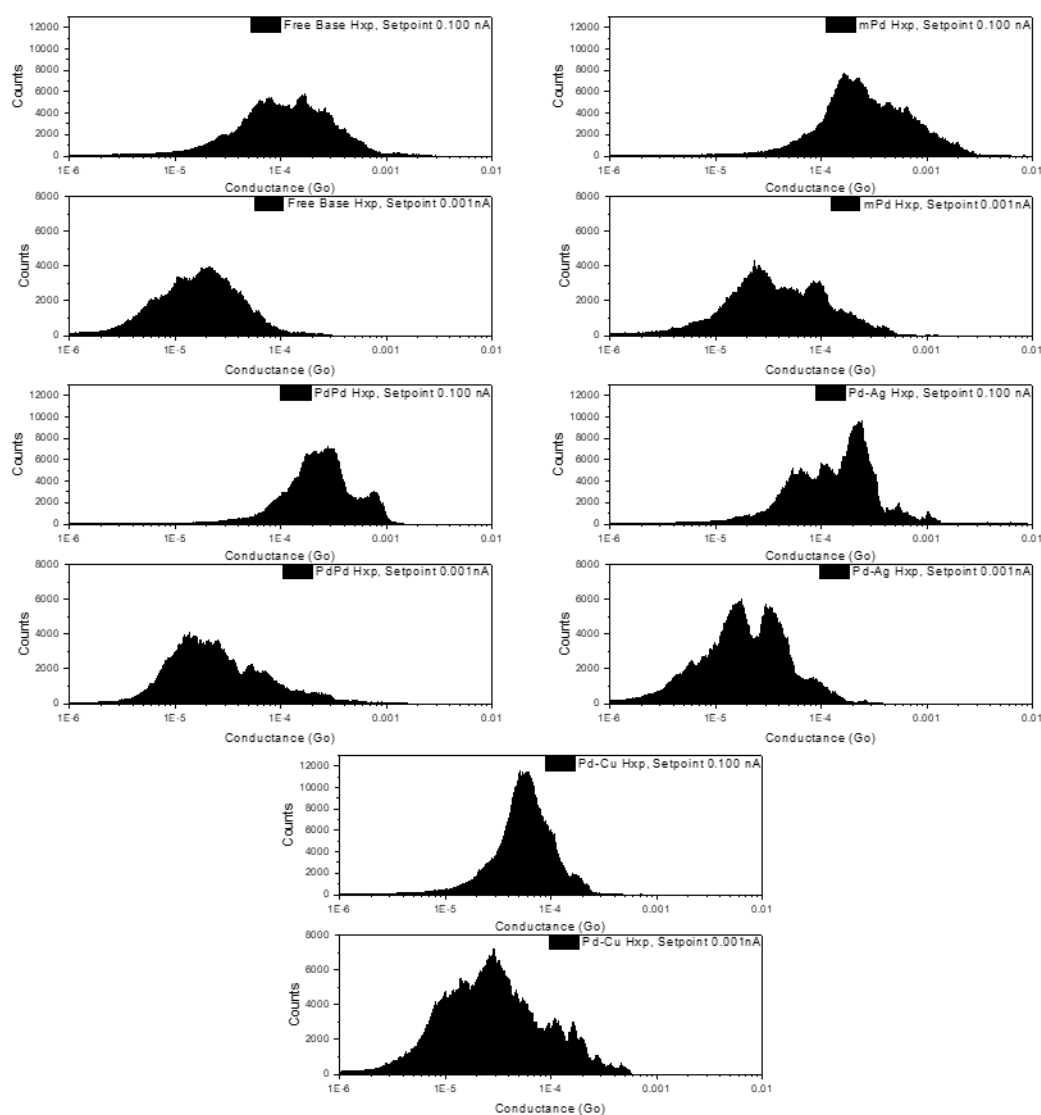


FIGURE 6.19 – Histograms acquired through blinking on 4-(thiomethyl) pyridine modified Au for all the molecules synthesized at setpoint 0.1 nA or 1 pA. 1,2,4-trichlorobenzene as solvent. The working bias voltage was set on +15 mV, employing a tip electrode.

Fig. 6.20 shows the 1d conductance histogram for all the studied hexaphyrins at setpoint 1 pA and a blink event from each current signature. Comparing the several 1d histograms on same setpoint, it is possible to observe trends when a metal centre is added to molecule. The free base hexaphyrin has the current signatures corresponding to the backbone of the macrocycle, which can be observed on all molecules and, for this reason, not highlighted. Upon addition of Pd, there is a current signature at higher conductance range, around  $10^{-4}$  Go and highlighted with a circle. This current signature is present on all the

metallated systems, indicating that the tunnelling through this conformation is dependent on the presence of the Pd. Observing the blink sampling on Fig. 6.20 for these metals, the blinks for this conformation are often short and infrequent, resulting in a smaller amount of counts when compared to the macrocycle current signatures. Upon addition of a second metal centre, represented as a square on the conductance histogram, a second region is highlighted. On Pd-Ag hexaphyrin a second current signature is well defined at  $2 \times 10^{-5}$  Go. This current signature is present on the other histograms but not as enhanced, once the current signatures corresponding to the macrocycle are present on all this range. On the case of Pd-Cu hexaphyrin the featured current signature is at  $1 \times 10^{-5}$  Go, showing a similar current signature to the Ag interaction.

Lastly, an important information that can be retrieved is the average lifetime for the blinks at each current signature. The 2D blinking maps was created by the accumulation of hundreds of blinks, shown in Fig. 6.21. The stability of the blinks can be evaluated through the average lifetime of the current captures. For all molecules, there is a large distribution of current signature as shown in the 1d histograms, where the weak interactions between them and the modified electrodes made the blinks, on average, have a short lifetime of bellow 0.1 second. This is an issue that could be improved through proper functionalization of the molecule, as it is demonstrated with further experiments.

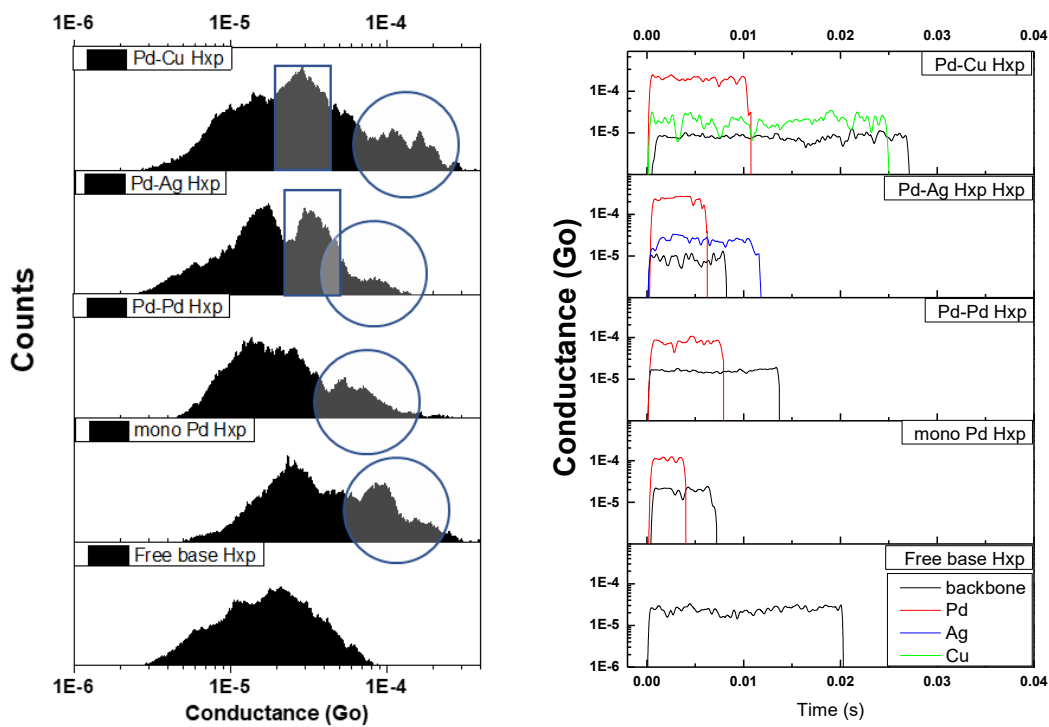


FIGURE 6.20 – Histograms (left) acquired through blinking on TPy modified Au for the studied hexaphyrins, TCB as solvent. The working bias voltage was set on +15 mV, employing a tip electrode. The setpoint for blinks was set as 1 pA. Example of blinks for each current signature (right) on same conditions.

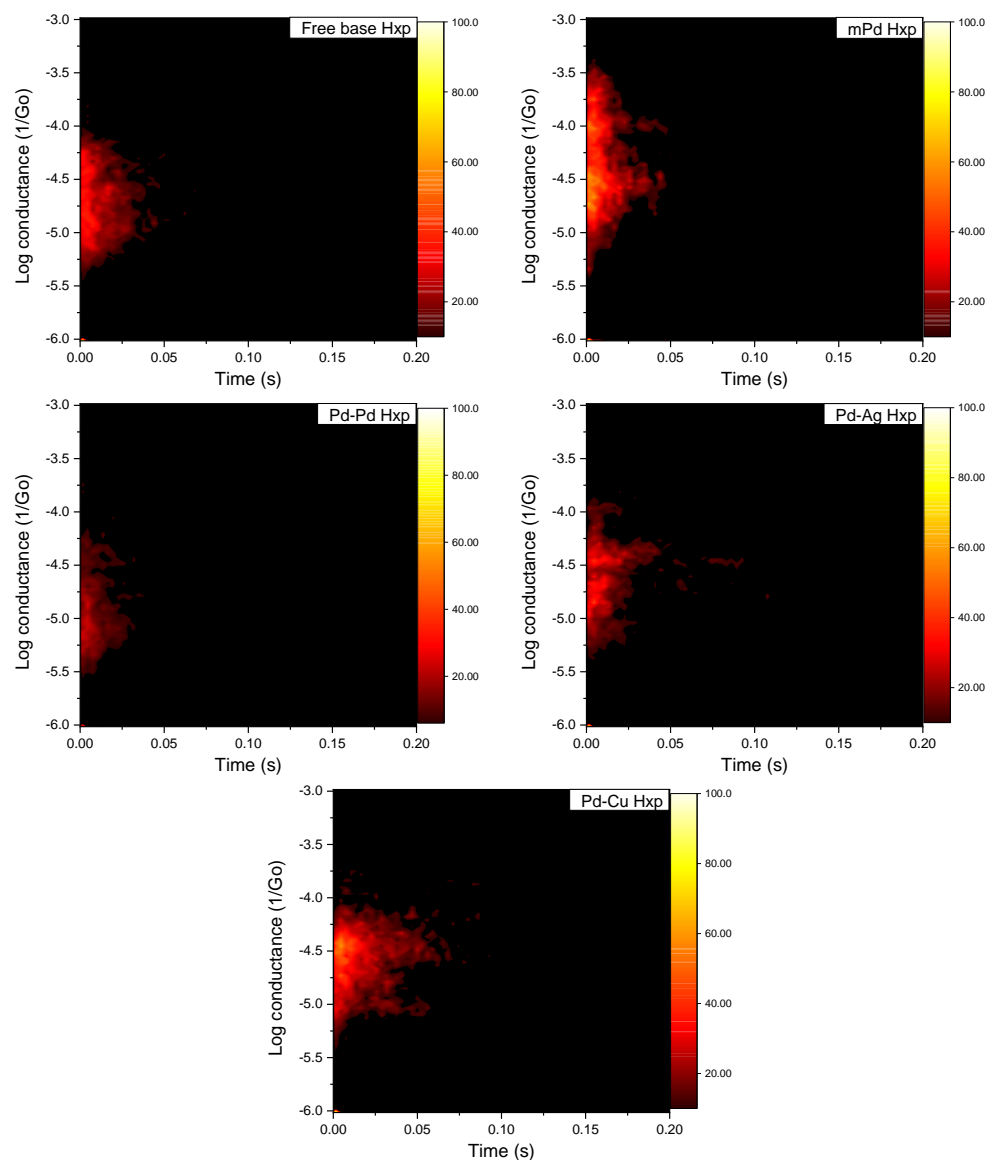


FIGURE 6.21 – 2-dimension blinking maps were built by the accumulation of hundreds of blinks at a common time x axis origin.

Fig. 6.22 shows the 1d conductance histogram for all the studied hexaphyrins at setpoint 0.1 nA. As previously discussed it was possible to restrict the current signatures by changing the setpoint of the measurements. While at setpoint 1 pA it was possible to observe a pattern between samples, at this condition there is no visible model for them. It is difficult without theoretical simulation to understand this behaviour, once the conductivity of the molecule depends of multiple factors, from the frontier orbitals energy difference from the fermi energy level of the electrodes or its coupling with the substrate,<sup>353</sup> as previously explained. To properly study this set of data, it is necessary

computation studies to determine its possible conformations between modified gold and then calculate its current signature.

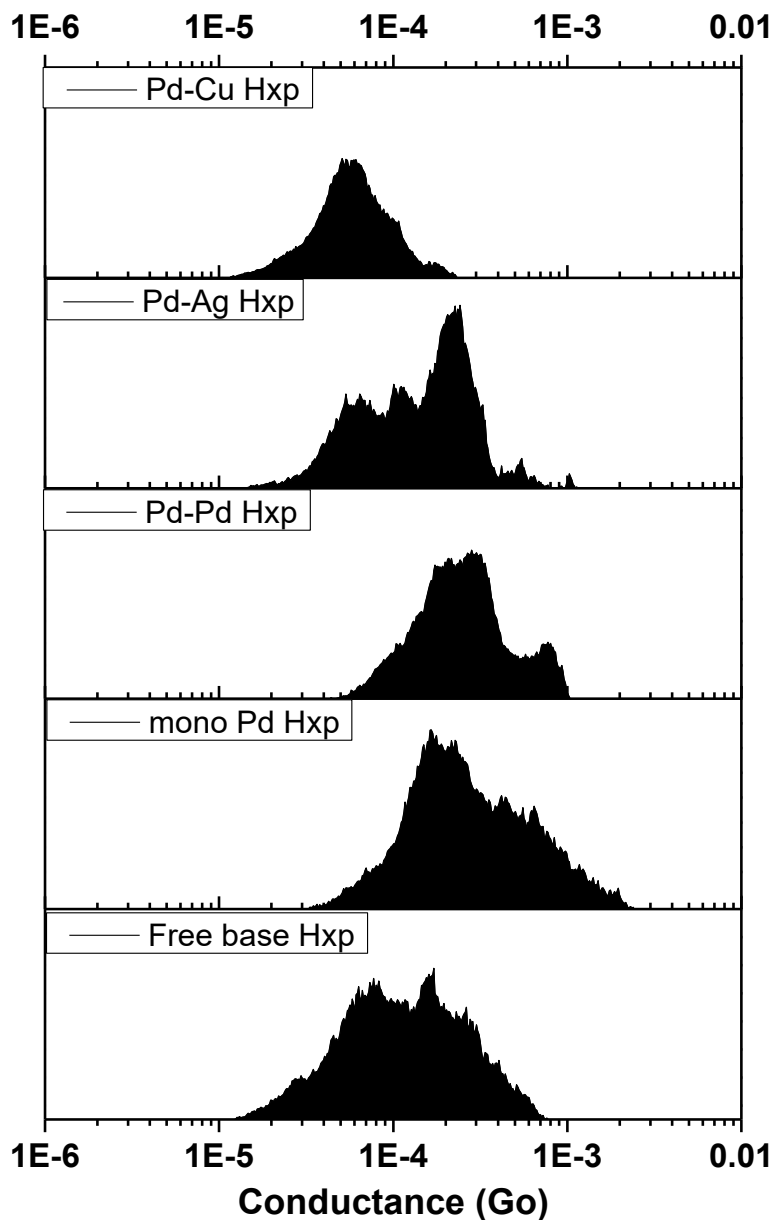


FIGURE 6.22 – Histograms acquired through blinking on TPy modified Au for the studied hexaphyrins, TCB as solvent. The working bias voltage was set on +15 mV, employing a tip electrode. The setpoint for blinks was set as 0.100 nA.

## 6.4 – Partial Conclusion

The molecular conductance signatures of the hexaphyrins could only be detected upon modification of the gold surface with 4-(thiomethyl)pyridine. This could be reasoned by the lack of a robust interaction from the molecules with non-functionalized electrodes and the difficulty of direct anchoring through octahedric chelation of the metal centres with the 4-mercaptopyridine.

Several conductance signatures in a same range were observed due to plausible multiple contact geometries between the molecule with the modified gold surface: from the several meso-pyrrolic ligands to the bulky macrocycle through  $\pi$ - $\pi$  stacking as it have been observed in previous works (refs). Some of these current signatures were evident to be the due electron pathways directly through the metal centre over the macrocycle, in which specific current signatures were observed uniquely under the presence of the metal centres: around  $1 \cdot 10^{-4}$  Go for Pd-Hxp ,  $2 \cdot 10^{-5}$  Go for Ag-Hxp and  $1 \cdot 10^{-5}$  Go for Cu-Hxp. The blinks corresponding to the macrocycle has shown a higher stability than those related to the metal centres. All blinks were brief with an average lifetime bellow 0.1 s. Upon decreasing the distance between tip and substrate by 1.7 nm, several new current signatures could be observed with a higher conductance value, up to  $10^{-3}$  Go. This is possibly caused by stronger interactions between the macrocycle and its metals centres and the TPy anchor. However, due to the number of distinct current signatures and the broad histograms obtained, it is not possible to infer over what interaction results in each conductance. For further details on this experimental setup, it would be necessary the study of related contact geometries and its conductance through theoretical simulation, which is not the scope of this thesis.

There is a design flaw of the molecules of the study, in which the presence of several meso-ligands is present, giving many distinct interaction positions with similar current signatures. Further, the lack of a functionalized group with strong interaction to the gold surface to further restrict

the possible conformations of the molecular junction lead to broad bands in which is difficult to distinguish the effect of the macrocycle and the metal centres as other studies could achieve.



## 7 – Conclusion

The absorption spectrum of the hexaphyrins is complex and the band gap of the material cannot be easily determined through it. The optimal way to determine its band gap is through fluorimetry, showing that for Free base Hexaphyrin the optical band gap is 1.12V. With the metalation of the macrocycle, there is a quench in its emission intensity until it is barely detectable. The optical band gap is 1.12eV (monoPd Hxp), 1.17V (Pd-Pd Hxp), 1.20V (PdAg Hxp). The insertion of the metal may lead to distinct decay modes, either vibrational or with interaction with other molecules. The Pd-Cu Hxp doesn't have an observable emission spectrum.

The electrochemical behaviour of the hexaphyrins show distinct quasi-reversible redox pairs. Upon addition of distinct metal centres, the potential in which the reactions occur changes in function of the electronegativity of the added metal. A similar behaviour with potential spacing between redox pairs could be observed for all molecules, indicating a criterion for determining the macrocycle processes potentials. The distance between first and second reductions half wave potentials is in the range of 0.30V to 0.42V, from second to third reduction half wave potential from 0.70V to 0.84V and from the third to fourth reduction half wave potential from 0.41V to 0.49V. The remaining potentials can be easily related to each other because they have a strong influence from the metal nature in the macrocycle.

The molecular conductance signatures of the hexaphyrins could only be detected upon modification of the gold surface with 4-(thiomethyl)pyridine. This could be reasoned by the lack of interactions from the molecules with non-functionalized electrodes and the difficulty of direct anchoring through octahedral chelation of the metal centres with the 4-mercaptopyridine. In the case of the 4-(thiomethyl)pyridine it is likely that the molecule is also interacting through  $\pi$ - $\pi$  stacking with the macrocycle. Several conductance signatures in a broad range could be observed due to several contact geometries possible between molecule and modified Au substrate. These could be separated by a change in the distance between tip-substrate. It was possible to detect conductance ranges specific for current signatures for pathways through the metal centre over the macrocycle: of

$1 \times 10^{-4}$  Go for Pd-Hxp,  $2 \times 10^{-5}$  Go for Ag-Hxp and  $1 \times 10^{-5}$  Go for Cu-Hxp. However, several other current signatures were registered which interaction between TPy and molecule cannot be easily explained.

Overall, while all these molecules could be characterized in this study, several hindrances were observed due to improper molecule design. For its electrochemistry analysis, the functionalization for better interaction with the substrate would lead to an easier study and a possibility of its use in electro catalysis, since a monolayer of these materials could be done and measured over distinct solvents. For molecular electronics, reducing the number of meso-pyrrolic ligands would lead to a great reduction in the current signatures observed. Further, with the exception of the free base Hxp and the Pd-Pd Hxp, these molecules are not symmetrical. A further improvement would be to have a protected group such as acetomidomethyl group, which could be unprotected after adsorption on gold and guaranteeing a single orientation of the molecule.

This thesis covered several distinct fields: organometallic synthesis, electrochemistry and molecular electronics. Each of them could, by itself, be further developed and result full project by itself, provided time and material would be present. Time was a limiting factor for the synthesis, which the ideal molecular design couldn't be achieved for the study even after 2 years of dedication. The lack of expertise in electrochemistry in non-aqueous medium and the small number of molecules obtained, did not allow the application of coupled techniques for a thorough investigation. Lastly, while the molecular electronics of this molecules could be characterized, it was done only qualitatively due to the molecule design. Overall, several techniques were learnt and developed, but it was not possible to achieve the desire explanation on how the electron transfer occur on these molecules.

## 8 – References

1. DAYAN, F.E.; DAYAN, E. A.; “Porphyrins: One Ring in the Colors of Life”, *American Scientist*, **99**, 236, 2011.
2. TANAKA, T.; OSUKA, A.; “Chemistry of meso-Aryl-Substituted Expanded Porphyrins: Aromaticity and Molecular Twist”, *Chem. Rev.*; **117**, 2584, 2017.
3. SESSLER, J.L.; TOMAT, E.; “Transition-Metal Complexes of Expanded Porphyrins”, *Acc. Chem. Res.*; 2007, **40**, 371–379.
4. SUN, G.; LIU, X.S.; YU, C.H.; LIU, C.G.; “Theoretical investigation of structure diversity and electronic properties in the series isomeric [26]hexaphyrin (1.1.1.1.1.1) and [28]hexaphyrin (1.1.1.1.1.1)”, *Comp. Theor. Chem.*; **1087**, 18, 2016..
5. MOBIUS, K.; SAVITSKY, A; LUBITZ, W.; PLATO, M.; “Möbius–Hückel Topology Switching in Expanded Porphyrins: EPR, ENDOR, and DFT Studies of Doublet and Triplet Open-Shell Systems”, *Appl. Magn. Reson.*; **47**, 757, 2016.
6. KIM, K.S.; YOON, Z.S.; RUCKS, A.B.; SHIN, J.; MORI, S.; SANKAR, J.; SAITO, S.; JUNG, Y.M.; WASIELEWSKI, M.R.; OSUKA, A.; KIM, D.; “Conformational Changes of meso-Aryl Substituted Expanded Porphyrins upon Protonation: Effects on Photophysical Properties and Aromaticity”, *J. Phys. Chem. B* , **113**, 5794, 2009.
7. NOORI, M.; ARAGONES, A.C.; PALMA, D.C.; DARWISH, N.; BAILEY, S.W.D.; AL-GALIBY, Q.; GRACE, I.; AMABILINO, D.B.; GONZALEZ-CAMPO, A.; DIEZ-PEREZ, I. ; LAMBERT C.J.; “Tuning the electrical conductance of metalloporphyrin supramolecular wires”, *Scientific Reports*, **6**, 37352, 2016.
8. ARAGONES, A.C.; DARWISH, N.; SALETRA, W.J.; PEREZ-GARCIA, L.; SANZ, F.; PUIGMARTI-LUIZ, J.; AMABILINO, D.B.; DIEZ-PEREZ, I.; “Highly Conductive Single-Molecule Wires with Controlled Orientation by Coordination of Metalloporphyrins”, *Nano Lett.*; **14**, 4751, 2014.
9. PONCE, I.; ARAGONES, A.; DARWISH, N.; PLA-VILANOVA, P.; OÑATE, R.; REZENDE, M.; ZAGAL, J.; SANZ, F.; PAVEZ, J.; DIEZ-PEREZ, I.; "Building nanoscale molecular wires exploiting electrocatalytic interactions", *Electrochim. Acta*, **179**, 611, 2015.
10. THOMPSON, S.E.; PARTHASARATHY, S.; “Moore’s law: the future of Si microelectronics”, *Materials Today*, 9(6), 20, 2006.
11. RATNER, M.; “A brief history of molecular electronics”, *Nature Nanotechnology*, 8(6), 378, 2013.
12. DENNARD R.H.; GAENSSLEN F.H.; RIDEOUT V.L.; BASSOUS E.; LEBLANC A.R.; “Design of ion-implanted MOSFET’s with very small physical dimensions”, *IEEE J. Solid-State Circuits*, **9**, 256, 1974.
13. FERAIN, I.; COLINGE, C.A.; COLINGE, J.; “Multigate transistors as the future of classical metal-oxide-semiconductor field-effect transistors”, *Nature*, 479(7373), 310, 2011.
14. WALDROP, M.M.; “The chips are down for Moore’s law”, *Nature*, 530(7589), 144, 2016.

- 
15. XIU, L.; "Time Moore: Exploiting Moore's Law From The Perspective of Time", IEEE Solid-State Circuits Magazine, 11(1), 39, 2019.
  16. CAVIN, R. K.; LUGLI, P.; ZHIRNOV, V. V.; "Science and Engineering Beyond Moore's Law", Proceedings of the IEEE, **100**(Special Centennial Issue), 1720, 2012.
  17. GAMAL, A. EL; ELTOUKHY, H.; "BCMOS image sensors", IEEE Circuit Device Mag.; 21(3), 6, 2005.
  18. LEMME, M. C.; ECHTERMEYER, T. J.; BAUS, M.; KURZ H.; "A graphene field-effect device", IEEE Electron Device Lett.; 28(4), 282, 2007.
  19. BAE, S.; KIM, H. F.; LEE, Y.; XU, X. F.; PARK, J.-S.; ZHENG, Y.; BALAKRISHNAN, J.; LEI, T.; KIM, H.R.; SONG, Y. I.; KIM, Y.-J.; KIM, K.S.; O'ZYILMAZ, B.; AHN, J.-H.; HONG, B. H.; IIJIMA, S.; "Roll-to-roll production of 30-inch graphene films for transparent electrodes", Nature Nanotechnol.; 5, 574, 2010.
  20. STRUKOV, D. B.; SNIDER, G. S.; STEWART, D. R.; WILLIAMS, R. S.; "The missing memristor found", Nature, **453**, 80, 2008.
  21. CHUA, L. O.; "Memristor: The missing circuit element", IEEE Trans. Circuit Theory, 18(5), 507, 1971.
  22. ZHIRNOV, V.; CAVIN, R.; LEEMING, G; GALATSIK, K.; "An assessment of integrated digital cellular automata architectures", IEEE Computer, 41(1), 38, 2008.
  23. CONSTANT, E.W.; "II: The Origins of the Turbojet Revolution", The Johns Hopkins Univ. Press, Baltimore, 1980.
  24. Mirkin, C. A.; Ratner, M. A.; "Molecular Electronics", Annual Review of Physical Chemistry, 43(1), 719, 1992.
  25. CHOI, H.; MODY, C.C.M.; "The Long History of Molecular Electronics: Microelectronics Origins of Nanotechnology", Social Studies of Science, 39(1), 11, 2009.
  26. RATNER, M.A; "A brief history of molecular electronics", Nature Nanotechnology, 8(6), 378, 2013.
  27. AVIRAM, A.; RATNER, M.; "Molecular Rectifiers", Chem. Phys. Lett.; **29**, 277, 1974.
  28. JOACHIM, C.; GIMZEWSKI, J. K. ; AVIRAM, A.; "Electronics using hybrid-molecular and mono-molecular devices", Nature, 408, 541 (2000).
  29. JAYAMURUGAN G.; GOWRI V.; HERNANDEZ D.; MARTIN S.; GONZALEZ-ORIVE A.; DENGIZ C.; DUMELE O.; PEREZ-MURANO F.; GISSELBRECHT J.P.; BOUDON C.; SCHWEIZER W.B.; BREITEN, B.; FINKE, A.D.; JESHKE, G.; BERNET B.; RUHLMANN L.; CEA P.; DIERERICH F.; "Design and Synthesis of Aviram-Ratner-Type Dyads and Rectification Studies in Langmuir-Blodgett (LB) Films", Chem. Eur. J.; **22**, 10539, 2016.
  30. RATNER M.A.; "Does molecular electronics compute?", Nature Nanotechnology, **8**, 378, 2013.
  31. MANN B.; KUHN H.; "Tunneling through Fatty Acid Salt Monolayers", J. Appl. Phys.; **42**, 4398, 1971.
  32. BINNIG, G.; ROHRER, H.; GERBER, C.; WEIBEL, H.; "Surface Studies by Scanning Tunneling Microscopy", Phys. Rev. Lett.; **49**, 57, 1982.
  33. BINNIG G.; ROHRER H.; " Scanning tunneling microscopy", Surf.. Sci.; **126**, 236, 1983.

- 
34. REED M.A.; ZHOU C.; MULDER C.J.; BURGIN T.P.; TOUR J.M.; "Conductance of a Molecular Junction", *Science*, 279(5336), 252, 1997.
35. JEONG, H.; KIM, D.; XIANG, D.; LEE, T.; "High-Yield Functional Molecular Electronic Devices", *ACS Nano*, 11(7), 6511, 2017.
36. CHOI, H.; MODY, C. C. M.; "The Long History of Molecular Electronics: Microelectronics Origins of Nanotechnology", *Soc. Stud. Sci.*; 39, 11, 2009.
37. POLYMERPOULOS, E. E.; SAGIV, J.; "Electrical Conduction through Adsorbed Monolayers", *J. Chem. Phys.*; **69**, 1836, 1978.
38. TEMPERTON R.H.; O'SHEA J.N.; SCURR, D.J.; "On the suitability of high vacuum electrospray deposition for the fabrication of molecular electronic devices", *Chem phys letters*, **682**, 15, 2017.
39. REED M.A.; LEE T.; WANG W.; "Mechanism of electron conduction in self-assembled alkanethiol monolayer devices", *Phys. Rev. B*, **68**, 035416, 2003.
40. ZHOU, C.; DESHPANDE, M. R.; REED, M. A.; JONES, L.; TOUR, J. M.; "Nanoscale Metal Self Assembled Monolayer Metal Heterostructures", *Appl. Phys. Lett.*; **71**, 611, 1997.
41. KUSHMERICK, J. G.; ALLARA, D. L.; MALLOUK, T. E.; MAYER, T. S.; "Electrical and Spectroscopic Characterization of Molecular Junctions", *MRS Bull*, **29**, 396, 2004.
42. KUSHMERICK J. G.; HOLT D. B.; YANG J. C.; NACIRI J.; MOORE M. H.; SHASHIDHAR R.; "Metal-Molecule Contacts and Charge Transport across Monomolecular Layers: Measurement and Theory", *Phys. Rev. Lett.*; **89**, 086802, 2002.
43. AKKERMAN, H.B.; BOER, B.; "Electron Transport through Thin Organic Films in Metal-Insulator-Metal Junctions Based on Self-Assembled Monolayers", *J. of Phys: Con. Matt.*; 20(1), 013001, 2008.
44. BELLEW A.T.; MANNING, H.G.; ROCHA, C.G.; FERREIRA, M.S.; BOLAND J.J.; "Resistance of Single Ag Nanowire Junctions and Their Role in the Conductivity of Nanowire Networks", *ACS Nano*, **9**, 11422, 2015.
45. SLOWINSKI, K.; CHAMBERLAIN, R. V.; MILLER, C. J.; MAJDA, M.; "Through-Bond and Chain-to Chain Coupling. Two Pathways in Electron Tunneling through Liquid Alkanethiol Monolayers on Mercury Electrodes", *J. Am. Chem. Soc.*; **119**, 11910, 1997.
46. SLOWINSKI, K.; FONG, H. K. Y.; MAJDA, M.; "Mercury-Mercury Tunneling Junctions: 1. Electron Tunneling across Symmetric and Asymmetric Alkanthiolate Bilayers", *J. Am. Chem. Soc.*; **121**, 7257, 1999.
47. WEISS, E. A.; CHIECHI, R. C.; KAUFMAN, G. K.; KRIEBEL, J. K.; LI, Z.; DUATI, M.; RAMPI, M. A.; WHITESIDES, G. M.; "Influence of Defects on the Electrical Characteristics of Mercury-Drop Junctions: Self-Assembled Monolayers of N-Alkanethiolates on Rough and Smooth Silver", *J. Am. Chem. Soc.*; **129**, 4336, 2007.
48. THUO, M.M.; REUST, W.F.; NIJHUIS, C. A.; BARBER, J.R.; KIM, C.; SHULZ, M.D.; WHITESIDES, G.M.; "Defining the Value of Injection Current and Effective Electrical Contact Area for EGaIn-Based Molecular Tunneling Junctions" *J. Am. Chem. Soc.*; **135**, 18131, 2013.
49. LOO, Y.; LANG, D.V.; ROGERS J.A; HSU J.W.P.; "Electrical Contacts to Molecular Layers by Nanotransfer Printing", *Nano Letters*, 3(7), 913, 2003.

- 
50. CHU, C. W.; NA, J. S.; PARSONS, G. N.; "Conductivity in Alkylamine/Gold and Alkanethiol/Gold Molecular Junctions Measured in Molecule/Nanoparticle/Molecule Bridges and Conducting Probe Structures", *J. Am. Chem. Soc.*; **129**, 2287, 2007.
51. JAFRI, S. H. M.; BLOM, T.; LEIFER, K.; STRØMME, M.; LÖFÅS, H.; GRIGORIEV, A.; WELCH, K.; "Assessment of a nanoparticle bridge platform for molecular electronics measurements", *Nanotechnology*, 21(43), 435204, 2010.
52. KUMAR, A.; MANDAL, S.; SELVAKANNAN, P. R.; PASRICHA, R.; MANDALE, A. B.; SASTRY, M.; "Investigation into the Interaction between Surface-Bound Alkylamines and Gold Nanoparticles", *Langmuir*, **19**, 6277, 2003.
53. MULLER, C.J.; VAN RUITENBEEK, J.M.; DE JONGH, L.J.; "Experimental observation of the transition from weak link to tunnel junction", *Physica C: Superconductivity*, 191(3). 485, 1992.
54. HONG, W.; MANRIQUE, D.Z.; MORENO-GARCIA, P.; GULCUR, M.; MISHCHENKI, A. LAMBERT, C.J.; BRYCE, M.R.; WANDLOWSKI, T.; "Single Molecular Conductance of Tolanes: Experimental and Theoretical Study on the Junction Evolution Dependent on the Anchoring Group", *J. Am. Chem. Soc.*; **134**, 2292, 2012.
55. HAICK, H.; CAHEN, D.; "Making contact: Connecting molecules electrically to the macroscopic world", *Prog. Surf. Sci.*; **83**, 217, 2008.
56. MORELAND, J.; EKIN, J.W.; "Electron tunneling experiments using Nb-Sn "break" junctions", *J. Appl. Phys.*; 58(10), 3888, 1985.
57. PERRIN, M.L.; VERZIJJ, C.J.O.; MARTIN, C.A.; SHAIKH, A.J.; EELKEMA, R.; VAN ESCH, J.H.; VAN RUITENBEEK, J.M.; THIJSEEN, J.M.; VAN DER ZANT, H.S.J.; DULIC, D.; "Large tunable image-charge effects in single-molecule junctions.", *Nature Nanotech.*; 8(4), 282, 2013.
58. FRISENDA, R.; PARLATO, L.; BARRA, M.; VAN DER ZANT, H. S. J.; CASSINESE, A.; "Single-Molecule Break Junctions Based on a Perylene-Diimide Cyano-Functionalized (PDI8-CN2) Derivative.", *Nanoscale Research Letters*, 10(1), 305, 2015.
59. WOEDTKE, S.; Ph.D. thesis, Inst. f. Exp. u. Ang. Phys. der CAU Kiel, 2002.
60. OLESEN, L.; LAEGSGAARD, E.; STENSGAARD, I.; BESENBACHER, F.; SCHIO/TZ, J.; STOLTZE, P.; JACOBSEN, K. W.; NORSKOV J. K.; "Quantized conductance in an atom-sized point contact", *Physical Review Letters*, 72(14), 2251, 1994.
61. XU, B.; TAO, N.; "Measurement of single-molecule resistance by repeated formation of molecular junctions", *Science*, 301(5637), 1221, 2003.
62. DIEZ-PEREZ, I.; HIKATH, J.; LEE, Y.; YU, L.; ADAMSKA, L.; KOZHUSHNER, M.A.; OLEYNIK, I.I.; TAO, N.; "Rectification and stability of a single molecular diode with controlled orientation", *Nat. Chem.*; 1(8), 635, 2009.
63. FRENCH W.R.; IACOVELLA C.R.; RUNGGER I.; SOUZA A.M.; SANVITO S.; CUMMINGS P.T.; "Atomistic simulations of highly conductive molecular transport junctions under realistic conditions", *Nanoscale*, **5**, 3654, 2013.
64. HUMPHREY, W.; DALKE, A.; SCHULTEN, K.; "VMD: Visual molecular dynamics", *J. Mol. Graphics*, **14**, 33, 1996.
65. HAISS, W.; NICHOLS, R.J.; VAN ZALINGE, H.; HIGGINS, S.J.; BETHELL, D.; SCHIFFRIN, D.J.; "Measurement of single molecule conductivity using the

- 
- spontaneous formation of molecular wires.”, *Phys. Chem. Chem. Phys.*; **6**(17), 4330, 2004.
66. NICHOLS, R. J.; HAISS, W.; HIGGINS, S. J.; LEARY, E.; MARTIN, S.; BETHELL, D.; “The experimental determination of the conductance of single molecules”, *Phys. Chem. Chem. Phys.*; **12**(12), 2801, 2010.
67. CUI, B.; ZHAO W.; WANG H.; ZHAO J.; ZHAO H.; LI D.; JIANG X.; ZHAO P.; LIU D.; *J. Appl. Phys.*; “Effect of geometrical torsion on the rectification properties of diblock conjugated molecular diodes”, **16**, 73701, 2014.
68. OVGUN, A. PhD Thesis, “Tunneling Through a Potential Barrier”, Izmir Institute of Technology, 2010.
69. ATKINS, P.; PAULA, J.; “Physical Chemistry”, chapter 8, W.H. Freeman and Company, New York.
70. SIMMONS, J.G.; “Electric tunnel effect between dissimilar electrodes separated by a thin insulating film”, *Journal of Applied Physics*, **34**(9), 2581, 1963.
71. LANDAUER, R.; “Spatial variation of currents and fields due to localized scatterers in metallic conduction”, *IBM Journal of Research and Development*, **1**(3), 223, 1957.
72. AGRAIT, N.; YEYATI, A.L.; VAN RUITENBEEK J.M.; “Quantum properties of atomic-sized conductors.”, *Physics Reports*, **377**(2), 81, 2003.
73. CUEVAS J.C.; SCHEER, E.; FRONT MATTER. In *Molecular Electronics*, **1**, 1, WORLD SCIENTIFIC, 2010.
74. LANDAUER, R.; “Electrical resistance of disordered one-dimensional lattices.”, *Philosophical Magazine*, **21**(172), 863. 1970.
75. IMRY, Y.; TINKHAM, M.; “Introduction to Mesoscopic Physics.”, *Physics Today*, **51**:60, 1998.
76. DATTA, S.; “Electronic Transport in Mesoscopic Systems”, **3**. 1997.
77. MCCREERY, R.L.; “Molecular electronic junctions.”, *Chemistry of Materials*, **16**(23), 4477, 2004.
78. CUEVAS, J.C.; SCHEER, E.; “FRONT MATTER. In *Molecular Electronics*”, WORLD SCIENTIFIC , **1**, 1, 2010.
79. MARCUS, R.A.; “On the Theory of Electron-Transfer Reactions. VI. Unified Treatment for Homogeneous and Electrode Reactions”, *J. Chem. Phys.*; **43**, 1965, 679.
80. MARCUS, R. A.; “Tutorial on rate constants and reorganization energies”, *J. Electroanal. Chem.*; **67**(4), 2000, 2.
81. MARCUS, R.A.; “On the Theory of Oxidation - Reduction Reactions Involving Electron Transfer.”, *J. Chem. Phys.*, **24**, 1956, 966.
82. HUSH, N.S.; “Adiabatic theory of outer sphere electron-transfer reactions in solution”, *Transactions of the Faraday Soc.*, **57**, 1961, 577.
83. KASTLUNGER, G.; STADLER, R.; “Bias-induced conductance switching in single molecule junctions containing a redox-active transition metal complex”, *Monatsch Chem*, **147**(10), 2016, 1675.
84. KÜSTER, W.; DEIHLE, P.; “Bilirubin and haemin”, *Physiol. Chem.*; **82**, 463, 1912.
85. FIEDOR F. K. A.; MYSLIVA-KURDZIEL, B.; ORZEL, L.; STOCHEL, G.; “Understanding chlorophylls: Central magnesium ion and phytyl as structural

- 
- determinants”, *Biochimica et Biophysica Acta – Bioenergetics*, **1777**, 1491, 2008.
86. PERUTZ, M.F.; “Stereochemical mechanism of oxygen transport by haemoglobin.”, *Proc. R. Soc. Lond. B. Biol.*; **208**, 135, 1980.
87. MILGROM, L. R.; “The Colours of Life”, Oxford University Press, Oxford 1997.
88. BATTERSBY, A.R.; “Tetrapyrrole: the pigments of life”, *Natural. Prod. Reports*, **17**, 507, 2000.
89. ADLER, A. D.; LONGO F. R.; SHERGALIS, W.; “Mechanistic Investigations of Porphyrin Syntheses. I. Preliminary Studies on ms-Tetraphenylporphin”, *J. Am. Chem. Soc.*; **86**, 3145, 1964.
90. VOGEL, E.; HAAS, W.; KNIPP, B.; LEX, J.; SCHMICKLER, H.; “Tetraoxaporphycene Dication”, *Angew. Chem.*; **27**, 406, 1988.
91. VOGEL, E. J.; “Novel porphyrinoid macrocycles and their metal-complexes”, *Heterocycl. Chem.*; **33**, 1461, 1996.
92. LASH, T. D.; ROMANIC, J. L.; HAYES, J.; SPENCE, J. D.; “Towards hydrocarbon analogues of the porphyrins: synthesis and spectroscopic characterization of the first dicarbaporphyrin”, *Chem. Commun.*; **9**, 819, 1999.
93. HIROTO, S.; MIYAKE, Y.; SHINOKUBO, H.; “Synthesis and Functionalization of Porphyrins through Organometallic Methodologies”, *Chem. Rev.*; **117**, 2910, 2017.
94. TSUDA, A.; OSUKA, A.; “Fully conjugated porphyrin tapes with electronic absorption bands that reach into infrared.”, *Science*, **293**, 79, 2001.
95. VICENTE, M. G. H.; SMITH, K. M.; “Syntheses and Functionalizations of Porphyrin Macrocycles”, *J. Porphyrins Phthalocyanines*, **8**, 26, 2004.
96. KUROTOBI, K.; KIM, K. S.; NOH, S. B.; KIM, D.; OSUKA, A.; “A Quadruply Azulene-Fused Porphyrin with Intense Near-IR Absorption and a Large Two-Photon Absorption Cross Section”, *Angew. Chem.*; **118**, 4048, 2006.
97. XU, H.J.; MACK, J.; DESCALZO, A.B.; SHEN, Z.; KOBAYASHI, N.; YOU, X.-Z.; RURACK, K.; “meso-Aryl Phenanthroporphyrins, Synthesis and Spectroscopic Properties”, *Chem. Eur. J.*; **17**, 8965, 2011.
98. SWAVEY, S.; EDER, A.; “Enhanced O<sub>2</sub> electrocatalysis by a highly conjugated cobalt(II) porphyrin”, *In. Chem. Comm.*; **29**, 14, 2013.
99. ONO, N.; HIRONAGA, H.; ONO, K.; KANEKO, S.; MURASHIMA, T.; UEDA, T.; TSUKAMURA, C.; OGAWA, T.; “A new synthesis of pyrroles and porphyrins fused with aromatic rings”, *J. Chem. Soc. Perkin Trans.*; **5**, 417, 1996.
100. CHANG, C.; KUO, M.; “Reaction of iron(III) porphyrins and iodosoxylene. The active oxene complex of cytochrome P-450”, *J. Am. Chem. Soc.*; **101**, 3413, 1979.
101. MEUNIER, B.; “Metalloporphyrins as versatile catalysts for oxidation reactions and oxidative DNA cleavage”, *Chem. Rev.*; **92**, 1411, 1992.
102. TAYLOR, T.G.; TSUCHIYA, S.; “Perhalogenated tetraphenylhemins: stable catalysts of high turnover catalytic hydroxylations”, *Inorg. Chem.*; **26**, 1338, 1987.
103. HABER, J.; MATACHOWSKI, L.; PAMIN, K.; POLTOWICZ, J.; “The effect of peripheral substituents in metalloporphyrins on their catalytic activity in Lyons system”, *J. Mol. Catal. A Chem.*; **198**, 215, 2003.



- 
104. COSTAS, M.; "Selective C–H oxidation catalyzed by metalloporphyrins", *Coord. Chem. Rev.*; **255**, 2912, 2011.
105. BALDWIN, J.E.; CROSSLEY, M.J.; DEBERNARDI, J.; "Efficient peripheral functionalization of porphyrins", *Tetrahedron*, **38**, 685, 1982.
106. MURASHIMA, T.; TSUJIMOTO, S.; YAMADA, T.; MIYAZAWA T.; UNO, H.; ONO, N.; SUGIMOTO, N.; "Synthesis of water-soluble porphyrin and the corresponding highly planar benzoporphyrin without meso-substituents" *Tetrahedron Lett.*; **46**, 113, 2005.
107. MAKARSKA M.; RADSZKI, ST.; LEGENDZIEWIEZ, J.; "Spectroscopic characterization of the water-soluble cationic porphyrins and their complexes with Cu(II) in various solvents", *J. of Alloys and Compounds*, **341**, 233, 2002.
108. MAMARDASHVILI, G.M.; MAMARDASHVILI, N. Z.; BEREZIN, B. D.; "Solubility of Alkylporphyrins", *Molecules*, **5**, 762, 2000.
109. WHITE, W. I.; PLANE, R.A.; "A homologous series of water-soluble porphyrins and metalloporphyrins: synthesis, dimerization, protonation and self-complexation", *Bioinorganic Chem.*; **4**, 21, 1974.
110. FALK J.E.; *Porphyrins and Metalloporphyrins*, Elsevier, New York, 1975.
111. GOUTERMAN. M.; WAGNIÈRE, H.; "Spectra of porphyrins: Part II. Four orbital model", *J. of Mol. Spectroscopy*, **11**, 108, 1963.
112. SHKIRMAN S.F.; SOLOVEV K.N.; KACHURA, T.F.; ARABEI, S.A.; SKAKOVSKII, E.D.; "Interpretation of the Soret band of porphyrins based on the polarization spectrum of N-methyltetraphenylporphin fluorescence", *J. of Appl. Spec*, **66**, 68, 1999.
113. ZOLTAN T.; VARGAS F.; LÓPEZ V.; CHÁVEZ V.; RIVAS C.; RAMÍREZ A.H.; "Influence of charge and metal coordination of meso-substituted porphyrins on bacterial photoinactivation", *Spectrochimica Acta Part A: Molecular and Biomolecular Spectroscopy*, **135**, 747, 2015.
114. JOSEFSEN L.B.; BOYLE R.W.; "Photodynamic therapy and the development of metal-based photosensitisers.", *Met Based Drugs.*; **2008**, 276109, 2008.
115. FALK J.E.; *Porphyrins and Metalloporphyrins*, Elsevier, New York, 1975.
116. MONTI D.; NARDIS S.; STEFANELLI M.; PAOLESSE R.; NATALE C.; D'AMICO A.; "Porphyrin-Based Nanostructures for Sensing Applications", *J. of Sensors*, **2009**, 10, 2009.
117. DING, Y.; ZHU, W.; XIE, Y.; "Development of Ion Chemosensors Based on Porphyrin Analogues.", *Chem. Rev.*; **117**, 2203, 2017.
118. DOLCI L. S.; MARZOCCHI E.; MONTALTI M.; "Amphiphilic porphyrin film on glass as a simple and selective solid-state chemosensor for aqueous Hg<sup>2+</sup>." *Biosensors and Bioelectronics*, **22**, 399, 2006.
119. LVOVA, L.; NATALE, C.; PAOLESSE, R.; "Porphyrin-based chemical sensors and multisensor arrays operating in the liquid phase", *Sensors and Actuators B: Chemical*, **179**, 21, 2013.
120. ISHIHARA, S.; LABUTA, J, ROSSOM, W.V.; ISHIKAWA, D.; MINAMI, K.; HILL, J.P.; ARIGA, K.; "Porphyrin-based sensor nanoarchitectonics in diverse physical detection modes", *Phys. Chem. Chem. Phys.*; **16**, 9713, 2014.
121. EMA, T.; MIYAZAKI, Y.; TANIGUCHI T.; TAKADA, J.; "Robust porphyrin catalysts immobilized on biogenous iron oxide for the repetitive conversions of epoxides and CO<sub>2</sub> into cyclic carbonates", *Green Chem.*; **15**, 2485, 2013.

- 
122. CHEN Y.; JIE, S.; YANG, C.; LIU, Z.; "Active and efficient Co-N/C catalysts derived from cobalt porphyrin for selective oxidation of alkylaromatics", *Appl. Surf. Sci.*; **419**, 98, 2017.
123. JASINSKA, K.R.; SHAN, W.; ZAWADA K.; KADSIH, K.M.; GRYKO, D.; "Porphyrins as Photoredox Catalysts: Experimental and Theoretical Studies", *J. Am. Chem. Soc.*; **138**, 15451, 2016.
124. EMA T.; MIYAZAKI Y.; SHIMONISHI, JK.; MAEDA, C.; HASEGAWA JY.; "Bifunctional Porphyrin Catalysts for the Synthesis of Cyclic Carbonates from Epoxides and CO<sub>2</sub>: Structural Optimization and Mechanistic Study", *J. Am. Chem. Soc.*; **136**, 15270, 2014.
125. AMBRE, R.B.; DANIEL, Q.; FAN, T.; CHEN, H.; ZHANG, B.; WANG, L.; AHLQUIST, M.S.G.; DUAN, L.; SUN, L.; "Molecular engineering for efficient and selective iron porphyrin catalysts for electrochemical reduction of CO<sub>2</sub> to CO", *Chem. Commun.*; **52**, 14478, 2016.
126. KUANG D.; UCHIDA S.; HUMPHRY-BAKER R.; ZAKEERUDDIN S. M.; GRÄTZEL M.; "Organic dye-sensitized ionic liquid based solar cells: remarkable enhancement in performance through molecular design of indoline sensitizers.", *Angew. Chem.; Int. Ed.*; **47**, 1923, 2008.
127. LEE C. Y.; SHE C. X.; JEONG N. C.; HUPP J. T.; "Porphyrin sensitized solar cells: TiO<sub>2</sub> sensitization with a  $\pi$ -extended porphyrin possessing two anchoring groups", *Chem. Commun.*; **46**, 6090, 2010.
128. HARDIN, B. E.; SNAITH H. J.; MCGEHEE, M. D.; "The renaissance of dye-sensitized solar cells", *Nat. Photonics*, **6**, 162, 2012.
129. GRATZEL, M.; "Recent advances in sensitized mesoscopic solar cells", *Acc. Chem. Res.*; **42**, 1788, 2009.
130. CHANG, K.; TANG, Y.; FANG, X.; YIN, S.; XU, H.; WU, C.; "Incorporation of porphyrin to  $\pi$ -conjugated backbone for polymer-dot-sensitized photodynamic therapy", *Biomacromolecules*, **17**, 2128, 2016.
131. SCHMITT, F.; GOVINDASWAMY P.; FINK, G.S.; ANG, W.H.; DYSON, P.J.; JEANNERET, L.J.; THERRIEN, B.; "Ruthenium porphyrin compounds for photodynamic therapy of cancer", *J. Med. Chem.*; **51**, 1811, 2008.
132. MOREIRA, L.M.; SANTOS, F.; V.; LYON, J. P.; COSTA, M.M.; SOARES, C.P.; SILVA, N.S.; "Photodynamic therapy: porphyrins and phthalocyanines as photosensitizers", *Aust. J. Chem.*; **61**, 741, 2008.
133. PUSHPAN SK, VENKATRAMAN S, ANAND VG, SANKAR J, PARMESWARAN D, GANESAN S, CHANDRASHEKAR TK.; "Porphyrins in photodynamic therapy-a search for ideal photosensitizers", *Curr. Med. Chem. Anticancer Agents*, **2**, 187, 2002.
134. STERNBERG, E.D.; DOLPHIN D.; BRUCKNER, C.; "Porphyrin-based photosensitizers for use in photodynamic therapy", *Tetrahedron*, **54**, 17, 1998.
135. ZHAO, C.; REHMAN, F.U.; YANG, Y.; LI, X.; ZHANG, D.; JIANG, H.; SELKE, M.; WANG, X.; LIU, C.; "Bio-imaging and Photodynamic Therapy with Tetra Sulphonatophenyl Porphyrin (TSPP)-TiO<sub>2</sub> Nanowhiskers: New Approaches in Rheumatoid Arthritis Theranostics", *Sci. Rep.*; **5**, 11518, 2015.
136. ETHIRAJAN, M.; CHEN, Y.; JOSHI, P.; PANDEY, R.K.; "The role of porphyrin chemistry in tumor imaging and photodynamic therapy", *Chem. Soc. Rev.*; **40**, 340, 2011.

- 
137. TANAKA, T.; OSUKA, A.; "Conjugated porphyrin arrays: synthesis, properties and applications for functional materials", *Chem. Soc. Rev.*; **44**, 943, 2015.
138. YOON, Z. S.; OSUKA, A.; KIM, D.; "Möbius aromaticity and antiaromaticity in expanded porphyrins", *Nature Chemistry*, **1**, 113, 2009.
139. BARATA, J.F.B.; NEVERS, M. G.; AMPARO, M.; FAUSTINO, F.; TOMÉ, A.C.; CAVALEIRO, J.A.S.; "Strategies for corrole functionalization", *Chem. Rev.*; **117**, 3192, 2017.
140. BARONACASTANO, J.C.; CARMONAVARGAS, C.C.; BROCKSON, R.J.; OLIVEIRA, K.T.; Porphyrins as catalysts in scalable organic reactions, *Molecules*, **21**, 310, 2016.
141. BIESAGA M, PYRRZYNSKA, K.; TROJANOWICZ, M, "Porphyrins in analytical chemistry. A review", *Talanta*, **51**, 209, 2000.
142. MANBECK, G.F.; "A review of iron and cobalt porphyrins, phthalocyanines and related complexes for electrochemical and photochemical reduction of carbon dioxide", *J. Porphyrins Phthalocyanines*, **19**, 45, 2015.
143. VICENTE, M.G.H.; SMITH, K.M.; "Syntheses and functionalizations of porphyrin macrocycles", *Curr Org Synth.*; **11**, 3, 2014.
144. CLAESSENS, C.G.; HAHN, U, TORRES, T.; "Phthalocyanines: From outstanding electronic properties to emerging applications", *Chem Record*, **8**, 75, 2008.
145. ORLOWSKI, R.; GRYKO, D.; GRYKO, D. T.; "Synthesis of corroles and their heteroanalogs", *Chem. Rev.*; **117**, 3102, 2017.
146. CLASSENS, C.G.; BLAU, W.K.; COOK, M.; HANACK, M.; NOLTE, R.K.M.; TORRES, T.; WÖHRLE, D.; "Phthalocyanines and phthalocyanine analogues: the quest for applicable optical properties", *Monatshefte für Chemie*, **132**, 3, 2001.
147. SOROKIN, A. B.; "Phthalocyanine metal complexes in catalysis", *Chem. Rev.*; **113**, 8152, 2013.
148. LU, H.; KOBAYASHI, N.; "Optically active porphyrin and phthalocyanine systems" *Chem. Rev.*; **116**, 6184, 2016.
149. HIROTO, S.; MIUYAKE, T.; SHINOKUBO, H.; "Synthesis and functionalization of porphyrins through organometallic methodologies", *Chem. Rev.*; **117**, 2910, 2017.
150. SESSLER, J. L.; SEIDEL, D.; "Synthetic expanded porphyrin chemistry", *Angew. Chem. Int. Ed.*; **42**, 5134, 2003.
151. FRANCK, B.; NONN, A.; "Novel porphyrinoids for chemistry and medicine by biomimetic syntheses", *Angew. Chem.; Int. Ed. Engl.*; **34**, 1795, 1995.
152. BAUER, V. J.; CLIVE, D. L. J.; DOLPHIN, D.; PAINE, J. B.; III; HARRIS, F. L.; KING, M. M.; LODER, J.; WANG, S.-W. C.; WOODWARD, R. B.; "Sapphyrins: novel aromatic pentapyrrolic macrocycles", *J. Am. Chem. Soc.*; **105**, 6429, 1983.
153. KOIDE T.; KASHIWAZAKI G.; SUZUKI M.; FURUKAWA K.; YOON M.-C.; CHO S.; KIM D.; OSUKA A.; "A Stable Radical Species from Facile Oxygenation of meso-Free 5,10,20,25-Tetrakis(pentafluorophenyl)-Substituted [26]Hexaphyrin(1.1.1.1.1)", *Angew. Chem.*; **47**, 9807, 2008.

- 
154. PAWLICKI, M. , COLLINS, H. A. , DENNING, R. G. , ANDERSON, H. L.; Two-photon absorption and the design of two-photon dyes, *Angew. Chem.*; **121**, 3292, 2009.
155. MORI, S.; OSUKA, A.; "Aromatic and Antiaromatic Gold (III) Hexaphyrins with Multiple Gold– Carbon Bonds", *J. Am. Chem. Soc.*; **127**, 8030, 2005.
156. XIE, Y.-S. , YAMAGUCHI, K. , TOGANOH, M.; UNO, H.; SUZUKI, M.; MORI, S.; SAITO, S.; OSUKA, A.; FURUTA, H.; "Triply N-Confused Hexaphyrins: Near-Infrared Luminescent Dyes with a Triangular Shape", *Angew. Chem.*; **121**, 5604, 2009.
157. SAITO, S.; OSUKA, A.; "Expanded porphyrins: intriguing structures, electronic properties, and reactivities", *Angew. Chem. Int. Ed.*; **50**, 4342, 2011.
158. RACHLEWICZ, K. , LATOS-GRAZ'YNSKI L.; GEBAUER, A. , VIVIAN, A. , SESSLER, J. L.; "NH tautomerization of 2, 7, 18, 23-tetramethyl-3, 8, 12, 13, 17, 22-hexaethylsapphyrin", *J. Chem. Soc. Perkin Trans.*; **2**, 2189, 1999.
159. NEVES M. G. P. M. S.; MARTINS, R. M.; TOM, A. C. , SILVESTRE A. J. D.; SILVA, A. M. S.; FELIX V. F, DREW M. G. B.; CAVALEIRO J. A. S.; "meso-Substituted expanded porphyrins: new and stable hexaphyrins", *Chem. Commun.* ; 385, 1999.
160. SUN, G.; LEI, E.; LIU, X.-S.; YU, C.-H.; DUAN, X.-X.; LIU, C.-G. "Theoretical investigation of structure diversity and electronic properties in the series isomeric [26]hexaphyrin (1.1.1.1.1.1) and [28]hexaphyrin (1.1.1.1.1.1)." *Computational and Theoretical Chemistry*, 1087, 18–25, 2016.
161. SANKAR, J. , MORI, S. SAITO, S. , RATH, H. SUZUKI M.; INOKUMA Y.; SHINOKUBO H.; KIM K. S.; YOON Z. S.; SHIN J.-Y.; LIM J. M.; MATSUZAKI Y.; MATSUSHITA O.; MURANAKA A.; KOBAYASHI N.; KIM D.; OSUKA A.; "Unambiguous Identification of Möbius Aromaticity for meso-Aryl-Substituted [28]Hexaphyrins(1.1.1.1.1.1)", *J. Am. Chem. Soc.*; **130**, 13568, 2008.
162. NAODA, K.; OSUKA, A.; "Iridium complexes of [26] hexaphyrin (1.1. 1.1. 1.1) and [36] octaphyrin (1.1. 1.1. 1.1. 1.1)", *J. of Porphyrins and Phthalocyanines*, **18**, 652, 2014.
163. MORI, S.; OSUKA, A.; "Heterobismetall Complexes of [26] Hexaphyrin (1.1. 1.1. 1.1)", *Inorganic Chemistry*, **47**, 3937, 2008.
164. MORI, S.; SHIMIZU, S.; SHIN, J. Y.; OSUKA, A.; "Group 12 Metal Complexes of [26] Hexaphyrin (1.1. 1.1. 1.1)", *Inorganic Chemistry*, **46**, 4374, 2007.
165. ALONSO, M.; PINTER, B.; GERRLINGS, P.; PROFT, F.; "Metalated Hexaphyrins: From Understanding to Rational Design", *Chem. Eur. J*, **21**, 17631, 2015.
166. SESSLER, J.L.; MELFI, P.J.; TOMAT, E, LYNCH, V. M.; "Copper (II) and oxovanadium (V) complexes of hexaphyrin (1.0. 1.0. 0.0)", *Dalton Transactions*, **6**, 629, 2007.
167. RATH, H, ARATANI N, LIM J M, LEE JS, KIM D, SHINOKUBO H, OSUKA A , "Bis-rhodium hexaphyrins: metalation of [28] hexaphyrin and a smooth Hückel aromatic–antiaromatic interconversion", *Chem. Comm.*; **25**, 3762, 2009.
168. MORI, H.; SUZUKI, M.; KIM, W.; LIM, J. M.; KIM, D.; & OSUKA, A.; "5, 20-Bis ( $\alpha$ -oligothienyl)-substituted [26] hexaphyrins possessing electronic circuits strongly perturbed by meso-oligothienyl substituents", *Chem. Sci.*; **6**, 1696, 2015.

- 
169. NAODA, K.; MORI, H.; OH, J. P.; KYU HYUNG KIM, D.; OSUKA, A.; "5,20-Di(pyridin-2-yl)-[28]hexaphyrin(1.1.1.1.1.1): A Stable Hückel Antiaromatic Hexaphyrin Stabilized by Intramolecular Hydrogen Bonding and Protonation-Induced Conformational Twist To Gain Möbius Aromaticity", *J. Org. Chem.*; **80**, 11726, 2015.
170. JANA, A.; ISHIDA, M.; CHO, K.; GHOSH, S.K.; KWAK, K.; OHKUBO, K.; SUNG, Y.M.; DAVIS, C.M.; LYNCH, V.M.; LEE, D.; FUKUZUMI, S.; KIM, D.; SESSLER, J.L.; "Tetrathiafulvalene-annulated [28]hexaphyrin(1.1.1.1.1.1): a multi-electron donor system subject to conformational control", *Chem. Commun.*; **49**, 8937, 2013.
171. KIM, D.; KWON, J. H.; AHN, T. K.; YOON, M. C.; KIM, D. Y.; KOH, M. K.; FURUTA, H.; SUZUKI, M.; OSUKA, A.; "Comparative photophysical properties of free-base, bis-Zn (II), bis-Cu (II), and bis-Co (II) doubly N-confused hexaphyrins (1.1. 1.1. 1.1)", *J. Phys. Chem. B*, **110**, 11683, 2006.
172. SUN, G.; DUAN, X.-X.; YU, C.-H.; LIU, C.-G.; "Theoretical investigation of the aromaticity and electronic properties of protonated and unprotonated molecules in the series hexaphyrin(1.0.0.1.0.0) to hexaphyrin(1.1.1.1.1.1)", *Journal of Molecular Modeling*, **21**, 315, 2015.
173. YOON, Z. S.; KWON, J. H.; YOON, M.; KOH, M. K.; NOH, S. B.; SESSLER, J. L.; "Nonlinear optical properties and excited-state dynamics of highly symmetric expanded porphyrins", *J. AM. CHEM. SOC.*; **128**, 14128, 2006.
174. SUN, G.; LI, H.; JIANG, S.; WANG, X.; LIE, C.; FU Q.; "Theoretical study on electronic spectrum properties of group 12 bis-metal (II) complexes of [26] hexaphyrin (1.1. 1.1. 1.1)", *Computational and theoretical Chemistry*, **976**, 68, 2011.
175. AHN, T.; KWON J.H.; KIM, D. Y.; CHO D. W.; JEONG, D. H.; KIM, S. K.; SUZUKI, M.; SHIMIZU, S.; OSUKA, A.; KIM, D.; "Comparative Photophysics of [26]-and [28] Hexaphyrins (1.1. 1.1. 1.1): Large Two-Photon Absorption Cross Section of Aromatic [26] Hexaphyrins (1.1. 1.1. 1.1)" *J. Am. Chem. Soc.*; **127**, 12856, 2005.
176. ZHU, Y.; ZHOU, S. KAN, Y.; SU, Z.; "Theoretical investigation of electronic structures and excitation energies of hexaphyrin and its group 11 transition metal (III) complexes", *J. Organometallic Chemistry*, **694**, 3012, 2009.
177. IKAWA, Y.; TAKEDA, M.; SUZUKI, M.; OSUKA, A.; FURUTA, H.; "Water-soluble doubly N-confused hexaphyrin: a near-IR fluorescent Zn (II) ion sensor in water", *Chemical Communications*, **46**, 5689, 2010.
178. HAGIWARA, H.; WATANABE, M.; DAI, T.; IDA, S.; ISHIIHARA T.; "Modification effects of meso-hexakis(pentafluorophenyl) [26]hexaphyrin aggregates on the photocatalytic water splitting", *Chem. Commun.*; **50**, 12515, 2014.
179. FURUTA, H.; YOZA, K.; IGARASHI, S.; OSUKA, A.; "meso-Aryl-Substituted Expanded Porphyrins", *J. Am. Chem. Soc.*; **123**, 2001.
180. YONEDA, T.; ARATANI, N.; OSUKA, A.; Regioselective fabrications of a Möbius aromatic [28]hexaphyrin palladium(II) complex, *J. Porphyrins Phthalocyanines*, **17**, 665, 2013.
181. YONEDA, T.; OSUKA, A.; "Synthesis of a [26]Hexaphyrin Bis-PdII Complex with a Characteristic Aromatic Circuit", *Chem. Eur. J.*, **19**, 7314, 2013.

- 
182. INOUE, M.; OSUKA, A.; "Redox-Induced Palladium Migrations that Allow Reversible Topological Changes between Palladium(II) Complexes of Möbius Aromatic [28]Hexaphyrin and Hückel Aromatic [26]Hexaphyrin", *Angewandte Chem.*; **49**, 49, 9488, 2010.
183. CHA, W.Y.; KIM, W.; MORI, H.; YONEDA, T.; OSUKA, A.; KIM, D.; "S<sub>2</sub> Fluorescence from [26]Hexaphyrin Dianion", *J. Phys. Chem. Lett.*, **8**, 3795, 2017.
184. AHN T.K.; KWON J.H.; KIM DY, CHO D.W.; JEONG DH.; KIM S.K.; SUZUKI, M.; SHIMIZU S.; OSUKA A.; KIM D.; "Comparative Photophysics of [26]- and [28] Hexaphyrins (1.1. 1.1. 1.1): Large Two-Photon Absorption Cross Section of Aromatic [26] Hexaphyrins (1.1. 1.1. 1.1)", *J. AM. CHEM. SOC.*, **127**, 12856, 2005.
185. IKAWA, Y.; TAKEDA, M.; SUZUKI, M.; OSUKA, A.; FURUTA, H.; "Water-soluble doubly N-confused hexaphyrin: a near-IR fluorescent Zn(ii) ion sensor in water.", *Chemical Communications*, 46(31), 5689, 2010.
186. HILL, J. P.; D'SOUZA, F.; ARIGA, K.; "Porphyrinoids: Highly Versatile, Redox-Active Scaffolds for Supramolecular Design and Biomimetic Applications. In *Supramolecular Chemistry*.", *Supramolecular Chemistry: From Molecules to Nanomaterials*, 2012.
187. KADISH, K. M.; VAN CAEMELBECKE, E.; "Electrochemistry of porphyrins and related macrocycles.", *Journal of Solid State Electrochemistry*, 7(5), 254, 2003.
188. LU X.; DEVARAMANI, S.; "Electrochemical Investigation of Porphyrin and Its Derivatives at Various Interfaces", *Phthalocyanines and some Current Applications*, 2017.
189. K. M KADISH, "electrochemical behaviour of porphyrins and their metal complexes", *Progress in Inorganic Chemistry*, **34**, 437-604, 1986.
190. SHELNUTT, J.; SONG, X.-Z.; MA, J.-G.; JIA, S.-L.; JENTZEN, W.; J. MEDFORTH, C.; J. MEDFORTH, C.; "Nonplanar porphyrins and their significance in proteins.", *Chemical Society Reviews*, 27(1), 31, 1998.
191. FERRADÁS, R. R.; MARQUÉS-GONZÁLEZ, S.; OSORIO, H. M.; FERRER, J.; CEA, P.; MILAN, D. C.; MARTÍN, S.; "Low variability of single-molecule conductance assisted by bulky metal–molecule contacts.", *RSC Adv.*; 6(79), 75111, 2016.
192. KADISH, K. M.; SMITH, K. M.; GUILARD, R.; *Handbook of Porphyrin Science*, **8**, 8, 2010.
193. MANBECK, G. F.; FUJITA, E. "A review of iron and cobalt porphyrins, phthalocyanines and related complexes for electrochemical and photochemical reduction of carbon dioxide. *Journal of Porphyrins and Phthalocyanines*", 19(1), 45, 2015.
194. WOLBERG, A.; MANASSEN, J.; "Electrochemical and electron paramagnetic resonance studies of metalloporphyrins and their electrochemical oxidation products", *J. Am. Chem. Soc.*; **92**, 2982, 1970.
195. TRAN, T. T. H.; CHANG, Y.-R.; HOANG, T. K. A.; KUO, M.-Y.; SU, Y. O. "Electrochemical Behavior of meso -Substituted Porphyrins: The Role of Cation Radicals to the Half-Wave Oxidation Potential Splitting.", *The Journal of Physical Chemistry A*, 120(28), 5504, 2016.

- 
196. FELTON, R.H.;" The Porphyrins", Dolphyn, D. Ed. Academic Press: New York, **5**, 1978.
197. FANG, Y.; SENGE, M. O.; VAN CAEMELBECKE, E.; SMITH, K. M.; MEDFORTH, C. J.; ZHANG, M.; KADISH, K. M.; "Impact of Substituents and Nonplanarity on Nickel and Copper Porphyrin Electrochemistry: First Observation of a Cu II /Cu III Reaction in Nonaqueous Media.", *Inorganic Chemistry*, **53**(19), 10772, 2014.
198. WORTHINGTON, P.; HAMBRIGHT, P.; WILLIAMS, R. F. X.; REID, J.; BURNHAM, C.; SHAMIM, A.; EISNER, U.; "Reduction potentials of seventy-five free base porphyrin molecules: Reactivity correlations and the prediction of potentials.", *Journal of Inorganic Biochemistry*, **12**(4), 281, 1980.
199. ZERNER M, GOUTERMAN M.; "Porphyrins - IV. Extended Hückel calculations on transition metal complexes", *Theoretica Chimica Acta*, **4**, 44 1966.
200. FUHRHOP, J. H.; KADISH, K. M.; DAVIS, D. G.; "Redox behavior of metallo octaethylporphyrins", *J. Am. Chem. Soc.*; **95**, 5140, 1973.
201. CLACK, D. W.; HUSH, N. S.; "Successive One-Electron Reduction Potentials of Porphins and Metal Porphins in Dimethylformamide", *J. Am. Chem. Soc.*; **87**, 4238, 1965.
202. KADISH, K. M.; VAN CAEMELBECKE, E.; D'SOUZA, F.; LIN, M.; NURCO, D. J.; MEDFORTH, C. J.; FORSYTH, T. P.; KRATTINGER, B.; SMITH, K. M.; FUKUZUMI, S.; NAKANISHI, I.; SHELNUTT, J. A.; "Synthesis and electrochemical studies of a series of fluorinated dodecaphenylporphyrins", *Inorg. Chem*, **38**, 2188, 1999.
203. KADISH, K. M.; VAN CAEMELBECKE, E.; D'SOUZA, F.; MEDFORTH, C. J.; SMITH, K. M.; TABARD, A.; GUILARD, R.; "Electrochemistry and Spectroelectrochemistry of  $\sigma$ -Bonded Iron(III) Porphyrins with Nonplanar Porphyrin Rings. Reactions of (OETPP)Fe(R) and (OETPP)FeCl, Where R = C<sub>6</sub>H<sub>5</sub>, C<sub>6</sub>F<sub>4</sub>H, or C<sub>6</sub>F<sub>5</sub> and OETPP Is the Dianion of 2,3,7,8,12,13,17,18-Octaethyl-5,10,15,20-tetraphenylporphyrin", *Inorg. Chem*, **34**, 2984, 1995.
204. KADISH, K. M.; LIN, M.; VAN CAEMELBECKE, E.; DE STEFANO, G.; MEDFORTH, C. J.; NURCO, D. J.; NELSON, N. Y.; KRATTINGER, B.; MUZZI, C. M.; JAQUINOD, L.; XU, Y.; SHYR, D. C.; SMITH, K. M.; SHELNUTT, J. A.; "Influence of electronic and structural effects on the oxidative behavior of nickel porphyrins", *Inorg. Chem*, **41**, 6673, 2002.
205. CHANG, D.; MALINSKI, T.; ULMAN, A.; KADISH, K. M.; "Electrochemistry of nickel(II) porphyrins and chlorins.", *Inorganic Chemistry*, **23**(7), 817, 1984.
206. PISTNER, A. J.; LUTTERMAN, D. A.; GHIDIU, M. J.; MA, Y.-Z.; ROSENTHAL, J.; "Synthesis, Electrochemistry, and Photophysics of a Family of Phlorin Macrocycles That Display Cooperative Fluoride Binding.", *Journal of the American Chemical Society*, **135**(17), 6601, 2013.
207. FUKUZUMI, S.; OHKUBO, K.; IMAHORI, H.; SHAO, J.; OU, Z.; ZHENG, G.; KADISH, K. M.; "Photochemical and electrochemical properties of zinc chlorin-C60 dyad as compared to corresponding free-base chlorin-C60, free-base porphyrin-C60, and zinc porphyrin-C60 dyads", *Journal of the American Chemical Society*, **123**(43), 10676, 2001.
208. MIWA, H.; MAKAROVA, E. A.; ISHII, K.; LUK'YANETS, E. A.; KOBAYASHI, N.; "Spectroscopy, Electrochemistry, and Molecular Orbital

- 
- Calculations of Metal-Free Tetraazaporphyrin, -chlorin, -bacteriochlorin, and -isobacteriochlorin.”, *Chemistry - A European Journal*, 8(5), 1082, 2002.
209. KADISH, K. M.; VAN CAEMELBECKE, E.; BOULAS, P.; D’SOUZA, F.; VOGEL, E.; KISTERS, M.; MEDFORTH, C. J.; SMITH, K. M.; “First reversible electrogeneration of triply oxidized nickel porphyrins and porphycenes. Formation of nickel (III). pi. Dications”, *Inorg. Chem*, **32**, 4177, 1993.
210. FANG, Y.; SENGE, M. O.; VAN CAEMELBECKE, E.; SMITH, K. M.; MEDFORTH, C. J.; ZHANG, M.; KADISH, K. M.; “Impact of Substituents and Nonplanarity on Nickel and Copper Porphyrin Electrochemistry: First Observation of a Cu II /Cu III Reaction in Nonaqueous Media.”, *Inorganic Chemistry*, 53(19), 10772, 2014.
211. CHEN, P.; FINIKOVA, O. S.; OU, Z.; VINOGRADOV, S. A.; KADISH, K. M.; “Electrochemistry of Platinum(II) Porphyrins: Effect of Substituents and  $\pi$ -Extension on Redox Potentials and Site of Electron Transfer.”, *Inorganic Chemistry*, 51(11), 6200, 2012.
212. GIRAudeau, A.; CALLOT, H. J.; GROSS, M.; “Effects of electron-withdrawing substituents on the electrochemical oxidation of porphyrins.”, *Inorganic Chemistry*, 18(1), 201, 1979.
213. GIRAudeau, A.; EZAHR, I.; GROSS, M.; CALLOT, H.J.; JORDAN, J.; “Effect of electrophilic substituents on the polarographic behavior of porphyrins”, *Bioelectrochemistry and Bioenergetics*, **3**, 519, 1976.
214. FEINBERG, B.; GROSS, M.; KADISH, K. M.; MARANO, R. S.; PACE, S. J.; JORDAN, J.; “Electrode Kinetics of Cytochrome c Models”, *Bioelectrochemistry and Bioenergetics*; **1**, 73, 1974.
215. MIRONOV, A., *Transition Metal Complexes of Porphyrins and Porphyrinoids.*, Handbook of porphyrin sciences, 2012.
216. SESSLER, J. L.; TOMAT, E.; “Transition-metal complexes of expanded porphyrins.”, *Accounts of Chemical Research*, 40(5), 371, 2007.
217. KADISH, K. M.; MONINOT, G.; HU, Y.; DUBOIS, D.; IBNLFASSI, A.; BARBE, J. M.; GUILARD, R.; “Double-decker actinide porphyrins and phthalocyanines. Synthesis and spectroscopic characterization of neutral, oxidized, and reduced homo- and heteroleptic complexes.”, *Journal of the American Chemical Society*, 115(18), 8153, 1993.
218. SESSLER, J. .; VIVIAN, A. .; SEIDEL, D.; BURRELL, A. .; HOEHNER, M.; MODY, T. .; LYNCH, V.; “Actinide expanded porphyrin complexes.”, *Coordination Chemistry Reviews*, **216**, 217, 411, 2001.
219. WONG, C.-P.; VENTEICHER, R. F.; HORROCKS, W. D.; “Lanthanide porphyrin complexes. Potential new class of nuclear magnetic resonance dipolar probe.”, *Journal of the American Chemical Society*, 96(22), 7149, 1974.
220. FUHRHOP, J. H.; KADISH, K. M.; DAVIS, D. G.; “Redox behavior of metallo oxaethylporphyrins”, *J. Am. Chem. Soc.*; 95, 5140, 1973.
221. BHUPATHIRAJU, N. V. S. D. K.; RIZVI, W.; BATTEAS, J. D.; DRAIN, C. M.; “Fluorinated porphyrinoids as efficient platforms for new photonic materials, sensors, and therapeutics.”, *Organic & Biomolecular Chemistry*, 14(2), 389, 2016.
222. RANA, M. K.; SINHA, M.; PANDA, S.; “Gas sensing behavior of metal-phthalocyanines: Effects of electronic structure on sensitivity.”, *Chemical Physics*, 513, 23, 2018.



- 
223. ZHOU, R.; JOSSE, F.; GAPEL, W.; AZTARK, Z. Z.; & BEKAROLU, A.; "Phthalocyanines as Sensitive Materials for Chemical Sensors.", *Applied Organometallic Chemistry*, 10(8), 557, 1996.
224. KLYAMER, D.; SUKHIKH, A.; GROMILOV, S.; KRASNOV, P.; BASOVA, T.; "Fluorinated Metal Phthalocyanines: Interplay between Fluorination Degree, Films Orientation, and Ammonia Sensing Properties.", *Sensors*, 18(7), 2018.
225. ÖZTÜRK, Z. Z.; KILINÇ, N.; ATILLA, D.; GÜREK, A. G.; AHSEN, V.; "Recent studies chemical sensors based on phthalocyanines." *Journal of Porphyrins and Phthalocyanines*, 13(11), 1179, 2009.
226. COLE, A.; MCILROY, R. J.; THORPE, S. C.; COOK, M. J.; MCMURDO, J.; RAY, A. K.; "Substituted phthalocyanine gas sensors.", *Sensors and Actuators B: Chemical*, 13(1–3), 416, 1993.
227. DING, Y.; ZHU, W.-H.; XIE, Y.; "Development of Ion Chemosensors Based on Porphyrin Analogues.", *Chemical Reviews*, 117(4), 2203, 2017.
228. ZAMADAR, M.; ORR, C.; UHEREK, M.; "Water Soluble Cationic Porphyrin Sensor for Detection of Hg 2+ , Pb 2+ , Cd 2+ , and Cu 2+.", *Journal of Sensors*, 2016, 1, 8, 2016.
229. LVOVA, L.; DI NATALE, C.; PAOLESSE, R.; "Porphyrin-based chemical sensors and multisensor arrays operating in the liquid phase." *Sensors and Actuators B: Chemical*, 179, 21, 2013.
230. ISHIHARA, S.; LABUTA, J.; VAN ROSSOM, W.; ISHIKAWA, D.; MINAMI, K.; HILL, J. P.; ARIGA, K.; "Porphyrin-based sensor nanoarchitectonics in diverse physical detection modes.", *Physical Chemistry Chemical Physics*, 16(21), 9713, 2014.
231. SOROKIN, A. B.; "Phthalocyanine Metal Complexes in Catalysis.", *Chemical Reviews*, 113(10), 8152, 2013.
232. FOSTER, C.; PILLAY, J.; METTERS, J.; BANKS, C.; FOSTER, C. W.; PILLAY, J.; BANKS, C. E.; "Cobalt Phthalocyanine Modified Electrodes Utilised in Electroanalysis: Nano-Structured Modified Electrodes vs. Bulk Modified Screen-Printed Electrodes.", *Sensors*, 14(11), 21905, 2014.
233. MA, W.; YU, P.; OHSAKA, T.; MAO, L.; "An efficient electrocatalyst for oxygen reduction reaction derived from a Co-porphyrin-based covalent organic framework." *Electrochemistry Communications*, 52, 53, 2015.
234. WU, Z.-Y.; WANG, T.; MENG, Y.-S.; RAO, Y.; WANG, B.-W.; ZHENG, J.; ZHANG, J.-L.; "Enhancing the reactivity of nickel( ii ) in hydrogen evolution reactions (HERs) by  $\beta$ -hydrogenation of porphyrinoid ligands." *Chemical Science*, 8(9), 5953, 2017.
235. WINDLE, C.; "Electrocatalysis: Reduced ring makes catalyst sing," *Nature Reviews Chemistry*, 1(8), 62, 2017.
236. KAMINSKY, C. J.; WRIGHT, J.; SURENDRANATH, Y.; "Graphite-Conjugation Enhances Porphyrin Electrocatalysis", *ACS Catalysis*, 9(4), 3667, 2019.
237. VAN DEN BRINK, F.; VISSCHER, W.; BARENDRECHT, E.; "Electrocatalysis of cathodic oxygen reduction by metal phthalocyanines: Part II. Cobalt phthalocyanine as electrocatalyst: A mechanism of oxygen reduction.", *Journal of Electroanalytical Chemistry and Interfacial Electrochemistry*, 157(2), 305, 1983.

- 
238. DING, L.; QIAO, J.; DAI, X.; ZHANG, J.; ZHANG, J.; TIAN, B.; "Highly active electrocatalysts for oxygen reduction from carbon-supported copper-phthalocyanine synthesized by high temperature treatment", *International Journal of Hydrogen Energy*, 37(19), 14103, 2012.
239. VASUDEVAN, P.; PHOUGAT, N.; SHUKLA, A. K.; "Metal Phthalocyanines as Electrocatalysts for Redox Reactions", *Applied Organometallic Chemistry*, 10(8), 591, 1996.
240. ZHANG, X.; WU, Z.; ZHANG, X.; LI, L.; LI, Y.; XU, H.; WANG, H.; "Highly selective and active CO<sub>2</sub> reduction electrocatalysts based on cobalt phthalocyanine/carbon nanotube hybrid structures", *Nature Communications*, 8(1), 14675, 2017.
241. MORLANES, N.; TAKANABE, K.; RODIONOV, V. ; "Simultaneous Reduction of CO<sub>2</sub> and Splitting of H<sub>2</sub>O by a Single Immobilized Cobalt Phthalocyanine Electrocatalyst", *ACS Catalysis*, 6(5), 3092, 2016 .
242. SUN, C.; LI, Z.; ZHONG, X.; WANG, S.; YIN, X.; WANG, L.; "Three-Dimensional Graphene-Supported Cobalt Phthalocyanine as Advanced Electrocatalysts for Oxygen Reduction Reaction." *Journal of The Electrochemical Society*, 165(2), F24, 2018.
243. SINHA, S.; AARON, M. S.; BLAGOJEVIC, J.; WARREN, J. J.; "Electrocatalytic Dioxygen Reduction by Carbon Electrodes Noncovalently Modified with Iron Porphyrin Complexes: Enhancements from a Single Proton Relay." *Chemistry - A European Journal*, 21(50), 18072, 2015.
244. GONG, M.; CAO, Z.; LIU, W.; NICHOLS, E. M.; SMITH, P. T.; DERRICK, J. S.; CHANG, C. J., "Supramolecular Porphyrin Cages Assembled at Molecular-Materials Interfaces for Electrocatalytic CO Reduction.", *ACS Central Science*, 3(9), 1032, 2017.
245. OLDACRE, A. N.; CRAWLEY, M. R.; FRIEDMAN, A. E.; COOK, T. R.; "Tuning the Activity of Heterogeneous Cofacial Cobalt Porphyrins for Oxygen Reduction Electrocatalysis through Self-Assembly.", *Chemistry - A European Journal*, 24(43), 10984, 2018.
246. LIONS, M.; TOMMASINO, J.-B.; CHATTOT, R.; ABEYKOON, B.; GUILLOU, N.; DEVIC, T.; FATEEVA, A.; "Insights into the mechanism of electrocatalysis of the oxygen reduction reaction by a porphyrinic metal organic framework." *Chemical Communications*, 53(48), 6496, 2017.
247. MESHITSUKA, S.; ICHIKAWA, M.; TAMARU, K. ; "Electrocatalysis by metal phthalocyanines in the reduction of carbon dioxide.", *Chemical Communications*, 5, 158, 1974.
248. VAROTTO, A.; NAM, C.-Y.; RADIVOJEVIC, I.; TOMÉ, J. P. C.; CAVALEIRO, J. A. S.; BLACK, C. T.; DRAIN, C. M.; "Phthalocyanine blends improve bulk heterojunction solar cells." *Journal of the American Chemical Society*, 132(8), 2552, 2010.
249. MILAN, R.; SELOPAL, G. S.; CAVAZZINI, M.; ORLANDI, S.; BOARETTO, R.; CARAMORI, S.; POZZI, G.; "Dye-sensitized solar cells based on a push-pull zinc phthalocyanine bearing diphenylamine donor groups: computational predictions face experimental reality", *Scientific Reports*, 7(1), 15675, 2017.
250. MARTÍN-GOMIS, L.; FERNÁNDEZ-LÁZARO, F.; SASTRE-SANTOS, Á. "Advances in phthalocyanine-sensitized solar cells (PcSSCs)." *J. Mater. Chem. A*, 2(38), 15672, 2014.

- 
251. MARTÍNEZ-DÍAZ, M. V.; DE LA TORRE, G.; TORRES, T.; "Lighting porphyrins and phthalocyanines for molecular photovoltaics", *Chemical Communications*, 46(38), 7090, (2010).
252. SUZUKI, A.; UEDA, H.; OKADA, Y.; OHISHI, Y.; YAMASAKI, Y.; OKU, T.; "Effects of Metal Phthalocyanines as Hole-transporting Layers of Perovskite-based Solar Cells." *Chemical and Materials Engineering*, 5(2), 34, 2017.
253. IWASE, T.; HAGA, Y.; "Photovoltaic Characteristics of Copper Phthalocyanine-poly( p -phenylene) Co-evaporation Films.", *Japanese Journal of Applied Physics*, **42**, 8, 5330, 2017.
254. URBANI, M.; RAGOUSI, M.-E.; NAZEERUDDIN, M. K.; TORRES, T.; "Phthalocyanines for dye-sensitized solar cells." *Coordination Chemistry Reviews*, **381**, 1, 2019.
255. BIREL, Ö.; NADEEM, S.; DUMAN, H.; "Porphyrin-Based Dye-Sensitized Solar Cells (DSSCs): a Review". *Journal of Fluorescence*, 27(3), 1075, 2017.
256. WALTER, M. G.; RUDINE, A. B.; WAMSER, C. C.; "Porphyrins and phthalocyanines in solar photovoltaic cells", *Journal of Porphyrins and Phthalocyanines*, 14(9), 759, 2010.
257. ZENG, K.; LU, Y.; TANG, W.; ZHAO, S.; LIU, Q.; ZHU, W.; XIE, Y.; "Efficient solar cells sensitized by a promising new type of porphyrin: dye-aggregation suppressed by double strapping", *Chemical Science*, 10(7), 2186, 2019.
258. YANG, G.; TANG, Y.; LI, X.; ÅGREN, H.; XIE, Y.; "Efficient Solar Cells Based on Porphyrin Dyes with Flexible Chains Attached to the Auxiliary Benzothiadiazole Acceptor: Suppression of Dye Aggregation and the Effect of Distortion", *ACS Applied Materials Interfaces*, 9(42), 36875, 2017.
259. XIE, Y.; TANG, Y.; WU, W.; WANG, Y.; LIU, J.; LI, X.; ZHU, W.-H.; "Porphyrin Cosensitization for a Photovoltaic Efficiency of 11.5%: A Record for Non-Ruthenium Solar Cells Based on Iodine Electrolyte." *Journal of the American Chemical Society*, 137(44), 14055, 2015.
260. PONCE, I.; SILVA, J. F.; OÑATE, R.; REZENDE, M. C.; PAEZ, M. A.; ZAGAL, J. H.; ARRATIA-PÉREZ, R.; "Enhancement of the Catalytic Activity of Fe Phthalocyanine for the Reduction of O<sub>2</sub> Anchored to Au(111) via Conjugated Self-Assembled Monolayers of Aromatic Thiols As Compared to Cu Phthalocyanine", *The Journal of Physical Chemistry C*, 116(29), 15329, 2012.
261. NAODA, K.; SHIMIZU, D.; KIM, J. O.; FURUKAWA, K.; KIM, D.; OSUKA, A.; "Thienylquinonoidal Porphyrins and Hexaphyrins with Singlet Diradical Ground States", *Chemistry - A European Journal*, 23(37), 8969, 2017.
262. YONEDA, T.; KIM, T.; SOYA, T.; NEYA, S.; OH, J.; KIM, D.; OSUKA, A.; "Conformational Fixation of a Rectangular Antiaromatic [28]Hexaphyrin Using Rationally Installed Peripheral Straps." *Chemistry - A European Journal*, 22(13), 4413, 2016.
263. TANAKA, T.; ARATANI, N.; LIM, J. M.; KIM, K. S.; KIM, D.; OSUKA, A.; "Porphyrin-hexaphyrin hybrid tapes", *Chemical Science*, 2(7), 1414, 2011.
264. MORI, H.; OSUKA, A.; "Bimetal complexes of 5,20-bis(5-formyl-2-pyrrolyl)-[26]hexaphyrin(1.1.1.1.1.1) exhibiting strong near-infrared region absorptions", *Chemistry - A European Journal*, 21(19), 7007, 2015.
265. MORI, H.; TANAKA, T.; LEE, S.; LIM, J. M.; KIM, D.; OSUKA, A.; "Meso-meso linked porphyrin-[26]hexaphyrin-porphyrin hybrid arrays and their triply

- 
- linked tapes exhibiting strong absorption bands in the NIR region.”, *Journal of the American Chemical Society*, 137(5), 2097, 2015.
266. JANA, A.; ISHIDA, M.; CHO, K.; GHOSH, S. K.; KWAK, K.; OHKUBO, K.; SESSLER, J. L.; “Tetrathiafulvalene-annulated [28]hexaphyrin(1.1.1.1.1.1): a multi-electron donor system subject to conformational control”, *Chemical Communications*, 49(79), 8937, 2013.
267. NAODA, K.; MORI, H.; ARATANI, N.; LEE, B. S.; KIM, D.; OSUKA, A. ; “Hexaphyrin fused to two anthracenes.” *Angewandte Chemie - International Edition*, 51(39), 9856, 2012.
268. HIGASHINO, T.; INOUE, M.; OSUKA, A., “Singly N-fused Möbius aromatic [28]Hexaphyrins(1.1.1.1.1.1)”, *Journal of Organic Chemistry*, 75(22), 7958, 2010.
269. KOIDE, T.; KASHIWAZAKI, G.; SUZUKI, M.; FURUKAWA, K.; YOON, M. C.; CHO, S.; OSUKA, A.; “A stable radical species from facile oxygenation of meso-free 5,10,20,25-tetrakis (pentafluorophenyl) -substituted [26]hexaphyrin(1.1.1.1.1.1)” *Angewandte Chemie - International Edition*, 47(50), 9661, 2008.
270. GOKULNATH, S.; TOGANO, M.; YAMAGUCHI, K.; MORI, S.; UNO, H.; FURUTA, H.; “Confusion of Möbius aromaticity: disruption of annulenic pathway in singly N-confused [28]hexaphyrin and its mono-Pd(ii) complex”, *Dalton Transactions*, 41(20), 6283, 2012.
271. HIGASHINO, T.; INOUE, M.; OSUKA, A.; “Singly N-fused Möbius aromatic [28]Hexaphyrins(1.1.1.1.1.1)”, *Journal of Organic Chemistry*, 75(22), 7958, 2010.
272. GOKULNATH, S.; NISHIMURA, K.; TOGANO, M.; MORI, S.; FURUTA, H. “Palladium-induced pyrrolic rearrangement of a singly to a doubly N-confused [26]hexaphyrin”, *Angewandte Chemie - International Edition*, 52(27), 6940, 2013.
273. NAODA, K.; OSUKA, A.; “Iridium complexes of [26]hexaphyrin(1.1.1.1.1.1) and [36]octaphyrin(1.1.1.1.1.1.1.1)”, *Journal of Porphyrins and Phthalocyanines*, 18(08n09), 652, 2014.
274. KE, S.-H.; YANG, W.; BARANGER, H. U.; “Quantum-Interference-Controlled Molecular Electronics”, *Nano Letters*, 8(10), 3257, 2008.
275. NOZAKI, D.; LOKAMANI, SANTANA-BONILLA, A.; DIANAT, A.; GUTIERREZ, R.; CUNIBERTI, G.; “Switchable Negative Differential Resistance Induced by Quantum Interference Effects in Porphyrin-based Molecular Junctions”, *The Journal of Physical Chemistry Letters*, 6(19), 3950, 2015.
276. MATHEW, P. T.; FANG, F.; “Advances in Molecular Electronics: A Brief Review”. *Engineering*, 4(6), 760, 2018.
277. ELEMANS, J. A. A. W.; VAN HAMEREN, R.; NOLTE, R. J. M.; ROWAN, A. E., “Molecular Materials by Self-Assembly of Porphyrins, Phthalocyanines, and Perylenes”, *Advanced Materials*, 18(10), 1251, 2006.
278. AKIYAMA T, IMAHORI H, AJAWAKOM A, SAKATA Y.; “Synthesis and self-assembly of porphyrin-linked fullerene on gold surface using S-Au linkage”, *Chem. Lett.* 25(10), 907, 1996.
279. AKIYAMA T., IMAHORI H., SAKATA Y.; “Preparation of Molecular Assemblies of Porphyrin-Linked Alkanethiol on Gold Surface and Their Redox Properties” *Chem. Lett.*, 23(8), 1447, 1994.

- 
280. ZAK J.; YUAN H.; HO M.; WOO LK.; PORTER MD.; "Thiol-derivatized metalloporphyrins: monomolecular films for the electrocatalytic reduction of dioxygen at gold electrodes" *Langmuir*, **9**, 2772, 1993.
281. POSTLETHWAITE T.A.; HUTCHISON J.E.; HATHCOCK K.W.; MURRAY RW.; "Optical, electrochemical, and electrocatalytic properties of self-assembled thiol-derivatized porphyrins on transparent gold films", *Langmuir*, **11**, 4109, 1995.
282. JUROW, M.; SCHUCKMAN, A.E.; BATTEAS, J.D.; DRAIN, C.M.; "Porphyrins as molecular electronic components of functional devices", *Coord Chem Rev.* 254(19-20), 2297, 2010.
283. HU, Y.; ZHU, Y.; GAO, H.; GUO, H.; "Conductance of an Ensemble of Molecular Wires: A Statistical Analysis", *Phys. Rev. Lett.*, **95**, 156803, 2005.
284. BASCH, H.; COHEN, R.; RATNER, M. A.; "Interface Geometry and Molecular Junction Conductance: Geometric Fluctuation and Stochastic Switching", *Nano Letters*, 5(9), 1668, 2005.
285. VENKATARAMAN, L.; KLARE, J. E.; NUCKOLLS, C.; HYBERTSEN, M. S.; STEIGERWALD, M. L.; "Dependence of single-molecule junction conductance on molecular conformation." *Nature*, 442(7105), 904, 2006.
286. CHEN, F.; LI, X.; HIHATH, J.; HUANG, Z.; TAO, N.; Effect of anchoring groups on single-molecule conductance: comparative study of thiol-, amine-, and carboxylic-acid-terminated molecules, *J. AM. CHEM. SOC.*, **128**, 15874, 2006.
287. WATCHARINYANON, S.; NILSSON, D.; MOONS, E.; SHAPORENKO, A.; ZHARNIKOV, M.; ALBINSSON, B.; MÅRTENSSON, J.; JOHANSSON, L.S.; "A spectroscopic study of self-assembled monolayer of porphyrin-functionalized oligo(phenyleneethynylene)s on gold: the influence of the anchor moiety.", *Phys. Chem. Chem. Phys.*; **10**, 5264, 2008.
288. BOECKL, M.S.; BRAMBLETT, A.L.; HAUCH, K.D.; SASAKI, T.; RATNER, B.D.; ROGERS, J.W.; Self-Assembly of Tetraphenylporphyrin Monolayers on Gold Substrates, *Langmuir*, **16**, 5644, 2000.
289. KRAWICZ, A.; PALAZZO, J.; WANG, G.-C.; DINOLFO, P. H.; "Layer-by-layer assembly of Zn(ii) and Ni(ii) 5,10,15,20-tetra(4-ethynylphenyl)porphyrin multilayers on Au using copper catalyzed azide-alkyne cycloaddition.", *RSC Advances*, 2(19), 7513, 2012.
290. XU, B. Q.; XIAO, X. Y.; TAO, N.; "Measurements of single-molecule electromechanical properties", *J. J. Am. Chem. Soc.*, **125**, 16164, 2003.
291. VENKATARAMAN, L.; KLARE, J. E.; TAM, I. W.; NUCKOLLS, C.; HYBERTSEN, M. S.; STEIGERWALD, M. L. *Nano Lett.* 2006, 6, 458-462.
292. KIM, B.; BEEBE, J. M.; JUN, Y.; ZHU, X. Y.; FRISBIE, C. D.; "Single-molecule circuits with well-defined molecular conductance", *J. Am. Chem. Soc.*, **128**, 4970, 2006.
293. ZHANG, Z. J.; IMAE, T.; Hydrogen-bonding stabilized self-assembled monolayer film of a functionalized diacid, protoporphyrin IX zinc (II), onto a gold surface, *Nano Lett.*; **1**, 241, 2001.
294. GHOSH, S.; MUKHERJEE, P.S.; "Self-Assembly of Metallamacrocycles via a Rigid Phosphorus Donor Linker", *Organometallics*, 26(14), 3362, 2007.
295. LI, Q.; SURTHI, S.; MATHUR, G.; GOWDA, S.; MISRA, V.; SORENSON, T. A.; TENENT, R. C.; KUHR, W. G.; TAMARU, S.-I.; LINDSEY, J. S.; LIU, Z.;

- 
- BOCIAN, D. F.; "Electrical Characterization of Redox-Active Molecular Monolayers on SiO<sub>2</sub> for Memory Applications.", *Appl. Phys. Lett.*; **83**, 198, 2003.
296. LI, Q.; SURTHI, S.; MATHUR, G.; GOWDA, S.; ZHAO, Q.; SORENSON, T. A.; TENENT, R. C.; MUTHUKUMARAN, K.; LINDSEY, J. S.; MISRA, V.; "Multiple-Bit Storage Properties of Porphyrin Monolayers on SiO<sub>2</sub>.", *Appl. Phys. Lett.*; **85**, 1829, 2004.
297. LUO, L.; FRISBIE, C. D.; "Length-Dependent Conductance of Conjugated Molecular Wires Synthesized by Stepwise "Click" Chemistry.", *Journal of the American Chemical Society*, **132**(26), 8854, 2010.
298. HUANG, K.; DUCLAIROIR, F.; PRO, T.; BUCKLEY, J.; MARCHAND, G.; MARTINEZ, E.; VINET, F.; "Ferrocene and Porphyrin Monolayers on Si(100) Surfaces: Preparation and Effect of Linker Length on Electron Transfer." *ChemPhysChem*, **10**(6), 963, 2009.
299. ULMAN, A.; "Formation and Structure of Self-Assembled-Monolayers", *Chem. Rev.*, **96**, 1533, 1996.
300. INKPEN, M. S.; LIU, Z.; LI, H.; CAMPOS, L. M.; NEATON, J. B.; VENKATARAMAN, L.; "Non-chemisorbed gold-sulfur binding prevails in self-assembled monolayers.", *Nature Chemistry*, **11**(4), 351, 2019.
301. SHIMAZU K, TAKECHI M, FUJII H, SUZUKI M, SAIKI H, YOSHIMURA T, UOSAKI K.; "Formation and characterization of thiol-derivatized zinc (II) porphyrin monolayers on gold", *Thin Solid Films*, **273**, 250, 1996.
302. VAN GALEN D.A.; MAJDA M.; "Irreversible self-assembly of monomolecular layers of a cobalt (II) hexadecyltetrapyrrolylporphyrin amphiphile at gold electrodes and its catalysis of oxygen reduction", *Anal. Chem.*, **60**, 1549, 1988.
303. BLAMBLETT, A.L.; BOECKL, M.S.; HAUCH, K.D.; RATNER, B.D.; SASAKI, T.; ROGERS JR., J.W.; "Determination of surface coverage for tetraphenylporphyrin monolayers using ultraviolet visible absorption and x-ray photoelectron spectroscopies", *Surf. Interface Anal.*; **33**, 506, 2002.
304. GRAY, H. B.; WINKLER, J. R.; "Electron flow through metalloproteins."; *Biochimica et Biophysica Acta (BBA) - Bioenergetics*, **1797**(9), 1563, 2010.
305. REGAN, J. J.; RAMIREZ, B. E.; WINKLER, J. R.; GRAY, H. B.; MALMSTRÖM, B. G.; "Pathways for Electron Tunneling in Cytochrome c Oxidase." *Journal of Bioenergetics and Biomembranes*, **30**(1), 35, 1998.
306. CLAUSEN, C.; GRYKO, D. T.; YASSERI, A. A.; DIERS, J. R.; BOCIAN, D. F.; KUHR, W. G.; LINDSEY, J. S.; "Investigation of Tightly Coupled Porphyrin Arrays Comprised of Identical Monomers for Multibit Information Storage." *The Journal of Organic Chemistry*, **65**(22), 7371, 2000.
307. CLAUSEN, C.; GRYKO, D. T.; DABKE, R. B.; DONTA, N.; BOCIAN, D. F.; KUHR, W. G.; LINDSEY, J. S.; "Synthesis of Thiol-Derivatized Porphyrin Dimers and Trimers for Studies of Architectural Effects on Multibit Information Storage." *The Journal of Organic Chemistry*, **65**(22), 7363, 2000.
308. LINDSEY, J. S.; BOCIAN, D. F.; "Molecules for Charge-Based Information Storage." *Accounts of Chemical Research*, **44**(8), 638, 2011.
309. LIU, Z.; YASSERI, A. A.; LINDSEY, J. S.; BOCIAN, D. F.; "Molecular Memories That Survive Silicon Device Processing and Real-World Operation", *Science*, **302**, 1543, 2003.

- 
310. WEI, L.; PADMAJA, K.; YOUNGBLOOD, W. J.; LYSENKO, A. B.; LINDSEY, J. S.; BOCIAN, D. F.; "Diverse Redox-Active Molecules Bearing Identical Thiol-Terminated Tripodal Tethers for Studies of Molecular Information Storage", *J. Org. Chem.*, 69, 1461, 2004.
311. THANOPULOS, I.; PASPALAKIS, E.; YANNOPAPAS, V.: Optical switching of electric charge transfer pathways in porphyrin: a light-controlled nanoscale current router", *Nanotechnology*, 19, 445202, 2008.
312. THANOPULOS, I.; PASPALAKIS, E.; "Molecular optoelectronics: the interaction of molecular conduction junctions with light", *Phys. Rev. B: Condens. Matter Mater. Phys.*; 76, 035317, 2007.
313. WOLLER, T.; GEERLINGS, P.; PROFT, F.; CHAMPAGNE, B.; ALONSO, M.; "Fingerprint of Aromaticity and Molecular Topology on the Photophysical Properties of Octaphyrins." *The Journal of Physical Chemistry C*, 123(12) , 7318, 2019.
314. AMBROISE, A.; KIRMAIER, C.; WAGNER, R.W.; LOEWE, R.S.; BOCIAN, D.F.; HOLTEN, D.; LINDSEY, J.S.; "Weakly Coupled Molecular Photonic Wires: Synthesis and Excited-State Energy-Transfer Dynamics.", *J. Org. Chem*, 67(11), 3811, 2002.
315. CHE, C.; XIANG, H.; CHUI, S. S.; XU, Z.; ROY, V. A. L.; YAN, J. J.; WILLIAMS, I. D.; "A High-Performance Organic Field-Effect Transistor Based on Platinum(II) Porphyrin: Peripheral Substituents on Porphyrin Ligand Significantly Affect Film Structure and Charge Mobility." *Chemistry – An Asian Journal*, 3(7), 1092, 2008.
316. CHO, W. J.; CHO, Y.; MIN, S. K.; KIM, W. Y.; KIM, K. S.; "Chromium Porphyrin Arrays As Spintronic Devices." *Journal of the American Chemical Society*, 133(24), 9364, 2011.
317. YASSERI, A.A.; SYOMIN, D.; MALINOVSKII, V.L.; LOEWE, R.S.; LINDSEY, J.S.; ZAERA, F.; BOCIAN\*, D.F.; "Characterization of Self-Assembled Monolayers of Porphyrins Bearing Multiple Thiol-Derivatized Rigid-Rod Tethers", *J. Am. Chem. Soc.*; 126(38), 11944, 2004.
318. MEISNER, J. S.; KAMENETSKA, M.; KRIKORIAN, M.; STEIGERWALD, M. L.; VENKATARAMAN, L.; NUCKOLLS, C.; „A Single-Molecule Potentiometer“, *Nano Letters*, 11(4), 1575, 2011.
319. FRISENDA, R.; TARKUÇ, S.; GALÁN, E.; PERRIN, M. L.; EELKEMA, R.; GROZEMA, F. C.; VAN DER ZANT, H. S. J.; "Electrical properties and mechanical stability of anchoring groups for single-molecule electronics", *Beilstein Journal of Nanotechnology*, 6, 1558, 2015.
320. KALIGINEDI, V.; V. RUDNEV, A.; MORENO-GARCÍA, P.; BAGHERNEJAD, M.; HUANG, C.; HONG, W.; WANDLOWSKI, T.; "Promising anchoring groups for single-molecule conductance measurements." *Phys. Chem. Chem. Phys.*; 16(43), 23529, 2014.
321. CHEN, F.; LI, X.; HIHATH, J.; HUANG, Z.; TAO, N.; "Effect of Anchoring Groups on Single-Molecule Conductance: Comparative Study of Thiol-, Amine-, and Carboxylic-Acid-Terminated Molecules.", *J. Am. Chem. Soc.*; 128(49), 15874, 2006.
322. MORENO-GARCÍA, P.; GULCUR, M.; MANRIQUE, D.Z.; POPE, T.; HONG, W.; KALIGINEDI, V.; HUANG, C.; BATSANOV, A.S.; BRYCE, M.R.; LAMBERT C.; WANDLOWSKI, T.; "Single-molecule conductance of

- 
- functionalized oligoynes: Length dependence and junction evolution”, *J. Am. Chem. Soc.*; **135**, 12228, 2013.
323. FERRADÁS, R. R. ; MARQUÉS-GONZÁLEZ, S. ; OSORIO, H. M. ; FERRER, J. ; CEA, P. ; MILAN, D. C. ; VEZZOLI, A. ; HIGGINS, S. J. ; NICHOLS, R. J. ; LOW, P. J. ; GARCÍA-SUÁREZ, V. M. ; MARTÍN, S.; “Low variability of single-molecule conductance assisted by bulky metal–molecule contacts”, *RSC Adv.*; **6**, 75111, 2016.
324. MILAN, D. C.; AL-OWAEDI, O. A.; OERTHEL, M. C.; MARQUÉS-GONZÁLEZ, S.; BROOKE, R. J.; BRYCE, M. R.; CEA, P.; FERRER, J.; HIGGINS, S. J.; LAMBERT, C. J. ; LOW, P. J. ; MANRIQUE, D. Z. ; MARTÍN, S. ; NICHOLS, R. J. ; SCHWARZACHER W. ; GARCÍA-SUÁREZ, V. M. ; “Solvent dependence of the single molecule conductance of oligoyne-based molecular wires”, *J. Phys. Chem. C*, 120(29), 15666, 2016.
325. AL-OWAEDI, O. A.; BOCK, S.; MILAN, D. C.; OERTHEL, M.-C.; INKPEN, M. S.; YUFIT, D. S.; LOW, P. J.; “Insulated molecular wires: inhibiting orthogonal contacts in metal complex based molecular junctions”, *Nanoscale*, 9(28), 9902, 2017.
326. PAN, C.; ZHAO, C.; TAKEUCHI, M.;SUGIYASU, K.; “Conjugated Oligomers and Polymers Sheathed with Designer Side Chains.”; *Chemistry - An Asian Journal*, 10(9), 1820, 2015.
327. MILAN, D. C.; KREMPE, M.; ISMAEL, A. K.; MOVSISYAN, L. D.; FRANZ, M.; GRACE, I.; NICHOLS, R. J.; “The single-molecule electrical conductance of a rotaxane-hexayne supramolecular assembly”; *Nanoscale*, 9(1), 355, 2017.
328. HUANG, J.; XU, K.; LEI, S.; SU, H.; YANG, S.; LI, Q.;YANG, J.; “Iron-phthalocyanine molecular junction with high spin filter efficiency and negative differential resistance”, *The Journal of Chemical Physics*, 136(6), 064707, 2012.
329. SEDGHI, G.; SAWADA, K.; ESDAILE, L. J.; HOFFMANN, M.; ANDERSON, H. L.; BETHELL, D.; NICHOLS, R. J.; “Single Molecule Conductance of Porphyrin Wires with Ultralow Attenuation.”, *Journal of the American Chemical Society*, 130(27), 8582, 2008.
330. DENG, X. Q.; ZHANG, Z. H.; TANG, G. P.; FAN, Z. Q.; SUN, L.;LI, C. X.; “Modulation of the spin transport properties of the iron-phthalocyanine molecular junction by carbon chains with different connection sites”, *Organic Electronics*, **35**, 1, 2016.
331. QIU, X. H.; NAZIN, G. V.;HO, W.; “Mechanisms of Reversible Conformational Transitions in a Single Molecule”, *Physical Review Letters*, 93(19), 196806, 2004.
332. MOL, J. A.; LAU, C. S.; LEWIS, W. J. M.; SADEGHI, H.; ROCHE, C.; CNOSSEN, A.; BRIGGS, G. A. D.; “Graphene-porphyrin single-molecule transistors”, *Nanoscale*, 7(31), 13181, 2015.
333. LI, Z.;BORGUET, E.; “Determining Charge Transport Pathways through Single Porphyrin Molecules Using Scanning Tunneling Microscopy Break Junctions”, *Journal of the American Chemical Society*, 134(1), 63, 2012.
334. S. W. WU, N. OGAWA, †, G. V. NAZIN, AND,HO\*, W.; “Conductance Hysteresis and Switching in a Single-Molecule Junction”, *J. Phys. Chem. C*, 112(14), 5241, 2008.



- 
335. QIAN, G.; SAHA, S.; LEWIS, K. M.; "Two-state conductance in single Zn porphyrin molecular junctions", *Applied Physics Letters*, 96(24), 243107, 2010.
336. PERRIN, M. L.; MARTIN, C. A.; PRINS, F.; SHAIKH, A. J.; EELKEMA, R.; VAN ESCH, J. H.; DULIĆ, D.; "Charge Transport in a Zn-Porphyrin single molecule junction." *Beilstein J. Nanotechnol.*; **2**, 714, 2011.
337. LI, Z.; SMEU, M.; RATNER, M. A.; BORGUET, E. ; "Effect of Anchoring Groups on Single Molecule Charge Transport through Porphyrins.", *The Journal of Physical Chemistry C*, 117(29), 14890, 2013.
338. PERRIN, M. L.; PRINS, F.; MARTIN, C. A.; SHAIKH, A. J.; EELKEMA, R.; VAN ESCH, J. H.; DULIĆ, D.; "Influence of the Chemical Structure on the Stability and Conductance of Porphyrin Single-Molecule Junctions", *Angewandte Chemie International Edition*, 50(47), 11223, 2011.
339. KIGUCHI, M.; TAKAHASHI, T.; KANEHARA, M.; TERANISHI, T.; MURAKOSHI, K.; "Effect of End Group Position on the Formation of a Single Porphyrin Molecular Junction.", *The Journal of Physical Chemistry C*, 113(21), 9014, 2009.
340. ARAGONÈS, A. C.; DARWISH, N.; SALETRA, W. J.; PÉREZ-GARCÍA, L.; SANZ, F.; PUIGMARTÍ-LUIS, J.; DÍEZ-PÉREZ, I.; "Orientation by Coordination of Metalloporphyrins", *Nano Letters*, 14(8), 4751, 2014.
341. NOORI, M.; ARAGONÈS, A. C.; DI PALMA, G.; DARWISH, N.; BAILEY, S. W. D.; AL-GALIBY, Q.; LAMBERT, C. J.; "Tuning the electrical conductance of metalloporphyrin supramolecular wires.", *Scientific Reports*, 6(1), 37352, 2016.
342. LIU, J.-Y.; EL-KHOULY, M. E.; FUKUZUMI, S.; NG, D. K. P.; "Mimicking Photosynthetic Antenna-Reaction-Center Complexes with a (Boron Dipyrromethene)3-Porphyrin-C60 Pentad.", *Chemistry - A European Journal*, 17(5), 1605, 2011.
343. WINTERS, M.U.; DAHLSTEDT, E.; BLADES, H.E.; WILSON, C.J.; FRAMPTON, M.J.; ANDERSON, H.L.; ALBINSSON, B.; "Probing the Efficiency of Electron Transfer through Porphyrin-Based Molecular Wires", *J. Am. Chem. Soc.*, 129(14)4291, 2007.
344. SEDGHI, G.; GARCÍA-SUÁREZ, V. M.; ESDAILE, L. J.; ANDERSON, H. L.; LAMBERT, C. J.; MARTÍN, S.; NICHOLS, R. J.; "Long-range electron tunnelling in oligo-porphyrin molecular wires.", *Nature Nanotechnology*, 6(8), 517, 2011.
345. SEDGHI, G.; SAWADA, K.; ESDAILE, L. J.; HOFFMANN, M.; ANDERSON, H. L.; BETHELL, D.; NICHOLS, R. J.; "Single Molecule Conductance of Porphyrin Wires with Ultralow Attenuation", *Journal of the American Chemical Society*, 130(27), 8582, 2008.
346. SUSUMU, K.; FRAIL, P. R.; ANGIOLILLO, P. J.; THERIEN, M. J.; "Conjugated Chromophore Arrays with Unusually Large Hole Polaron Delocalization Lengths", *Journal of the American Chemical Society*, 128(26), 8380, 2006.
347. SEDGHI, G.; ESDAILE, L. J.; ANDERSON, H. L.; MARTIN, S.; BETHELL, D.; HIGGINS, S. J.; NICHOLS, R. J.; "Comparison of the Conductance of Three Types of Porphyrin-Based Molecular Wires:  $\beta$ , meso,  $\beta$ - Fused Tapes, meso - Butadiyne-Linked and Twisted meso-meso Linked Oligomers", *Advanced Materials*, 24(5), 653, 2012.

- 
348. ALGETHAMI, N.; SADEGHI, H.; SANGTARASH, S.; LAMBERT, C. J.; "The conductance of porphyrin-based molecular nanowires increases with length", *Nano Lett.*; **18**(7), 4482, 2018.
349. STUYVER, T.; PERRIN, M.; GEERLINGS, P.; DE PROFT, F.; ALONSO, M.; Conductance Switching in Expanded Porphyrins through Aromaticity and Topology Changes. *Journal of the American Chemical Society*, **140**(4), 1313–2018.
350. ZHAO, Y.; ASHCROFT, B.; ZHANG, P.; LIU, H.; SEN, S.; SONG, W.; IM, J.; GYARFAS, B.; MANNA, S.; BISWAS, S.; BORGES, C.; LINDSAY, S.; "Single-molecule spectroscopy of amino acids and peptides by recognition tunnelling", *Nat. Nanotech.*; **9**, 466, 2014.
351. LI, Z.; BORGUET, E.; "Determining charge transport pathways through single porphyrin molecules using scanning tunneling microscopy break junctions", *J. Am. Chem. Soc.*, **134**, 63, 2011.
352. SEDGHI, G.; GARCÍA-SUÁREZ, V. M.; ESDAILE, L. J.; ANDERSON, H. L.; LAMBERT, J. C.; MARTÍN, S.; BETHEL, D.; HIGGINS, S. J.; ELLIOTT, M.; BENNETT, N.; MACDONALD, J. E.; NICHOLS, R. J.; "Long-range electron tunnelling in oligo-porphyrin molecular wires" *Nature Nanotechnol.*, **6**, 517, 2011.
353. STADLER, R.; JACOBSEN, K. W.; Fermi level alignment in molecular nanojunctions and its relation to charge transfer., *Physical Review B*, **74**(16), 161405, 2006.